Diplomarbeit

Transport through metal phthalocyanine molecular bridges

Benjamin Siegert
aus
Allersburg

November 2011

durchgeführt am Institut Physik I
Theoretische Physik
Universität Regensburg
unter Anleitung von Prof. Dr. Milena Grifoni

Contents

1. Introduction

In recent times, the calls for faster, cheaper and smaller electronic devices become more and more louder while the chip industry already struggles keeping up with Moore's law. However, halving the node size of transistors every two years will not be possible forever, as at some point quantum mechanical effects will come into play.
This could be the starting point for the success of molecular electronics, as the size of molecules is tipically in the sub-nanometer range. Further reasons for molecular devices to supersede conventional transistors are their synthetical fabrication and the adjustability of their electronic properties [Tou00]. At present, many different candidates for molecular electronic devices are subject to extensive research [PPL+00,KDH+03,PGAW11,LRM07].

The visionary talk "There's Plenty of Room at the Bottom", given by Richard Feynman [Fey60] at the annual meeting of the American Physical Society at the Californian Institute of Technology in December 1959, is regarded by many as the beginning point of nanotechnology. The first theoretical work that adressed the feasibility of molecular electronic devices was authored by Aviram and Ratner in 1974 [AR74]. In this work the possibility of using single molecules as electrical rectifiers has been proposed. However, the physics community had to wait a long time for an experimental realization of contacting and manipulating molecules or nano-scale devices, respectively. For sure, a breakthrough in this respect has been the invention of scanning tunneling microscopy (STM): In 1981 Gerd Binning and Heinrich Rohrer presented a technique to image surfaces in atomic resolution [BR82]. Five years later they were awarded the Nobel Prize.

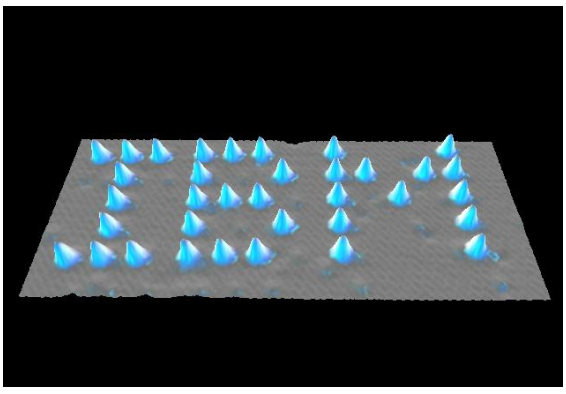

Figure 1.1.: *"The Beginning". Xenon atoms on nickel (110). Image originally created by IBM Corporation. Source: http://www.almaden.ibm.com/vis/stm/atomo.html*

Since then, STM has found an ever wider range of applications. Starting from surface microscopy via spectroscopy and imaging of molecular orbitals through to the actual manipulation of individual atoms and molecules [ES90, RM05, GRM+05].
The subject of the present thesis is to develop a semi-quantitative transport theory that allows us to reproduce two main applications of scanning tunneling microscopy: spectroscopy and imaging of molecular orbitals. The spectral properties of molecules are strongly influencing the electronic transport through molecules in the Coulomb Blockade Regime [GD92]. The molecule we have chosen to investigate is hydrogen phthalocyanine. Due to its size, an exact diagonalization is numerically intractable. Hence an important part of this thesis will be to search for alternative approaches and to check to which extent these approximations retain their validity.
The imaging of molecular orbitals allows the examination of the electronic structure of molecules. To this end, molecules are placed on a thin insulating film, that sets them apart from the substrate. This is important, since the electrons in the substrate are wielding heavy influence on the electrons in the molecule [RM05]. As we will see later in this work, the shape of the recorded images is also strongly related to the orbital structure of the tip. By comparison with expected results we will be able to check the validity of our mathematical description of the tip.

The present thesis is outlined as follows: In Chap. 2 we specify the Hamiltonian which describes our system and derive the tunneling matrix elements for an organic molecule in an STM tunneling junction. In the third chapter we evaluate the General Master Equation for the reduced density matrix up to second order in the tunneling Hamiltonian. Finally we obtain the stationary solution for the reduced density matrix and derive the current operator. Its expectation value, evaluated using the stationary solution, will be the fundament of our transport calculations. Eventually, in the fourth chapter we adress phthalocyanine, to be precise hydrogen phthalocyanine and copper phthalocyanine. We diagonalize their single particle Hamiltonians in order to obtain the molecular orbitals and the corresponding eigenenergies. After setting up a reasonable many-body representation, we finally give the results of our transport calculations in Chap. 5 and compare these to experimental data.

2. STM setup and tunneling matrix elements

At first, we specify the setup of our system and give the single particle Hamilton operators which describe the dynamics of the different subsystems. These are coupled amongst themselves through a tunneling Hamiltonian. Finally, to mirror the functional principle of a scanning tunneling microscope we have to derive so-called tunneling matrix elements. These are determining the tunneling properties between the different subsystems.

2.1. The model Hamiltonian

The Hamiltonian of our system consists of four terms:

$$\hat{\mathcal{H}} = \hat{\mathcal{H}}_{mol} + \hat{\mathcal{H}}_{sub} + \hat{\mathcal{H}}_{tip} + \hat{\mathcal{H}}_{T}. \tag{2.1}$$

Here $\hat{\mathcal{H}}_{mol}$ is the Hamiltonian of the molecule, $\hat{\mathcal{H}}_{sub}$ and $\hat{\mathcal{H}}_{tip}$ describe the Hamiltonians of the substrate or the tip respectively and $\hat{\mathcal{H}}_{T}$ is the tunneling term (see Fig. 2.1). The single particle Hamiltonian of the molecule is given by:

$$\hat{\mathcal{H}}_{mol} = \sum_{\nu} \epsilon_{\nu}\, \hat{\mathrm{d}}_{\nu}^{\dagger} \hat{\mathrm{d}}_{\nu} + \sum_{\langle \nu, \nu' \rangle} b_{\nu\nu'}\, \hat{\mathrm{d}}_{\nu}^{\dagger} \hat{\mathrm{d}}_{\nu'}, \tag{2.2}$$

where the indices $\nu = (\alpha, l_m, \tau)$ and $\nu' = (\alpha', l'_{m'}, \tau')$ are given in multi-index notation. They include the index of the atomic site α, the quantum number l_m of an atomic orbital

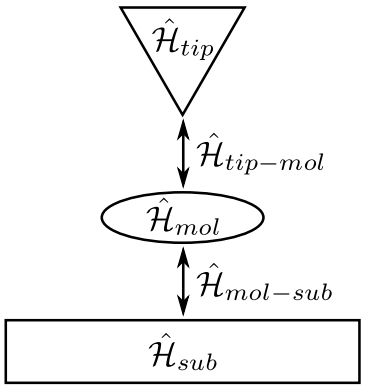

Figure 2.1.: *Schematic sketch of a molecule underlying an STM setup.*

at the specified site and a spin index τ. The operators $\hat{\mathrm{d}}_\nu^\dagger$ and $\hat{\mathrm{d}}_\nu$ are the creation or annihilation operators for an electron on the molecule, with quantum numbers $\nu = (\alpha, l_m, \tau)$. Due to the fact that there are no spin-dependent interactions in our system we will leave out the spin index in our further notations, but will keep in mind that we are treating fermionic particles. By diagonalizing the Hamiltonian of the molecule we get the single particle molecular orbitals $|i\rangle$ and their corresponding energies ϵ_i:

$$\hat{\mathcal{H}}_{mol} = \sum_i \epsilon_i \, \hat{\mathrm{d}}_i^\dagger \hat{\mathrm{d}}_i . \tag{2.3}$$

The operator $\hat{\mathrm{d}}_i^\dagger$ creates an electron in the molecular orbital specified by the orbital quantum number i. For further details about the diagonalization and the molecular orbitals the reader is referred to Sec. 4.1.2. The Hamiltonians for the substrate and the tip are single particle Hamiltonians of noninteracting electrons in a metal, where $\hat{\mathrm{c}}_\mathbf{k}^\dagger/\hat{\mathrm{a}}_\mathbf{k}^\dagger$ and $\hat{\mathrm{c}}_\mathbf{k}/\hat{\mathrm{a}}_\mathbf{k}$ create or annihilate an electron with momentum $\mathbf{k}$ in the substrate or the tip, respectively. They read:

$$\hat{\mathcal{H}}_{sub} = \sum_\mathbf{k} \epsilon_\mathbf{k} \, \hat{\mathrm{c}}_\mathbf{k}^\dagger \hat{\mathrm{c}}_\mathbf{k}, \tag{2.4}$$

$$\hat{\mathcal{H}}_{tip} = \sum_\mathbf{k} \epsilon_\mathbf{k} \, \hat{\mathrm{a}}_\mathbf{k}^\dagger \hat{\mathrm{a}}_\mathbf{k}. \tag{2.5}$$

The tunneling Hamiltonian $\hat{\mathcal{H}}_T$ can be split into two parts. The first one, $\hat{\mathcal{H}}_{tip-mol}$, is associated with tunneling between the tip and the molecule whereas the second term, $\hat{\mathcal{H}}_{mol-sub}$, gives the tunneling between the molecule and the substrate:

$$\hat{\mathcal{H}}_T = \hat{\mathcal{H}}_{tip-mol} + \hat{\mathcal{H}}_{mol-sub}. \tag{2.6}$$

Explicitly the terms read:

$$\hat{\mathcal{H}}_{tip-mol} = \sum_{\mathbf{k},i} \left(t_{\mathbf{k}i}^T \, \hat{\mathrm{a}}_\mathbf{k}^\dagger \hat{\mathrm{d}}_i + \left(t_{\mathbf{k}i}^T\right)^* \, \hat{\mathrm{d}}_i^\dagger \hat{\mathrm{a}}_\mathbf{k} \right), \tag{2.7}$$

$$\hat{\mathcal{H}}_{mol-sub} = \sum_{\mathbf{k},i} \left(t_{\mathbf{k}i}^S \, \hat{\mathrm{c}}_\mathbf{k}^\dagger \hat{\mathrm{d}}_i + \left(t_{\mathbf{k}i}^S\right)^* \, \hat{\mathrm{d}}_i^\dagger \hat{\mathrm{c}}_\mathbf{k} \right). \tag{2.8}$$

Tunneling is realized by creating an electron in the molecule and annihilating one electron in the tip or the substrate, or by its inverse process. The coefficients $t_{\mathbf{k}i}^T$ and $t_{\mathbf{k}i}^S$ are called tunneling matrix elements and depend on the momentum of the electron in the tip or the substrate, respectively, and the orbital quantum number of the electron in the molecule.

2.2. STM tunneling matrix elements

The tunneling matrix elements (TMEs) $t_{\mathbf{k}i}^\eta$, with η denoting either substrate or tip, are of great importance to describe the transport properties of the STM setup. They are

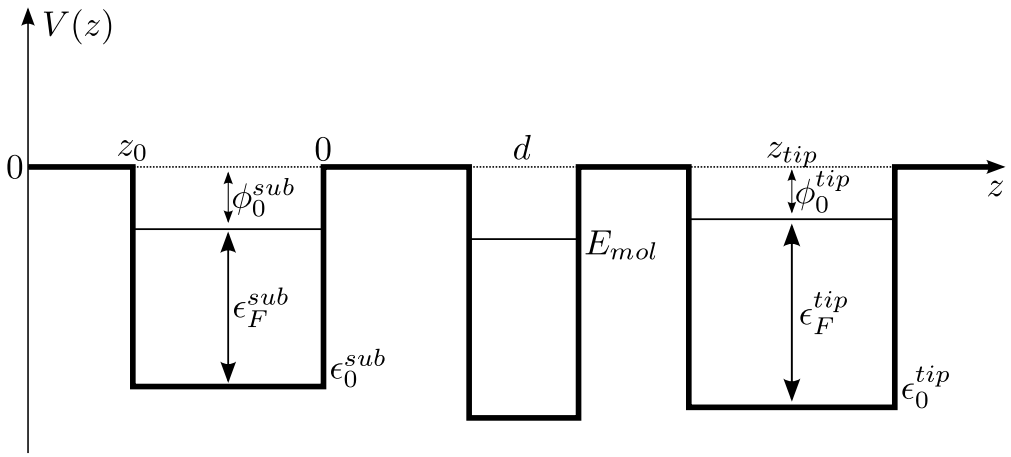

Figure 2.2.: *Potential for the STM setup.*

obtained by calculating the matrix elements of the underlying single particle Hamiltonians $\hat{h}_\eta$ between the eigenstates of the molecule and those of the substrate or tip, respectively. In both cases we have matrix elements of the form

$$t^{\eta}_{\mathbf{k}i} = \langle \eta\mathbf{k}| \hat{h}_\eta |i\rangle = \langle \eta\mathbf{k}| \hat{\mathrm{T}} + \hat{\mathrm{V}}_{mol} + \hat{\mathrm{V}}_\eta |i\rangle \,. \tag{2.9}$$

Here $|\eta\mathbf{k}\rangle$ and $|i\rangle$ are the eigenstates of the contact and molecule single particle Hamiltonians, $\hat{\mathrm{T}}$ is the kinetic term, $\hat{\mathrm{V}}_{mol}$ denotes the potential in the molecule and $\hat{\mathrm{V}}_\eta$ describes the potential in the region near the contact η. The form of the potential is shown in Fig. 2.2. On the one hand the wavefunctions of the molecule are decaying exponentially with the distance perpendicular to the molecular plane. On the other hand we assume, that $\hat{\mathrm{V}}_\eta$ is equal to zero in the regions between the molecule and the substrate and tip. Hence we are allowed to neglect the contribution of the last term $\langle \mathbf{k}| \hat{\mathrm{V}}_\eta |i\rangle$ and arrive at:

$$t^{\eta}_{\mathbf{k}i} = \langle \eta\mathbf{k}| \hat{\mathrm{T}} + \hat{\mathrm{V}}_{mol} |i\rangle = \langle \eta\mathbf{k}| \hat{h}_{mol} |i\rangle \,. \tag{2.10}$$

Since $|i\rangle$ is an eigenstate of the single particle Hamilton operator of the molecule with eigenenergy ϵ_i, Eq. (2.10) simplifies to:

$$t^{\eta}_{\mathbf{k}i} = \epsilon_i \langle \eta\mathbf{k}|i\rangle \,. \tag{2.11}$$

By using the fact that the molecular orbitals $|i\rangle$ are linear combinations of the atomic p_z orbitals $|\alpha\rangle$ with coefficients $c_{\alpha i}$ (see Sec. 4.1.1), the tunneling matrix elements are given by:

$$t^{\eta}_{\mathbf{k}i} = \epsilon_i \sum_\alpha c_{\alpha i} \langle \eta\mathbf{k}|\alpha\rangle \,. \tag{2.12}$$

In the following we will calculate the TMEs for the two different tunneling regions.

2.2.1. The substrate-molecule tunneling matrix elements

In a first step we calculate the wavefunctions of the electrons in the conduction band of the substrate. According to Fig. 2.2, in z-direction the electrons are bound to a finite potential well with energy at the bottom $\epsilon_0 < 0$. In x- and y-direction they behave like Bloch states with wavevectors k_x and k_y. In Fig. 2.2 we see that the Fermi energy of the electrons and the workfunction, which is the energy needed to remove an electron from the Fermi level of the conduction band, are connected to ϵ_0 via $\epsilon_0 + \epsilon_F + \phi_0 = 0$. The associated Schrödinger equation for an electron with energy $\epsilon_k = \epsilon_x + \epsilon_y + \epsilon_z + \epsilon_0$ then reads:

$$\begin{aligned}\left[\frac{\hat{\mathbf{p}}^2}{2m} + V(z)\right]\Psi(\vec{r}) &= \epsilon_{\mathbf{k}}\Psi(\vec{r}) \\ &= (\epsilon_0 + \epsilon_x + \epsilon_y + \epsilon_z)\Psi(\vec{r}),\end{aligned} \tag{2.13}$$

where $V(z)$ is given by

$$V(z) = \begin{cases} 0, & z < z_0 \\ \epsilon_0, & z_0 < z < 0 \\ 0, & z > 0 \end{cases}. \tag{2.14}$$

Using the separation ansatz $\Psi(\vec{r}) = \Psi(x)\Psi(y)\Psi(z)$, we can solve the Schrödinger equation to obtain the eigenstates of the substrate in x- and y-direction:

$$\Psi(x) = \frac{1}{\sqrt{L}}\, e^{-ik_x x} \tag{2.15}$$

$$\Psi(y) = \frac{1}{\sqrt{L}}\, e^{-ik_y y}, \tag{2.16}$$

Here $\frac{1}{\sqrt{L}}$ with $L^2 = S$ being the surface area of the substrate is the normalization factor for the wavefunctions. With the abbreviation $\xi = 1 + i\frac{\kappa}{k_z}$, the solution of the Schrödinger equation in the z-direction reads:

$$\Psi(z) = \Omega \begin{cases} -\sin(k_z z_0)\, \frac{\kappa^2 + k_z^2}{2\kappa k_z}\, e^{\kappa(z - z_0)} & z < z_0 \\ \frac{1}{2}\left(\xi e^{ik_z z} + \xi^* e^{-ik_z z}\right) & z_0 < z < 0 \\ e^{-\kappa z} & z > 0 \end{cases}. \tag{2.17}$$

For the wavevectors we have the relations

$$k_j = \sqrt{\frac{2m}{\hbar^2}\epsilon_j} \quad \text{with} \quad j = x, y, z \tag{2.18}$$

$$\kappa = \sqrt{\frac{2m}{\hbar^2}(\epsilon_F + \phi_0 - \epsilon_z)}. \tag{2.19}$$

Finally, the normalization factor Ω is given by:

$$\Omega = \sqrt{2\kappa}\left(1 - \kappa z_0\left(1+\frac{\kappa^2}{k_z^2}\right) + \frac{1}{2}\sin^2(k_z z_0)\left(1+\frac{k_z^2}{\kappa^2}\right)\left(1+\frac{\kappa^2}{k_z^2}\right)^2\right)^{-\frac{1}{2}}. \tag{2.20}$$

After calculating the eigenstates of the substrate, we have to specify the atomic orbitals of the molecule. We consider the p_z-orbitals for hydrogen-like atoms

$$p_z(\mathbf{r}-\mathbf{r}_\alpha) = \frac{1}{4\sqrt{2\pi}}\left(\frac{Q_\alpha}{a_0}\right)^{5/2}|\mathbf{r}-\mathbf{r}_\alpha|\cos(\vartheta)\, e^{-\frac{Q_\alpha}{2a_0}|\mathbf{r}-\mathbf{r}_\alpha|}, \tag{2.21}$$

where Q_α is the atomic number of the atom α located at $\mathbf{r}_\alpha = (x_\alpha, y_\alpha, d)^T$ and $a_0 \simeq 0.53\,\text{Å}$ is the Bohr radius. Then the overlap integral we have to calculate is:

$$\langle \mathbf{k}|\alpha\rangle = S^{-1/2}\int \mathrm{d}^3 r\, e^{-ik_x x}e^{-ik_y y}\,\Psi(z)p_z(\mathbf{r}-\mathbf{r}_\alpha). \tag{2.22}$$

The resulting tunneling matrix elements for the substrate region are ultimately given by:

$$t^S_{\mathbf{k}i} = \epsilon_i \sum_\alpha c_{\alpha i}\,\langle \mathbf{k}|\alpha\rangle = \epsilon_i \sum_\alpha c_{\alpha i} V_\alpha(k_z, k_\parallel, \kappa)\, e^{-i(k_x x_\alpha + k_y y_\alpha)}, \tag{2.23}$$

where the function $V_\alpha(k_z, k_\parallel, \kappa)$ condenses the results of the integration in Eq. (2.22). It depends on the type of atom α and on the k-vectors of the substrate wavefunction in z-direction, in the plane and in the region outside the substrate, respectively. As tunneling into the substrate represents a delocalized process, we have in Eq. (2.23) an exponential, whose phase contains the in-plane wavevectors. For the interested reader, an explicit derivation of Eq. (2.23) is given in App. A.2.

2.2.2. The tip-molecule tunneling matrix elements

Now we calculate the tunneling elements in the tip region. For sure, the easiest way to model the tip wavefunction would be the use of a delta function

$$\langle \mathbf{r} \mid \mathbf{k}\rangle = \mathcal{N}_\mathbf{k}\delta(\mathbf{r}-\mathbf{r}_{tip}), \tag{2.24}$$

where $\mathbf{r}_{tip}$ is the position of the apex of the tip and $\mathcal{N}_\mathbf{k}$ is a $\mathbf{k}$-dependent prefactor. Calculating the overlap integral with a p_z orbital of the molecule yields:

$$\langle \mathbf{k}|\alpha\rangle = \mathcal{N}_\mathbf{k}\, p_z(\mathbf{r}_{tip}-\mathbf{r}_\alpha). \tag{2.25}$$

Thus the tunneling matrix elements for delta-like tip wavefunctions read:

$$t^T_{\mathbf{k}i} = \epsilon_i \mathcal{N}_\mathbf{k} \sum_\alpha c_{\alpha i}\, p_z(\mathbf{r}_{tip}-\mathbf{r}_\alpha) = \epsilon_i \mathcal{N}_\mathbf{k}\psi_i(\mathbf{r}_{tip}). \tag{2.26}$$

Despite its simplicity, we will not use this approach, as it gives no information about the explicit form of the prefactor $\mathcal{N}_\mathbf{k}$. However, up to the prefactor, Eq. (2.26) coincides with

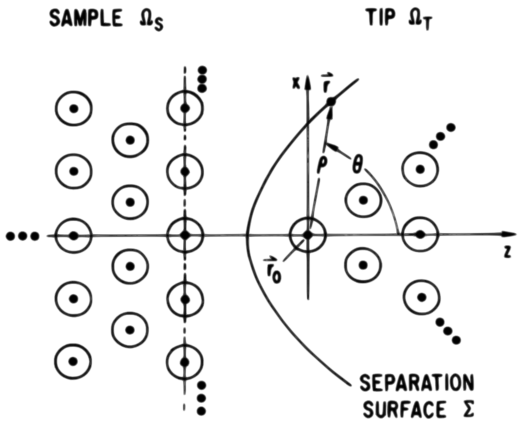

Figure 2.3.: *Geometrical situation for the calculation of the TMEs of the tip. Taken from [Che90].*

the result proposed by C. Julian Chen in [Che90], where Bessel functions are used to model the "tail" of the tip wavefunctions in the vacuum between the molecule and the tip. This approach does not care about the explicit form of the wavefunctions inside the tip but rather distinguishes between their different spatial orientations. For spherical symmetric, thus s-type tip wavefunctions the tunneling coefficients are predicted to be proportional to the wavefunctions of the sample evaluated at the position of the tip. In the following we will adapt this approach to our formalism. It is based on Bardeen's tunneling theory [Bar61], which assumes that a tunneling matrix element between two wavefunctions χ and ψ living in different regions can be represented by the following surface integral:

$$M = \frac{\hbar^2}{2m} \int_\Sigma \mathrm{d}\mathbf{S} \left(\chi \boldsymbol{\nabla} \psi - \psi \boldsymbol{\nabla} \chi\right). \tag{2.27}$$

Here Σ denotes the separation surface that isolates the two regions.

Modeling the tip states

Consider a tip wavefunction $\chi_{\mathbf{k}}(\mathbf{r})$ which is the solution of a Schrödinger equation for an electron with wavevector κ in the vacuum:

$$\left(\boldsymbol{\nabla}^2 - \boldsymbol{\kappa}^2\right) \chi_{\mathbf{k}}(\mathbf{r}) = 0. \tag{2.28}$$

Here $\kappa = \sqrt{\boldsymbol{\kappa}^2}$ is, in analogy to the calculations we have done for the substrate, given by

$$\kappa = \sqrt{\frac{2m}{\hbar^2}\left(\epsilon_F^{tip} + \phi_0^{tip} - \epsilon_{\mathbf{k}}\right)}. \tag{2.29}$$

Note that Eq. (2.28) is only valid for $\chi_{\mathbf{k}}(\mathbf{r})$ in the region that is lying to the left of the separation surface and on the separation surface itself, as depicted in Fig. 2.3. However, the chosen approach disregards the behavior of $\chi_{\mathbf{k}}(\mathbf{r})$ inside the separation surface Σ. One further assumption we have to make is that Eq. (2.28) is also valid for the sample

wavefunction on the separation surface and to the right of it. In the words of Julian Chen, the latter assumption is "valid by definition". The next step is to do a separation ansatz and to write $\chi_{\mathbf{k}}(\mathbf{r})$ in terms of an angular part given by spherical harmonics $Y_{lm}(\theta,\varphi)$ and a radial part $R_{lm}(\kappa\rho)$ with $\rho = |\mathbf{r} - \mathbf{r}_{tip}|$, where $\mathbf{r}_{tip}$ is the position of the apex of the tip:

$$\chi_{\mathbf{k}}(\mathbf{r}) = \sum_{l,m} \chi_{\mathbf{k}}^{lm}(\mathbf{r}) = \sum_{l,m} C_{lm} R_{lm}(\kappa\rho) Y_{lm}(\theta,\varphi). \tag{2.30}$$

The functions $Y_{lm}(\theta,\varphi)$ are solutions of the angular part of Eq. (2.28) per se, so we only have to care about its radial part. This reads:

$$\frac{\partial}{\partial\rho}\rho^2\frac{\partial}{\partial\rho} - l(l+1)R_{lm}(\kappa\rho) = \kappa^2\rho^2 R_{lm}(\kappa\rho). \tag{2.31}$$

We see that $R_{lm}(k\rho)$ does not depend on m and with the substitution $x = \kappa\rho$ we arrive at:

$$\frac{\partial}{\partial x}x^2\frac{\partial}{\partial x}R_l(x) - \left[x^2 + l(l+1)\right]R_l(x) = 0, \tag{2.32}$$

whose solutions are the modified spherical Bessel functions. Here we use the definition given in [Arf85], which is basically the same as in [AS72] up to the prefactor. As we are interested in solutions that do not diverge for large x, our functions of choice are the modified spherical Bessel functions of the third kind,

$$k_l(x) = \sqrt{\frac{2}{\pi x}}K_{l+\frac{1}{2}}(x). \tag{2.33}$$

They are defined by:

$$k_0(x) = \frac{e^{-x}}{x}, \tag{2.34}$$

$$k_{l+1}(x) = -x^l\frac{\mathrm{d}}{\mathrm{d}x}x^{-l}k_l(x), \tag{2.35}$$

and are subject to the following useful recurrence relations:

$$\frac{2l+1}{x}k_l(x) = k_{l+1}(x) - k_{l-1}(x) \tag{2.36}$$

$$(2l+1)\frac{\mathrm{d}k_l(x)}{\mathrm{d}x} = -(l+1)k_{l+1}(x) - l\,k_{l-1}(x). \tag{2.37}$$

For completeness we give $k_{1/2}(x)$ explicitly:

$$k_1(x) = \left(\frac{1}{x} + \frac{1}{x^2}\right)e^{-x}, \tag{2.38}$$

$$k_2(x) = \left(\frac{1}{x} + \frac{3}{x^2} + \frac{3}{x^3}\right)e^{-x}. \tag{2.39}$$

$l\|m\|$	Orientation	Wavefunction
00	s	$C_s\, k_0(\kappa\rho)$
10	p_z	$C_z\, k_1(\kappa\rho)\cos(\theta)$
11	p_x	$C_x\, k_1(\kappa\rho)\sin(\theta)\cos(\varphi)$
11	p_y	$C_y\, k_1(\kappa\rho)\sin(\theta)\sin(\varphi)$
20	d_{z^2}	$C_{z^2}\, k_2(\kappa\rho)(\cos^2(\theta) - \frac{1}{3})$
21	d_{xz}	$C_{xz}\, k_2(\kappa\rho)\sin(2\theta)\cos(\varphi)$
21	d_{yz}	$C_{yz}\, k_2(\kappa\rho)\sin(2\theta)\sin(\varphi)$
22	d_{xy}	$C_{xy}\, k_2(\kappa\rho)\sin^2(\theta)\sin(2\varphi)$
22	$d_{x^2-y^2}$	$C_{x^2-y^2}\, k_2(\kappa\rho)\sin^2(\theta)\cos(2\varphi)$

Table 2.1.: *The different tip states, depending on their orientations.*

Inserting Eq. (2.33) into Eq. (2.30) yields:

$$\chi_{\mathbf{k}}(\mathbf{r}) = \sum_{l,\,m} \chi_{\mathbf{k}}^{lm}(\mathbf{r}) = \sum_{l,\,m} C_{lm} k_l(\kappa\rho) Y_{lm}(\theta,\varphi). \tag{2.40}$$

The factors C_{lm}, depending on the electronic configuration of the tip material, have to be chosen in a way that $\chi_{\mathbf{k}}(\mathbf{r})$ is normalized. In Tab. 2.1 all tip states up to $l = 2$ are listed, where we put the spherical harmonics for $m \neq 0$ in their real representation by taking linear combinations of the following form:

$$\frac{1}{\sqrt{2}}\left(Y_{lm} + (-1)^m Y_{l,-m}\right) \qquad \text{for} \quad m > 0, \tag{2.41}$$

$$\frac{1}{i\sqrt{2}}\left(Y_{l,-m} - (-1)^m Y_{lm}\right) \qquad \text{for} \quad m < 0. \tag{2.42}$$

From now on we will label our functions by their spatial orientations instead of the two indices l and m. For example $\chi_{\mathbf{k}}^{z}$ is equivalent to $\chi_{\mathbf{k}}^{10}$. As more convenient for the later calculations, we now calculate the Green's function for the problem. The differential equation the Green's function reads:

$$\left(\nabla^2 - \kappa^2\right) G(\mathbf{r} - \mathbf{r}_{tip}) = -\delta(\mathbf{r} - \mathbf{r}_{tip}). \tag{2.43}$$

After transforming Eq. (2.43) into momentum space, we are directly able to write down $G(\mathbf{q})$:

$$G(\mathbf{q}) = \frac{1}{q^2 + \kappa^2}. \tag{2.44}$$

Now we only have to do one more Fourier transform to obtain $G(\mathbf{r} - \mathbf{r}_{tip})$. We immediately see that it is proportional to $k_0(\kappa|\mathbf{r} - \mathbf{r}_{tip}|)$:

$$G(\mathbf{r} - \mathbf{r}_{tip}) = \frac{e^{-\kappa|\mathbf{r}-\mathbf{r}_{tip}|}}{4\pi|\mathbf{r} - \mathbf{r}_{tip}|} = \frac{\kappa}{4\pi} k_0(\kappa|\mathbf{r} - \mathbf{r}_{tip}|). \tag{2.45}$$

This means the s-wave tip state $\chi^s_{\mathbf{k}}$ can be represented through the Green's function:

$$\chi^s_{\mathbf{k}}(\mathbf{r}) = \frac{4\pi C_s}{\kappa} G(\mathbf{r} - \mathbf{r}_{tip}). \tag{2.46}$$

However, not only the s-wave tip wavefunction, but all other tip wavefunctions can be related to the Green's function $G(\mathbf{r} - \mathbf{r}_{tip})$. This we will demonstrate first for the p_z-type tip state. We start by differentiating Eq. (2.45) with respect to z_{tip}:

$$\frac{\partial}{\partial z_{tip}} G(\mathbf{r} - \mathbf{r}_{tip}) = \frac{\kappa}{4\pi} \frac{\partial}{\partial z_{tip}} k_0(\kappa\rho) = \frac{\kappa^2}{4\pi} \frac{\partial k_0(\kappa\rho)}{\partial(\kappa\rho)} \frac{\partial \rho}{\partial z_{tip}}. \tag{2.47}$$

If we exploit the fact that $\frac{\mathrm{d}k_0(x)}{\mathrm{d}x} = -k_1(x)$ and, according to Fig. 2.3, notice that

$$\frac{\partial \rho}{\partial z_{tip}} = -\frac{z - z_{tip}}{\rho} = -\cos(\theta), \tag{2.48}$$

we get for the derivative of $G(\mathbf{r} - \mathbf{r}_{tip})$ with respect to z_{tip}:

$$\frac{\partial}{\partial z_{tip}} G(\mathbf{r} - \mathbf{r}_{tip}) = \frac{\kappa^2}{4\pi} \cos(\theta) k_1(\kappa\rho), \tag{2.49}$$

which is proportional to the p_z tip wavefunction $\chi^z_{\mathbf{k}}$. As it holds that

$$\frac{\partial \rho}{\partial x_{tip}} = -\sin(\theta)\cos(\varphi) \qquad \text{and} \qquad \frac{\partial \rho}{\partial y_{tip}} = -\sin(\theta)\sin(\varphi), \tag{2.50}$$

we are immediately able give the tip states for $l = 1$ in terms of derivatives of the Greens's function:

$$\chi^x_{\mathbf{k}}(\mathbf{r}) = \frac{4\pi C_x}{\kappa^2} \frac{\partial}{\partial x_{tip}} G(\mathbf{r} - \mathbf{r}_{tip}) \tag{2.51}$$

$$\chi^y_{\mathbf{k}}(\mathbf{r}) = \frac{4\pi C_y}{\kappa^2} \frac{\partial}{\partial y_{tip}} G(\mathbf{r} - \mathbf{r}_{tip}) \tag{2.52}$$

$$\chi^z_{\mathbf{k}}(\mathbf{r}) = \frac{4\pi C_z}{\kappa^2} \frac{\partial}{\partial z_{tip}} G(\mathbf{r} - \mathbf{r}_{tip}). \tag{2.53}$$

The tip wavefunctions for $l = 2$ can be generated by further differentiating the above equations with respect to other components of $\mathbf{r}_{tip}$. As an example, if we want to calculate the tip state $\chi^{z^2}_k(\mathbf{r})$, in a first step we have to pick up Eq. (2.49) and take the derivative with respect to z_{tip} on both sides of it:

$$\frac{\partial^2}{\partial z^2_{tip}} G(\mathbf{r} - \mathbf{r}_{tip}) = \frac{\kappa^2}{4\pi} \frac{\partial}{\partial z_{tip}} \left(\cos(\theta) k_1(\kappa\rho)\right). \tag{2.54}$$

Notice that $\cos(\theta)$ also depends on z_{tip}. Using Eq. (2.48), we get for the derivative of the cosine:

$$\frac{\partial}{\partial z_{tip}} \cos(\theta) = \frac{1}{\rho} \left(\cos^2(\theta) - 1 \right). \tag{2.55}$$

The chain rule and Eq. (2.37) tells us that

$$\frac{\partial}{\partial z_{tip}} k_1(\kappa\rho) = \frac{1}{3} \kappa \cos(\theta) \left(2k_2(\kappa\rho) + k_0(\kappa\rho) \right). \tag{2.56}$$

Collecting the results, we obtain

$$\frac{\partial^2}{\partial z_{tip}^2} G(\mathbf{r} - \mathbf{r}_{tip}) = \frac{\kappa^3}{4\pi} \left[\left(\cos^2(\theta) - 1 \right) \frac{k_1(\kappa\rho)}{\kappa\rho} + \frac{1}{3} \cos^2(\theta) \left(2k_2(\kappa\rho) + k_0(\kappa\rho) \right) \right]. \tag{2.57}$$

Now we only have to use the recurrence relation Eq. (2.37) and to remind the definition of the Green's function Eq. (2.45) and the form of the d_{z^2} tip wavefunction (see Tab. 2.1) to finally relate $\chi_{\mathbf{k}}^{z^2}(\mathbf{r})$ to $G(\mathbf{r} - \mathbf{r}_{tip})$ and its second derivative:

$$\chi_{\mathbf{k}}^{z^2}(\mathbf{r}) = \frac{4\pi C_{z^2}}{\kappa^3} \left(\frac{\partial^2}{\partial z_{tip}^2} G(\mathbf{r} - \mathbf{r}_{tip}) - \frac{1}{3} \kappa^2 G(\mathbf{r} - \mathbf{r}_{tip}) \right). \tag{2.58}$$

In the next part of this section we will see why we put such great effort to model the various tip states by using the Green's function and its derivatives.

Calculation of the tunneling matrix elements

To actually calculate the tunneling matrix elements, we have to evaluate Eq. (2.27). As a first example we will do this for a s-wave tip state. Consequently, the according tunneling matrix element $M_{\mathbf{k}i}^s$ reads:

$$M_{\mathbf{k}i}^s = \frac{\hbar^2}{2m} \int_\Sigma \mathrm{d}\mathbf{S} \left(\chi_k^s(\mathbf{r}) \boldsymbol{\nabla} \psi_i(\mathbf{r}) - \psi_i(\mathbf{r}) \boldsymbol{\nabla} \chi_{\mathbf{k}}^s(\mathbf{r}) \right). \tag{2.59}$$

Inserting Eq. (2.46) we get:

$$M_{\mathbf{k}i}^s = \frac{2\pi\hbar^2 C_s}{m\kappa} \int_\Sigma \mathrm{d}\mathbf{S} \left(G(\mathbf{r} - \mathbf{r}_{tip}) \boldsymbol{\nabla} \psi_i(\mathbf{r}) - \psi_i(\mathbf{r}) \boldsymbol{\nabla} G(\mathbf{r} - \mathbf{r}_{tip}) \right). \tag{2.60}$$

Using one of Green's theorems,

$$\int_{\partial\Omega} \mathrm{d}\mathbf{S}\, \mathbf{F} = \int_\Omega \mathrm{d}V\, \boldsymbol{\nabla}\mathbf{F}, \tag{2.61}$$

we can convert our integral into a volume integral over Ω_{tip} that is enclosed by the separation surface:

$$M_{\mathbf{k}i}^s = \frac{2\pi\hbar^2 C_s}{m\kappa} \int_{\Omega_{tip}} \mathrm{d}^3 r \left(G(\mathbf{r} - \mathbf{r}_{tip}) \boldsymbol{\nabla}^2 \psi_i(\mathbf{r}) - \psi_i(\mathbf{r}) \boldsymbol{\nabla}^2 G(\mathbf{r} - \mathbf{r}_{tip}) \right). \tag{2.62}$$

tip state	t. matrix element	tip state	t. matrix element
s	$\frac{2\pi\hbar^2 C_s}{m\kappa}\ \psi(\mathbf{r}_{tip})$	d_{z^2}	$\frac{2\pi\hbar^2 C_{z^2}}{m\kappa^3}\left(\frac{\partial^2}{\partial z_{tip}^2}-\frac{1}{3}\kappa^2\right)\psi(\mathbf{r}_{tip})$
p_z	$\frac{2\pi\hbar^2 C_z}{m\kappa^2}\ \frac{\partial}{\partial z_{tip}}\psi(\mathbf{r}_{tip})$	d_{xz}	$\frac{2\pi\hbar^2 C_{xz}}{m\kappa^3}\ \frac{\partial^2}{\partial x_{tip}\partial z_{tip}}\psi(\mathbf{r}_{tip})$
p_x	$\frac{2\pi\hbar^2 C_x}{m\kappa^2}\ \frac{\partial}{\partial x_{tip}}\psi(\mathbf{r}_{tip})$	d_{yz}	$\frac{2\pi\hbar^2 C_{yz}}{m\kappa^3}\ \frac{\partial^2}{\partial y_{tip}\partial z_{tip}}\psi(\mathbf{r}_{tip})$
p_y	$\frac{2\pi\hbar^2 C_y}{m\kappa^2}\ \frac{\partial}{\partial y_{tip}}\psi(\mathbf{r}_{tip})$	$d_{x^2-y^2}$	$\frac{2\pi\hbar^2 C_{x^2-y^2}}{m\kappa^3}\left(\frac{\partial^2}{\partial x_{tip}^2}-\frac{\partial^2}{\partial y_{tip}^2}\right)\psi(\mathbf{r}_{tip})$

Table 2.2.: *Tunneling matrix elements for the tip up to second order in l.*

Now we have to make use of Eq. (2.43) and claim that ψ_i fulfills Eq. (2.28) to obtain:

$$M^s_{\mathbf{k}i} = \frac{2\pi\hbar^2 C_s}{m\kappa}\int_{\Omega_{tip}} \mathrm{d}^3 r\Big(G(\mathbf{r}-\mathbf{r}_{tip})\kappa^2\psi_i(\mathbf{r}) - \psi_i(\mathbf{r})\big[-\delta(\mathbf{r}-\mathbf{r}_{tip})+\kappa^2 G(\mathbf{r}-\mathbf{r}_{tip})\big]\Big). \quad (2.63)$$

This integral can be solved easily, yielding:

$$M^s_{\mathbf{k}i} = \frac{2\pi\hbar^2 C_s}{m\kappa}\,\psi_i(\mathbf{r}_{tip}) = \frac{2\pi\hbar^2 C_s}{m\kappa}\sum_\alpha c_{\alpha i}\, p_z(\mathbf{r}_{tip}-\mathbf{r}_\alpha), \quad (2.64)$$

where we already inserted the explicit form of the sample wavefunction. The tunneling matrix element for a p_z-oriented tip state can be gained with a similar calculation. As above, we obtain for $M^z_{\mathbf{k}i}$:

$$M^z_{\mathbf{k}i} = \frac{2\pi\hbar^2 C_z}{m\kappa^2}\int_\Sigma \mathrm{d}\mathbf{S}\left(\frac{\partial}{\partial z_{tip}}G(\mathbf{r}-\mathbf{r}_{tip})\boldsymbol{\nabla}\psi_i(\mathbf{r}) - \psi_i(\mathbf{r})\boldsymbol{\nabla}\frac{\partial}{\partial z_{tip}}G(\mathbf{r}-\mathbf{r}_{tip})\right). \quad (2.65)$$

Only the Green's function depends on z_{tip}, so we can put the partial derivative out of it. After applying Green's theorem, we are left with the same integral as in the s-wave case:

$$M^z_{\mathbf{k}i} = \frac{2\pi\hbar^2 C_z}{m\kappa^2}\frac{\partial}{\partial z_{tip}}\int_{\Omega_{tip}} \mathrm{d}^3 r\left(G(\mathbf{r}-\mathbf{r}_{tip})\boldsymbol{\nabla}^2\psi_i(\mathbf{r}) - \psi_i(\mathbf{r})\boldsymbol{\nabla}^2 G(\mathbf{r}-\mathbf{r}_{tip})\right) \quad (2.66)$$

$$= \frac{2\pi\hbar^2 C_z}{m\kappa^2}\frac{\partial}{\partial z_{tip}}\psi_i(\mathbf{r}_{tip}). \quad (2.67)$$

In the same way, we get for the TME of a d_{z^2}-oriented tip state:

$$M^{z^2}_{\mathbf{k}i} = \frac{2\pi\hbar^2 C_z}{m\kappa^3}\int_\Sigma \mathrm{d}\mathbf{S}\Big(\left[\frac{\partial^2}{\partial z_{tip}^2}-\frac{1}{3}\kappa^2\right]G\,\boldsymbol{\nabla}\psi_i - \psi_i\boldsymbol{\nabla}\left[\frac{\partial^2}{\partial z_{tip}^2}-\frac{1}{3}\kappa^2\right]G\Big). \quad (2.68)$$

For brevity, we left out the arguments of the functions. Notice that, still, the only term that depends on z_{tip} is the Green's function. Performing the same steps as before it takes minimal effort to arrive at

$$M_{\mathbf{k}i}^{z^2} = \frac{2\pi\hbar^2 C_z}{m\kappa^3}\left(\frac{\partial^2}{\partial z_{tip}^2}\int_{\Omega_{tip}} \mathrm{d}^3 r\, \psi_i(\mathbf{r})\delta(\mathbf{r}-\mathbf{r}_{tip}) - \frac{1}{3}\kappa^2 \int_{\Omega_{tip}} \mathrm{d}^3 r\, \psi_i(\mathbf{r})\delta(\mathbf{r}-\mathbf{r}_{tip})\right), \quad (2.69)$$

which yields for the tunneling matrix element of a d_{z^2}-oriented tip state:

$$M_{\mathbf{k}i}^{z^2} = \frac{2\pi\hbar^2 C_z}{m\kappa^3}\left(\frac{\partial^2}{\partial z_{tip}^2}\psi_i(\mathbf{r}_{tip}) - \frac{1}{3}\kappa^2\psi_i(\mathbf{r}_{tip})\right). \quad (2.70)$$

With this result we can construct the tunneling matrix element $t_{\mathbf{k}i}^T$ for the tip by summing up the various matrix elements $M_{\mathbf{k}i}^{\xi}$ with $\xi \in \{s,\, x,\, y,\, z,\, z^2,\, xz,\, yz,\, x^2-y^2\}$:

$$t_{\mathbf{k}i}^T = \sum_{\xi} M_{\mathbf{k}i}^{\xi}. \quad (2.71)$$

A complete list of them up to second order of l is given in Tab. (2.2). The composition of the tip state regarding its different spatial orientations is then determined through the choice of the prefactors C_ξ. A proof for the consistency of this approach with Eq. (2.12) is given in [Rei95].

3. Transport in an STM setup

In order to calculate the current through our system, we have to evaluate the expectation value of the current operator $\hat{I}$. This is related to the time derivative of the expectation value of the total charge in the system:

$$\langle \hat{I} \rangle = \frac{\mathrm{d}}{\mathrm{d}t} \langle \hat{Q} \rangle = e \frac{\mathrm{d}}{\mathrm{d}t} \langle \hat{N} \rangle = e \frac{\mathrm{d}}{\mathrm{d}t} \, \mathrm{tr}_{mol} \left\{ \hat{N} \hat{\rho}^S_{red} \right\}. \tag{3.1}$$

Here $\hat{N}$ is the particle number operator in the sample and tr_{mol} denotes the trace over the eigenstates of the molecule. The quantity $\hat{\rho}^S_{red}$ is the reduced density matrix of our system in the Schrödinger picture. As $\hat{N} = \sum_i \hat{\mathrm{d}}^\dagger_i \hat{\mathrm{d}}_i$ does not depend on time, we can write Eq. (3.1) as:

$$\langle \hat{I} \rangle = e \, \mathrm{tr}_{mol} \left\{ \hat{N} \dot{\hat{\rho}}^S_{red} \right\} = \mathrm{tr}_{mol} \left\{ \hat{I} \hat{\rho}^S_{red} \right\}. \tag{3.2}$$

We can write the expectation value $\langle \hat{I} \rangle$ as a sum of the currents through the substrate and the tip,

$$\langle \hat{I} \rangle = \langle \hat{I}_{sub} + \hat{I}_{tip} \rangle \, , \tag{3.3}$$

and use the convention that the current is positive when increasing the number of particles. Therefore, the net current through the sample is zero in the stationary limit $t \to \infty$. The stationary current in the substrate or in the tip is then given by:

$$I^{stat}_\eta = \mathrm{tr}_{mol} \left\{ \hat{I}_\eta \rho^{stat}_{red} \right\} = -I^{stat}_{\bar{\eta}}, \tag{3.4}$$

with $\eta = sub, tip$. Hence we have to find an expression for the time evolution of the reduced density matrix of the system and evaluate it in the stationary limit. On the other hand we need also an expression for the current operator $\hat{I}_\eta$.

3.1. The Generalized Master Equation for the reduced density matrix

In this section we express the time evolution of the reduced density matrix of our system in terms of a generalized master equation (GME), following [Blu96, DBDG09]. The calculations are performed in the interaction picture. Here we treat $\hat{\mathcal{H}}_T$ as a perturbation, while the intrinsic time dependence of the system comes from $\hat{\mathcal{H}}_0 \equiv \hat{\mathcal{H}}_{mol} + \hat{\mathcal{H}}_{tip} + \hat{\mathcal{H}}_{sub}$. States and operators are transformed into the interaction picture by:

$$|\psi_I(t)\rangle = e^{\frac{i}{\hbar}\hat{\mathcal{H}}_0 t}\,|\psi(t)\rangle\,, \tag{3.5}$$

$$\hat{\mathrm{O}}_I(t) = e^{\frac{i}{\hbar}\hat{\mathcal{H}}_0 t}\,\hat{\mathrm{O}}\,e^{-\frac{i}{\hbar}\hat{\mathcal{H}}_0 t}. \tag{3.6}$$

We start with the density matrix $\hat{\rho}^I(t)$ of the whole system in the interaction picture. To evolve $\hat{\rho}^I(t)$ from t_0 to t we need to evaluate

$$\hat{\rho}^I(t) = \hat{U}_I(t,t_0)\,\hat{\rho}^I(t_0)\,\hat{U}_I^\dagger(t,t_0). \tag{3.7}$$

The time evolution operator in the interaction picture for our problem is defined by the following equation:

$$\begin{aligned}\hat{U}_I(t,t_0) &= \hat{U}_0^\dagger(t,t_0)\,\hat{U}(t,t_0)\\ &= e^{\frac{i}{\hbar}\hat{\mathcal{H}}_0(t-t_0)}\,e^{-\frac{i}{\hbar}(\hat{\mathcal{H}}_0+\hat{\mathcal{H}}_T)(t-t_0)}.\end{aligned} \tag{3.8}$$

For the time derivative of $\hat{U}_I(t,t_0)$ we get:

$$i\hbar\frac{\partial}{\partial t}\hat{U}_I(t,t_0) = \hat{\mathcal{H}}_T^I(t)\hat{U}_I(t,t_0). \tag{3.9}$$

This yields the following differential equation describing the time evolution of the density matrix in the interaction picture:

$$i\hbar\,\frac{\mathrm{d}\hat{\rho}^I(t)}{\mathrm{d}t} = [\hat{\mathcal{H}}_T^I(t),\,\hat{\rho}^I(t)]. \tag{3.10}$$

The formal solution of Eq. (3.10) is:

$$\hat{\rho}^I(t) = \hat{\rho}^I(t_0) - \frac{i}{\hbar}\int_{t_0}^{t}\mathrm{d}t_1\,[\hat{\mathcal{H}}_T^I(t_1),\,\hat{\rho}^I(t_1)]. \tag{3.11}$$

Reinserting Eq. (3.11) into Eq. (3.10) we obtain:

$$\dot{\hat{\rho}}^I(t) = -\frac{i}{\hbar}\,[\hat{\mathcal{H}}_T^I(t),\,\hat{\rho}^I(t_0)] + \left(\frac{i}{\hbar}\right)^2\int_{t_0}^{t}\mathrm{d}t_1\,\left[\hat{\mathcal{H}}_T^I(t),\,[\hat{\mathcal{H}}_T^I(t_1),\,\hat{\rho}^I(t_1)]\right]. \tag{3.12}$$

We trace out the substrate and tip degrees of freedom to obtain the reduced density matrix (RDM) that describes only the dynamics of the molecule:

$$\hat{\rho}_{red}^I(t) = \mathrm{tr}_{sub,\,tip}\left\{\hat{\rho}^I(t)\right\}, \tag{3.13}$$

$$\begin{aligned}\dot{\hat{\rho}}_{red}^I(t) = &-\frac{i}{\hbar}\,\mathrm{tr}_{sub,\,tip}\left\{[\hat{\mathcal{H}}_T^I(t),\,\hat{\rho}^I(t_0)]\right\}\\ &+\left(\frac{i}{\hbar}\right)^2\int_{t_0}^{t}\mathrm{d}t_1\,\mathrm{tr}_{sub,\,tip}\left\{\left[\hat{\mathcal{H}}_T^I(t),\,[\hat{\mathcal{H}}_T^I(t_1),\,\hat{\rho}^I(t_1)]\right]\right\}.\end{aligned} \tag{3.14}$$

If we assume the molecule to be uncorrelated with the contacts initially ($t = t_0$) we can factorize the density matrix at $t = t_0$:

$$\hat{\rho}^I(t_0) = \hat{\rho}^I_{red}(t_0)\hat{\rho}_{tip}(t_0)\hat{\rho}_{sub}(t_0), \tag{3.15}$$

Assuming that the substrate and the tip subsystems behave like large thermal reservoirs, their density matrices at time t_0 are described by equilibrium density operators:

$$\hat{\rho}_{sub/tip}(t_0) \equiv \hat{\rho}_{sub/tip} = \frac{e^{-\beta(\hat{\mathcal{H}}_{sub/tip} - \mu_{sub/tip}\hat{N}_{sub/tip})}}{Z_{sub/tip}}. \tag{3.16}$$

If we now consider the coupling between the molecule and the contacts to be weak, the interaction between the subsystems will only have very small influence on the contacts, so that they stay in thermal equilibrium. Therefore the total density matrix at time t can be approximated by

$$\hat{\rho}^I(t) = \hat{\rho}^I_{red}(t)\hat{\rho}_{tip}\hat{\rho}_{sub} + \Delta\rho, \tag{3.17}$$

with $\Delta\rho = \mathcal{O}(\hat{\mathcal{H}}_T)$. Inserting it into Eq. (3.14) yields:

$$\begin{aligned}\dot{\hat{\rho}}^I_{red}(t) = &-\frac{i}{\hbar}\,\mathrm{tr}_{sub,\,tip}\left\{[\hat{\mathcal{H}}^I_T(t),\ \hat{\rho}^I_{red}(t_0)\hat{\rho}_{tip}\hat{\rho}_{sub}]\right\} \\ &-\frac{1}{\hbar^2}\int_{t_0}^{t}\mathrm{d}t_1\ \mathrm{tr}_{sub,\,tip}\left\{\left[\hat{\mathcal{H}}^I_T(t),\,[\hat{\mathcal{H}}^I_T(t_1),\,\hat{\rho}^I_{red}(t_1)\hat{\rho}_{tip}\hat{\rho}_{sub}]\right]\right\},\end{aligned} \tag{3.18}$$

where we performed a Born-approximation and dropped the $\Delta\rho$ terms as they contribute in $\mathcal{O}(\hat{\mathcal{H}}^3_T)$. The first term in this equation vanishes because it contains matrix elements of single annihilation and creation operators. As the trace implies that

$$\mathrm{tr}_{sub/tip}\left\{\hat{\rho}_{sub/tip}\hat{\mathrm{O}}\right\} = \langle\hat{\mathrm{O}}\rangle\,, \tag{3.19}$$

for any arbitrary quantum mechanical operator $\hat{\mathrm{O}}$, the matrix elements that stem from the first term are zero because they do not conserve the particle number:

$$\mathrm{tr}_{sub}\left\{\rho_{sub}\,\hat{\mathrm{c}}^\dagger_k\right\} = \mathrm{tr}_{sub}\left\{\hat{\rho}_{sub}\,\hat{\mathrm{c}}_k\right\} = 0, \tag{3.20}$$

$$\mathrm{tr}_{tip}\left\{\rho_{tip}\,\hat{\mathrm{a}}^\dagger_k\right\} = \mathrm{tr}_{tip}\left\{\hat{\rho}_{tip}\,\hat{\mathrm{a}}_k\right\} = 0. \tag{3.21}$$

The equation for $\dot{\hat{\rho}}^I_{red}$ then reduces to:

$$\dot{\hat{\rho}}^I_{red}(t) = -\frac{1}{\hbar^2}\int_{t_0}^{t}\mathrm{d}t_1\ \mathrm{tr}_{sub,\,tip}\left\{\left[\hat{\mathcal{H}}^I_T(t),\,[\hat{\mathcal{H}}^I_T(t_1),\,\hat{\rho}^I_{red}(t_1)\hat{\rho}_{tip}\hat{\rho}_{sub}]\right]\right\}. \tag{3.22}$$

As $\dot{\hat{\rho}}^I_{red}(t)$ depends on time t_1 with $t_0 \le t_1 \le t$ in the above equation, the latter is nonlocal in time and thus very difficult to calculate. However, products of $\hat{\mathcal{H}}^I_T(t)$ and $\hat{\mathcal{H}}^I_T(t_1)$

imply expectation values of creation and annihilation operators of the tip and substrate at different times. They decay much faster than the characteristic timescale of the subsystem of the molecule, thus the latter will not notice such rapid changes [Blu96]. This means we can change $\hat{\rho}^I_{red}(t_1)$ to $\hat{\rho}^I_{red}(t)$ in Eq. (3.22):

$$\dot{\hat{\rho}}^I_{red}(t) = -\frac{1}{\hbar^2}\int_{t_0}^{t} \mathrm{d}t_1 \ \mathrm{tr}_{sub,tip}\left\{ \left[\hat{\mathcal{H}}^I_T(t), \left[\hat{\mathcal{H}}^I_T(t_1), \hat{\rho}^I_{red}(t)\hat{\rho}_{tip}\hat{\rho}_{sub}\right]\right] \right\}. \tag{3.23}$$

Notice that even within this approximation, in the stationary limit, where t goes to infinity, we regain an exact solution. The next step is to perform a variable transformation $t_1 = t - t_2$. As we are interested in the dynamics of the system for $t \gg t_0$, we set $t_0 \to \infty$. Execution of the traces and resolving the time dependence of $\hat{\mathcal{H}}^I_T(t)$ in Eq. (3.23) yields:

$$\begin{aligned}
\dot{\hat{\rho}}^I_{red}(t) = -\frac{1}{\hbar^2}\int_0^\infty \mathrm{d}t_2 \sum_{\mathbf{k}}\sum_{i,j}\sum_{\eta}\Big[& \\
& + t^\eta_{\mathbf{k}i}(t^\eta_{\mathbf{k}j})^*\, f^+_\eta(\epsilon_{\mathbf{k}})\ \hat{\mathrm{d}}_i(t)\hat{\mathrm{d}}^\dagger_j(t-t_2)\,\hat{\rho}^I_{red}(t)\, e^{\frac{i}{\hbar}\epsilon_{\mathbf{k}}t_2} \\
& + (t^\eta_{\mathbf{k}i})^* t^\eta_{\mathbf{k}j}\, f^-_\eta(\epsilon_{\mathbf{k}})\ \hat{\mathrm{d}}^\dagger_i(t)\hat{\mathrm{d}}_j(t-t_2)\,\hat{\rho}^I_{red}(t)\, e^{-\frac{i}{\hbar}\epsilon_{\mathbf{k}}t_2} \\
& + t^\eta_{\mathbf{k}i}(t^\eta_{\mathbf{k}j})^*\,\hat{\rho}^I_{red}(t)\, f^+_\eta(\epsilon_{\mathbf{k}})\ \hat{\mathrm{d}}_i(t-t_2)\hat{\mathrm{d}}^\dagger_j(t)\, e^{-\frac{i}{\hbar}\epsilon_{\mathbf{k}}t_2} \\
& + (t^\eta_{\mathbf{k}i})^* t^\eta_{\mathbf{k}j}\,\hat{\rho}^I_{red}(t)\, f^-_\eta(\epsilon_{\mathbf{k}})\ \hat{\mathrm{d}}^\dagger_i(t-t_2)\hat{\mathrm{d}}_j(t)\, e^{\frac{i}{\hbar}\epsilon_{\mathbf{k}}t_2} \\
& - t^\eta_{\mathbf{k}i}(t^\eta_{\mathbf{k}j})^*\, f^-_\eta(\epsilon_{\mathbf{k}})\ \hat{\mathrm{d}}_i(t)\hat{\rho}^I_{red}(t)\hat{\mathrm{d}}^\dagger_j(t-t_2)\, e^{\frac{i}{\hbar}\epsilon_{\mathbf{k}}t_2} \\
& - (t^\eta_{\mathbf{k}i})^* t^\eta_{\mathbf{k}j}\, f^+_\eta(\epsilon_{\mathbf{k}})\ \hat{\mathrm{d}}^\dagger_i(t)\hat{\rho}^I_{red}(t)\hat{\mathrm{d}}_j(t-t_2)\, e^{-\frac{i}{\hbar}\epsilon_{\mathbf{k}}t_2} \\
& - t^\eta_{\mathbf{k}i}(t^\eta_{\mathbf{k}j})^*\, f^-_\eta(\epsilon_{\mathbf{k}})\ \hat{\mathrm{d}}_i(t-t_2)\hat{\rho}^I_{red}(t-t_2)\hat{\mathrm{d}}^\dagger_j(t)\, e^{-\frac{i}{\hbar}\epsilon_{\mathbf{k}}t_2} \\
& - (t^\eta_{\mathbf{k}i})^* t^\eta_{\mathbf{k}j}\, f^+_\eta(\epsilon_{\mathbf{k}})\ \hat{\mathrm{d}}^\dagger_i(t-t_2)\hat{\rho}^I_{red}(t-t_2)\hat{\mathrm{d}}_j(t)\, e^{\frac{i}{\hbar}\epsilon_{\mathbf{k}}t_2}\Big].
\end{aligned} \tag{3.24}$$

Here $f^+_\eta(\epsilon_{\mathbf{k}})$, with η denoting either *sub* or *tip*, is the Fermi distribution of an electron with chemical potential μ_η in the substrate or tip respectively:

$$f^+_\eta(\epsilon_{\mathbf{k}}) = f(\epsilon_{\mathbf{k}} - \mu_\eta), \tag{3.25}$$

$$f^-_\eta(\epsilon_{\mathbf{k}}) = 1 - f^+_\eta(\epsilon_{\mathbf{k}}), \tag{3.26}$$

with

$$f(E) = \frac{1}{1 + \exp\left(\frac{E}{k_B T}\right)}. \tag{3.27}$$

For the calculations that we have left out, see App. A.1.1 and App. A.1.2. Now we transform Eq. (3.24) back into the Schrödinger picture (see App. A.1.3). After that, we project the reduced density matrix onto the subspace of particle number N and energy

E, in which it has block-diagonal form. This is done by using the projection operator $\hat{\mathcal{P}}_{\mathrm{NE}} = \sum_l |\mathrm{N\,E}\, l\rangle \langle \mathrm{N\,E}\, l|$, where the index l denotes orbitally degenerate states. For a more detailed description of the properties and the application of the operator $\hat{\mathcal{P}}_{\mathrm{NE}}$ see App. (A.1.4). Having the GME in the basis of the energy and the particle number, we are able to perform the time integrations. They are all of the form $\int_0^\infty \mathrm{d}t\, e^{\frac{i}{\hbar}Xt}$ and can be calculated rather easily by including a small convergence factor λ to avoid divergences at $t \to \infty$:

$$\int_0^\infty \mathrm{d}t\, e^{\frac{i}{\hbar}Xt} = \lim_{\lambda\to 0} \int_0^\infty \mathrm{d}t\, e^{\frac{i}{\hbar}(X+i\lambda)t} \tag{3.28}$$

$$= \lim_{\lambda\to 0} \left(\frac{\hbar\lambda}{X^2+\lambda^2} + \frac{i\hbar X}{X^2+\lambda^2} \right). \tag{3.29}$$

This result is, in accordance to the Sokhatsky–Weierstrass theorem and the definition of the delta distribution, equivalent to

$$\int_0^\infty \mathrm{d}t\, e^{\frac{i}{\hbar}Xt} = \pi\hbar\,\delta(X) + i\hbar\ \mathrm{p.v.}\left(\frac{1}{X}\right), \tag{3.30}$$

where p.v. denotes the principal value. Note that

$$\delta(-x) = \delta(x) \quad \text{and} \quad \mathrm{p.v.}\left(\frac{1}{-X}\right) = -\mathrm{p.v.}\left(\frac{1}{X}\right). \tag{3.31}$$

Collecting the results, we finally obtain:

$$
\begin{aligned}
\dot{\rho}^{\mathrm{N}}_{\mathrm{EE}'} = &-\frac{i}{\hbar}(\mathrm{E}-\mathrm{E}')\rho^{\mathrm{N}}_{\mathrm{EE}'} - \frac{1}{\hbar}\sum_{\mathbf{k}}\sum_{i,j}\sum_{\mathrm{F}}\sum_{\eta}\Big\{ \\
&\hat{\mathcal{P}}_{\mathrm{NE}}\,\hat{\mathrm{d}}_i\Big[t^{\eta}_{\mathbf{k}i}(t^{\eta}_{\mathbf{k}j})^*\,f^{+}_{\eta}(\epsilon_{\mathbf{k}})\left(\pi\,\delta(\mathrm{F}-\hat{\mathcal{H}}_{mol}+\epsilon_{\mathbf{k}})+i\,\mathrm{p.v.}\left(\frac{1}{\mathrm{F}-\hat{\mathcal{H}}_{mol}+\epsilon_{\mathbf{k}}}\right)\right)\Big]\hat{\mathrm{d}}^{\dagger}_j\,\rho^{\mathrm{N}}_{\mathrm{FE}'} \\
&+\hat{\mathcal{P}}_{\mathrm{NE}}\,\hat{\mathrm{d}}^{\dagger}_i\Big[(t^{\eta}_{\mathbf{k}i})^*t^{\eta}_{\mathbf{k}j}\,f^{-}_{\eta}(\epsilon_{\mathbf{k}})\left(\pi\,\delta(\mathrm{F}-\hat{\mathcal{H}}_{mol}-\epsilon_{\mathbf{k}})+i\,\mathrm{p.v.}\left(\frac{1}{\mathrm{F}-\hat{\mathcal{H}}_{mol}-\epsilon_{\mathbf{k}}}\right)\right)\Big]\hat{\mathrm{d}}_j\,\rho^{\mathrm{N}}_{\mathrm{FE}'} \\
&+\rho^{\mathrm{N}}_{\mathrm{EF}}\,\hat{\mathrm{d}}_i\Big[t^{\eta}_{\mathbf{k}i}(t^{\eta}_{\mathbf{k}j})^*\,f^{+}_{\eta}(\epsilon_{\mathbf{k}})\left(\pi\,\delta(\hat{\mathcal{H}}_{mol}-\mathrm{F}-\epsilon_{\mathbf{k}})+i\,\mathrm{p.v.}\left(\frac{1}{\hat{\mathcal{H}}_{mol}-\mathrm{F}-\epsilon_{\mathbf{k}}}\right)\right)\Big]\hat{\mathrm{d}}^{\dagger}_j\,\hat{\mathcal{P}}_{\mathrm{NE}'} \\
&+\rho^{\mathrm{N}}_{\mathrm{EF}}\,\hat{\mathrm{d}}^{\dagger}_i\Big[(t^{\eta}_{\mathbf{k}i})^*t^{\eta}_{\mathbf{k}j}\,f^{-}_{\eta}(\epsilon_{\mathbf{k}})\left(\pi\,\delta(\hat{\mathcal{H}}_{mol}-\mathrm{F}+\epsilon_{\mathbf{k}})+i\,\mathrm{p.v.}\left(\frac{1}{\hat{\mathcal{H}}_{mol}-\mathrm{F}+\epsilon_{\mathbf{k}}}\right)\right)\Big]\hat{\mathrm{d}}_j\,\hat{\mathcal{P}}_{\mathrm{NE}'} \\
&-\hat{\mathcal{P}}_{\mathrm{NE}}\,\hat{\mathrm{d}}_i\sum_{\mathrm{F}'}\rho^{\mathrm{N}+1}_{\mathrm{FF}'}\Big[t^{\eta}_{\mathbf{k}i}(t^{\eta}_{\mathbf{k}j})^*\,f^{-}_{\eta}(\epsilon_{\mathbf{k}})\left(\pi\,\delta(\mathrm{E}'-\mathrm{F}'+\epsilon_{\mathbf{k}})+i\,\mathrm{p.v.}\left(\frac{1}{\mathrm{E}'-\mathrm{F}'+\epsilon_{\mathbf{k}}}\right)\right)\Big]\hat{\mathrm{d}}^{\dagger}_j\,\hat{\mathcal{P}}_{\mathrm{NE}'} \\
&-\hat{\mathcal{P}}_{\mathrm{NE}}\,\hat{\mathrm{d}}^{\dagger}_i\sum_{\mathrm{F}'}\rho^{\mathrm{N}-1}_{\mathrm{FF}'}\Big[(t^{\eta}_{\mathbf{k}i})^*t^{\eta}_{\mathbf{k}j}\,f^{+}_{\eta}(\epsilon_{\mathbf{k}})\left(\pi\,\delta(\mathrm{E}'-\mathrm{F}'-\epsilon_{\mathbf{k}})+i\,\mathrm{p.v.}\left(\frac{1}{\mathrm{E}'-\mathrm{F}'-\epsilon_{\mathbf{k}}}\right)\right)\Big]\hat{\mathrm{d}}_j\,\hat{\mathcal{P}}_{\mathrm{NE}'} \\
&-\hat{\mathcal{P}}_{\mathrm{NE}}\,\hat{\mathrm{d}}_i\sum_{\mathrm{F}'}\rho^{\mathrm{N}+1}_{\mathrm{FF}'}\Big[t^{\eta}_{\mathbf{k}i}(t^{\eta}_{\mathbf{k}j})^*\,f^{-}_{\eta}(\epsilon_{\mathbf{k}})\left(\pi\,\delta(\mathrm{F}-\mathrm{E}-\epsilon_{\mathbf{k}})+i\,\mathrm{p.v.}\left(\frac{1}{\mathrm{F}-\mathrm{E}-\epsilon_{\mathbf{k}}}\right)\right)\Big]\hat{\mathrm{d}}^{\dagger}_j\,\hat{\mathcal{P}}_{\mathrm{NE}'} \\
&-\hat{\mathcal{P}}_{\mathrm{NE}}\,\hat{\mathrm{d}}^{\dagger}_i\sum_{\mathrm{F}'}\rho^{\mathrm{N}-1}_{\mathrm{FF}'}\Big[(t^{\eta}_{\mathbf{k}i})^*t^{\eta}_{\mathbf{k}j}\,f^{+}_{\eta}(\epsilon_{\mathbf{k}})\left(\pi\,\delta(\mathrm{F}-\mathrm{E}+\epsilon_{\mathbf{k}})+i\,\mathrm{p.v.}\left(\frac{1}{\mathrm{F}-\mathrm{E}+\epsilon_{\mathbf{k}}}\right)\right)\Big]\hat{\mathrm{d}}_j\,\hat{\mathcal{P}}_{\mathrm{NE}'}\Big\}.
\end{aligned}
\tag{3.32}
$$

Eq. (3.32) is the so-called non-secular part of the GME. It contains coherences between states with different energies but the same particle number. The secular part, which does not contain these coherences, can be gained analogously. We only have to sandwich Eq. (3.24) between two projection operators with the same index for the energy, yielding:

$$
\begin{aligned}
\dot{\rho}^{\mathrm{N}}_{\mathrm{E}} = &-\frac{1}{\hbar}\sum_{\mathbf{k}}\sum_{i,j}\sum_{\mathrm{E}'}\sum_{\eta}\Big\{ \\
&\hat{\mathcal{P}}_{\mathrm{NE}}\,\hat{\mathrm{d}}_i\,\hat{\mathcal{P}}_{(\mathrm{N}+1)\mathrm{E}'}\,\hat{\mathrm{d}}^{\dagger}_j\,\rho^{\mathrm{N}}_{\mathrm{E}}\Big[t^{\eta}_{\mathbf{k}i}(t^{\eta}_{\mathbf{k}j})^*\,f^{+}_{\eta}(\epsilon_{\mathbf{k}})\left(\pi\,\delta(\mathrm{E}-\mathrm{E}'+\epsilon_{\mathbf{k}})+i\,\mathrm{p.v.}\left(\frac{1}{\mathrm{E}-\mathrm{E}'+\epsilon_{\mathbf{k}}}\right)\right)\Big] \\
&+\mathrm{h.c.} \\
&+\hat{\mathcal{P}}_{\mathrm{NE}}\,\hat{\mathrm{d}}^{\dagger}_i\,\hat{\mathcal{P}}_{(\mathrm{N}-1)\mathrm{E}'}\,\hat{\mathrm{d}}_j\,\rho^{\mathrm{N}}_{\mathrm{E}}\Big[(t^{\eta}_{\mathbf{k}i})^*t^{\eta}_{\mathbf{k}j}\,f^{-}_{\eta}(\epsilon_{\mathbf{k}})\left(\pi\,\delta(\mathrm{E}-\mathrm{E}'-\epsilon_{\mathbf{k}})+i\,\mathrm{p.v.}\left(\frac{1}{\mathrm{E}-\mathrm{E}'-\epsilon_{\mathbf{k}}}\right)\right)\Big] \\
&+\mathrm{h.c.} \\
&-2\pi\,\hat{\mathcal{P}}_{\mathrm{NE}}\,\hat{\mathrm{d}}_i\,\rho^{\mathrm{N}+1}_{\mathrm{E}'}\,\hat{\mathrm{d}}^{\dagger}_j\,\hat{\mathcal{P}}_{\mathrm{NE}}\,t^{\eta}_{\mathbf{k}i}(t^{\eta}_{\mathbf{k}j})^*\,f^{-}_{\eta}(\epsilon_{\mathbf{k}})\,\delta(\mathrm{E}-\mathrm{E}'+\epsilon_{\mathbf{k}}) \\
&-2\pi\,\hat{\mathcal{P}}_{\mathrm{NE}}\,\hat{\mathrm{d}}^{\dagger}_i\,\rho^{\mathrm{N}-1}_{\mathrm{E}'}\,\hat{\mathrm{d}}_j\,\hat{\mathcal{P}}_{\mathrm{NE}}\,(t^{\eta}_{\mathbf{k}i})^*t^{\eta}_{\mathbf{k}j}\,f^{+}_{\eta}(\epsilon_{\mathbf{k}})\,\delta(\mathrm{E}-\mathrm{E}'-\epsilon_{\mathbf{k}})\Big\}.
\end{aligned}
\tag{3.33}
$$

In our further calculations we will focus on the secular part of the GME. Now we are able to perform the sum over $\mathbf{k}$ in Eq. (3.33). As the substrate and the tip are considered to be macroscopic objects, we use a continuum limit and let the sums go over into integrals:

$$\sum_{\mathbf{k}} \to \int \mathrm{d}\epsilon_{\mathbf{k}} D(\epsilon_{\mathbf{k}}). \tag{3.34}$$

Here $D(\epsilon_{\mathbf{k}})$ is the density of states in the tip or the substrate, respectively. As the tip states and the substrate states have different symmetries respective to their dependence on $\mathbf{k}$, we have to treat each contribution on its own.
We start with the tip part of the GME. Inserting Eq. (3.34) we get:

$$\begin{aligned}
\left(\dot{\rho}^{\mathrm{N}}_{\mathrm{E}}\right)_{tip} = -\frac{1}{\hbar}\sum_{i,j}\sum_{\mathrm{E}'}\int_{0}^{-\epsilon_0^{tip}} \mathrm{d}\epsilon_{\mathbf{k}} D(\epsilon_{\mathbf{k}})\Big\{ & \\
\hat{\mathcal{P}}_{\mathrm{NE}}\,\hat{\mathrm{d}}_i\,\hat{\mathcal{P}}_{(\mathrm{N}+1)\mathrm{E}'}\,\hat{\mathrm{d}}_j^{\dagger}\,\rho^{\mathrm{N}}_{\mathrm{E}}\Big[t^T_{\mathbf{k}i}(t^T_{\mathbf{k}j})^*\,f^+_{\eta}\left(\epsilon_{\mathbf{k}}\right)\left(\pi\,\delta(\mathrm{E}-\mathrm{E}'+\epsilon_{\mathbf{k}})+i\,\mathrm{p.v.}\left(\frac{1}{\mathrm{E}-\mathrm{E}'+\epsilon_{\mathbf{k}}}\right)\right)\Big] & \\
+\mathrm{h.c.} & \\
+\hat{\mathcal{P}}_{\mathrm{NE}}\,\hat{\mathrm{d}}_i^{\dagger}\,\hat{\mathcal{P}}_{(\mathrm{N}-1)\mathrm{E}'}\,\hat{\mathrm{d}}_j\,\rho^{\mathrm{N}}_{\mathrm{E}}\Big[(t^T_{\mathbf{k}i})^* t^T_{\mathbf{k}j}\,f^-_{\eta}\left(\epsilon_{\mathbf{k}}\right)\left(\pi\,\delta(\mathrm{E}-\mathrm{E}'-\epsilon_{\mathbf{k}})+i\,\mathrm{p.v.}\left(\frac{1}{\mathrm{E}-\mathrm{E}'-\epsilon_{\mathbf{k}}}\right)\right)\Big] & \\
+\mathrm{h.c.} & \\
-2\pi\,\hat{\mathcal{P}}_{\mathrm{NE}}\,\hat{\mathrm{d}}_i\,\rho^{\mathrm{N}+1}_{\mathrm{E}'}\,\hat{\mathrm{d}}_j^{\dagger}\,\hat{\mathcal{P}}_{\mathrm{NE}}\,t^T_{\mathbf{k}i}(t^T_{\mathbf{k}j})^*\,f^-_{\eta}\left(\epsilon_{\mathbf{k}}\right)\delta(\mathrm{E}-\mathrm{E}'+\epsilon_{\mathbf{k}}) & \\
-2\pi\,\hat{\mathcal{P}}_{\mathrm{NE}}\,\hat{\mathrm{d}}_i^{\dagger}\,\rho^{\mathrm{N}-1}_{\mathrm{E}'}\,\hat{\mathrm{d}}_j\,\hat{\mathcal{P}}_{\mathrm{NE}}\,(t^T_{\mathbf{k}i})^* t^T_{\mathbf{k}j}\,f^+_{\eta}\left(\epsilon_{\mathbf{k}}\right)\delta(\mathrm{E}-\mathrm{E}'-\epsilon_{\mathbf{k}})\Big\}. &
\end{aligned} \tag{3.35}$$

Note that $t^T_{\mathbf{k}i} = (t^T_{\mathbf{k}i})^*$, as they are real numbers. Hence the terms which are containing the principal parts are vanishing. For the borders of the integral see Fig. 2.2. Evaluating Eq. (3.35) yields:

$$\begin{aligned}
\left(\dot{\rho}^{\mathrm{N}}_{\mathrm{E}}\right)_{tip} = -\sum_{i,j}\sum_{\mathrm{E}'}\Big\{ & T^T_{ij}(\mathrm{E}'-\mathrm{E})\,\hat{\mathcal{P}}_{\mathrm{NE}}\,\hat{\mathrm{d}}_i\,\hat{\mathcal{P}}_{(\mathrm{N}+1)\mathrm{E}'}\,\hat{\mathrm{d}}_j^{\dagger}\,\rho^{\mathrm{N}}_{\mathrm{E}}\,f^+_T\left(\mathrm{E}'-\mathrm{E}\right) \\
& +T^T_{ij}(\mathrm{E}-\mathrm{E}')\,\hat{\mathcal{P}}_{\mathrm{NE}}\,\hat{\mathrm{d}}_i^{\dagger}\,\hat{\mathcal{P}}_{(\mathrm{N}-1)\mathrm{E}'}\,\hat{\mathrm{d}}_j\,\rho^{\mathrm{N}}_{\mathrm{E}}\,f^-_T\left(\mathrm{E}-\mathrm{E}'\right) \\
& -T^T_{ij}(\mathrm{E}'-\mathrm{E})\,\hat{\mathcal{P}}_{\mathrm{NE}}\,\hat{\mathrm{d}}_i\,\rho^{\mathrm{N}+1}_{\mathrm{E}'}\,\hat{\mathrm{d}}_j^{\dagger}\,\hat{\mathcal{P}}_{\mathrm{NE}}\,f^-_T\left(\mathrm{E}'-\mathrm{E}\right) \\
& -T^T_{ij}(\mathrm{E}-\mathrm{E}')\,\hat{\mathcal{P}}_{\mathrm{NE}}\,\hat{\mathrm{d}}_i^{\dagger}\,\rho^{\mathrm{N}-1}_{\mathrm{E}'}\,\hat{\mathrm{d}}_j\,\hat{\mathcal{P}}_{\mathrm{NE}}\,f^+_T\left(\mathrm{E}-\mathrm{E}'\right)\Big\}.
\end{aligned} \tag{3.36}$$

The function $T^T_{ij}(E)$ stems from the product of two tunneling matrix elements, whose energy dependence results from their $\kappa(\mathbf{k})$ dependent prefactors. The exact form of $T^T_{ij}(E)$ depends on the type of the tip wavefunction. In the simplest case of an s-type tip state it takes the form:

$$T_{ij}^{T}(E) = \frac{(2\pi\hbar)^3 C_s^2 D(E)}{m^2\kappa^2(E)}\psi_i(\mathbf{r}_{tip})\psi_j(\mathbf{r}_{tip}) \tag{3.37}$$

$$= \frac{(2\pi\hbar)^3 C_s^2 D(E)}{m^2\kappa^2(E)}\sum_{\alpha,\,\beta} c_{\alpha i}c_{\beta j}\, p_z(\mathbf{r}_{tip}-\mathbf{r}_\alpha)p_z(\mathbf{r}_{tip}-\mathbf{r}_\beta), \tag{3.38}$$

with

$$\kappa(E) = \sqrt{\frac{2m}{\hbar^2}(\epsilon_F^{tip} + \phi_0^{tip} - E)} \qquad \text{and} \qquad D(E) = \frac{(2m)^{\frac{3}{2}}V}{2\pi^2\hbar^3}\sqrt{E}. \tag{3.39}$$

The calculation of the substrate part of the GME will be more complicated. Hence, in a first step we have a look at the product $t_{\mathbf{k}i}^S(t_{\mathbf{k}j}^S)^*$:

$$t_{\mathbf{k}i}^S(t_{\mathbf{k}j}^S)^* = \epsilon_i\epsilon_j\sum_{\alpha,\,\beta} c_{\alpha i}c_{\beta j}^* V_\alpha(k_z,k_\parallel,\kappa)V_\beta(k_z,k_\parallel,\kappa)\, e^{-i\mathbf{k}_\parallel\cdot\mathbf{r}_{\alpha\parallel}}e^{+i\mathbf{k}_\parallel\cdot\mathbf{r}_{\beta\parallel}}$$

$$= \epsilon_i\epsilon_j\sum_{\alpha,\,\beta} c_{\alpha i}c_{\beta j} V_\alpha(k_z,k_\parallel,\kappa)V_\beta(k_z,k_\parallel,\kappa)\, e^{-i\mathbf{k}_\parallel\cdot\left(\mathbf{r}_{\alpha\parallel}-\mathbf{r}_{\beta\parallel}\right)}, \tag{3.40}$$

We see that we do best if we split the sum over $\mathbf{k}$ into two sums over k_z and $k_\parallel$ and then replace the sums with energy integrals. This yields cylindrical integrations in energy. The associated densities of states are:

$$D^{(1D)}(\epsilon) = \frac{\sqrt{m}L}{\pi\hbar\sqrt{2\epsilon}} \qquad \text{and} \qquad D^{(2D)} = \frac{mS}{\pi\hbar^2}. \tag{3.41}$$

Now we are able to apply Eq. (3.34). In Fig. 2.2 we see that we have to integrate ϵ_z from 0 to $-\epsilon_0^{sub}$, because ϵ_z is defined positive. Therefore we set

$$\sum_{\mathbf{k}} = \sum_{k_\parallel}\sum_{k_z} \to \frac{\sqrt{\frac{1}{2}m^3}}{\pi^2\hbar^3}\int_0^\infty \mathrm{d}\epsilon_\parallel \int_0^{-\epsilon_0^{sub}} \mathrm{d}\epsilon_z \frac{1}{\sqrt{\epsilon_z}}. \tag{3.42}$$

We once again recall the definitions given in section 2.1 for the energies,

$$\epsilon_{\mathbf{k}} = \epsilon_\parallel + \epsilon_z + \epsilon_0^{sub},$$

$$k_z(\epsilon_z) = \sqrt{\frac{2m}{\hbar^2}\epsilon_z},$$

$$k_\parallel(\epsilon_\parallel) = \sqrt{\frac{2m}{\hbar^2}\epsilon_\parallel},$$

$$\kappa(\epsilon_z) = \sqrt{\frac{2m}{\hbar^2}(\epsilon_F^{sub} + \phi_0^{sub} - \epsilon_z)}.$$

The substrate part of the GME in energy-dependent form reads:

$$
\begin{aligned}
\left(\dot{\rho}^{\mathrm{N}}_{\mathrm{E}}\right)_{sub} = -\frac{\sqrt{2m^3}}{\pi\hbar^4}\sum_{i,j}\sum_{\mathrm{E}'}\int_0^{\infty}\mathrm{d}\epsilon_{\parallel}\int_0^{-\epsilon_0^{sub}}\mathrm{d}\epsilon_z\frac{1}{\sqrt{\epsilon_z}}\Big\{ \\
\hat{\mathcal{P}}_{\mathrm{NE}}\,\hat{\mathrm{d}}_i\,\hat{\mathcal{P}}_{(\mathrm{N}+1)\mathrm{E}'}\,\hat{\mathrm{d}}_j^{\dagger}\,\rho^{\mathrm{N}}_{\mathrm{E}}\,t^S_{ki}(t^S_{kj})^*\,f_S^+\left(\epsilon_{\parallel}+\epsilon_z+\epsilon_0^{sub}\right)\delta(\mathrm{E}-\mathrm{E}'+\epsilon_{\parallel}+\epsilon_z+\epsilon_0^{sub}) \\
+\hat{\mathcal{P}}_{\mathrm{NE}}\,\hat{\mathrm{d}}_i^{\dagger}\,\hat{\mathcal{P}}_{(\mathrm{N}-1)\mathrm{E}'}\,\hat{\mathrm{d}}_j\,\rho^{\mathrm{N}}_{\mathrm{E}}\,t^S_{ki}(t^S_{kj})^*\,f_S^-\left(\epsilon_{\parallel}+\epsilon_z+\epsilon_0^{sub}\right)\delta(\mathrm{E}-\mathrm{E}'-(\epsilon_{\parallel}+\epsilon_z+\epsilon_0^{sub})) \\
-\hat{\mathcal{P}}_{\mathrm{NE}}\,\hat{\mathrm{d}}_i\,\rho^{\mathrm{N}+1}_{\mathrm{E}'}\,\hat{\mathrm{d}}_j^{\dagger}\,\hat{\mathcal{P}}_{\mathrm{NE}}\,t^S_{ki}(t^S_{kj})^*\,f_S^-\left(\epsilon_{\parallel}+\epsilon_z+\epsilon_0^{sub}\right)\delta(\mathrm{E}-\mathrm{E}'+\epsilon_{\parallel}+\epsilon_z+\epsilon_0^{sub}) \\
-\hat{\mathcal{P}}_{\mathrm{NE}}\,\hat{\mathrm{d}}_i^{\dagger}\,\rho^{\mathrm{N}-1}_{\mathrm{E}'}\,\hat{\mathrm{d}}_j\,\hat{\mathcal{P}}_{\mathrm{NE}}\,t^S_{ki}(t^S_{kj})^*\,f_S^+\left(\epsilon_{\parallel}+\epsilon_z+\epsilon_0^{sub}\right)\delta(\mathrm{E}-\mathrm{E}'-(\epsilon_{\parallel}+\epsilon_z+\epsilon_0^{sub}))\Big\}.
\end{aligned}
\tag{3.43}
$$

Assuming non-degenerate states and using the properties of the projection operators $\hat{\mathcal{P}}_{\mathrm{NE}}$ (see Eq. (A.19)) one can easily check, that also for the substrate part of the GME the terms containing the principal parts are canceling. After performing the integration over $\epsilon_{\parallel}$ we arrive at:

$$
\begin{aligned}
\left(\dot{\rho}^{\mathrm{N}}_{\mathrm{E}}\right)_{sub} = -\sum_{i,j}\sum_{\mathrm{E}'}\Big\{&\hat{\mathcal{P}}_{\mathrm{NE}}\,\hat{\mathrm{d}}_i\,\hat{\mathcal{P}}_{(\mathrm{N}+1)\mathrm{E}'}\,\hat{\mathrm{d}}_j^{\dagger}\,\rho^{\mathrm{N}}_{\mathrm{E}}\,T^S_{ij}(\mathrm{E}'-\mathrm{E})\,f_S^+\left(\mathrm{E}'-\mathrm{E}\right) \\
&+\hat{\mathcal{P}}_{\mathrm{NE}}\,\hat{\mathrm{d}}_i^{\dagger}\,\hat{\mathcal{P}}_{(\mathrm{N}-1)\mathrm{E}'}\,\hat{\mathrm{d}}_j\,\rho^{\mathrm{N}}_{\mathrm{E}}\,T^S_{ij}(\mathrm{E}-\mathrm{E}')\,f_S^-\left(\mathrm{E}-\mathrm{E}'\right) \\
&-\hat{\mathcal{P}}_{\mathrm{NE}}\,\hat{\mathrm{d}}_i\,\rho^{\mathrm{N}+1}_{\mathrm{E}'}\,\hat{\mathrm{d}}_j^{\dagger}\,\hat{\mathcal{P}}_{\mathrm{NE}}\,T^S_{ij}(\mathrm{E}'-\mathrm{E})\,f_S^-\left(\mathrm{E}'-\mathrm{E}\right) \\
&-\hat{\mathcal{P}}_{\mathrm{NE}}\,\hat{\mathrm{d}}_i^{\dagger}\,\rho^{\mathrm{N}-1}_{\mathrm{E}'}\,\hat{\mathrm{d}}_j\,\hat{\mathcal{P}}_{\mathrm{NE}}\,T^S_{ij}(\mathrm{E}-\mathrm{E}')\,f_S^+\left(\mathrm{E}-\mathrm{E}'\right)\Big\}.
\end{aligned}
\tag{3.44}
$$

The function $T^S_{ij}(\xi)$ is given by:

$$
T^S_{ij}(\xi) = \epsilon_i\epsilon_j\frac{\sqrt{2m^3}}{\pi\hbar^4}\sum_{\alpha,\beta}c_{\alpha i}c_{\beta j}\int_0^{-\epsilon_0^{sub}}\mathrm{d}\epsilon_z\frac{1}{\sqrt{\epsilon_z}}W_{\alpha\beta}(\epsilon_z,\xi),
\tag{3.45}
$$

where we introduced $W_{\alpha\beta}(\epsilon_z,\xi)$ for brevity. It is defined by:

$$
\begin{aligned}
W_{\alpha\beta}(\epsilon_z,\xi) =& V_{\alpha}\left(k_z(\epsilon_z),k_{\parallel}(\epsilon_z,\xi),\kappa(\epsilon_z)\right)\,V_{\beta}\left(k_z(\epsilon_z),k_{\parallel}(\epsilon_z,\xi),\kappa(\epsilon_z)\right) \\
&\times\frac{1}{2\pi}\int_0^{2\pi}\mathrm{d}\theta_k\,\exp\left(-i\mathbf{k}_{\parallel}(\epsilon_z,\xi)\cdot\mathbf{r}_{\alpha\beta}\right).
\end{aligned}
\tag{3.46}
$$

Note that $k_{\parallel}(\epsilon_z,\xi)$ is given by:

$$
k_{\parallel}(\epsilon_z,\xi) = \sqrt{\frac{2m}{\hbar^2}(\xi-\epsilon_z-\epsilon_0^{sub})}.
\tag{3.47}
$$

Although not mentioned, in the derivation of the two-dimensional density of states we already evaluated the integral over the angle θ_k in the k space. But as the scalar product

$$\mathbf{k}_{\parallel} \cdot \left(\mathbf{r}_{\alpha\parallel} - \mathbf{r}_{\beta\parallel}\right) = k_{\parallel} r_{\alpha\beta} \cos(\theta_k) \tag{3.48}$$

in Eq. (3.46) depends on this angle, we have to repeat the integration here and divide by 2π. It is

$$\int_0^{2\pi} \mathrm{d}\theta \, e^{-ix\cos(\theta)} = 2\pi J_0(x), \tag{3.49}$$

where J_0 is the zeroth Bessel function of the first kind. In series representation it reads:

$$J_0(x) = \sum_n^{\infty} (-1)^n \frac{\left(\frac{1}{4}x^2\right)^n}{(n!)^2}. \tag{3.50}$$

Thus we get for $W_{\alpha\beta}$:

$$W_{\alpha\beta}(\epsilon_z, \xi) = V_\alpha\left(k_z, k_{\parallel}, \kappa\right) V_\beta\left(k_z, k_{\parallel}, \kappa\right) J_0\left(k_{\parallel} r_{\alpha\beta}\right). \tag{3.51}$$

Because of the nontrivial structure of this function we have to integrate it numerically to obtain the tunneling matrix elements for the substrate. After evaluating the tunneling matrix elements, we are able to write down the final secular GME:

$$\begin{aligned}
\dot{\rho}_{\mathrm{E}}^{\mathrm{N}} = -\sum_{\eta} \sum_{i,j} \sum_{\mathrm{E}'} \Big\{ & \hat{\mathcal{P}}_{\mathrm{NE}} \, \hat{\mathrm{d}}_i \, \hat{\mathcal{P}}_{(\mathrm{N}+1)\mathrm{E}'} \, \hat{\mathrm{d}}_j^{\dagger} \, \rho_{\mathrm{E}}^{\mathrm{N}} \, T_{ij}^{\eta}(\mathrm{E}' - \mathrm{E}) \, f_{\eta}^{+}\left(\mathrm{E}' - \mathrm{E}\right) \\
& + \hat{\mathcal{P}}_{\mathrm{NE}} \, \hat{\mathrm{d}}_i^{\dagger} \, \hat{\mathcal{P}}_{(\mathrm{N}-1)\mathrm{E}'} \, \hat{\mathrm{d}}_j \, \rho_{\mathrm{E}}^{\mathrm{N}} \, T_{ij}^{\eta}(\mathrm{E} - \mathrm{E}') \, f_{\eta}^{-}\left(\mathrm{E} - \mathrm{E}'\right) \\
& - \hat{\mathcal{P}}_{\mathrm{NE}} \, \hat{\mathrm{d}}_i \, \rho_{\mathrm{E}'}^{\mathrm{N}+1} \, \hat{\mathrm{d}}_j^{\dagger} \, \hat{\mathcal{P}}_{\mathrm{NE}} \, T_{ij}^{\eta}(\mathrm{E}' - \mathrm{E}) \, f_{\eta}^{-}\left(\mathrm{E}' - \mathrm{E}\right) \\
& - \hat{\mathcal{P}}_{\mathrm{NE}} \, \hat{\mathrm{d}}_i^{\dagger} \, \rho_{\mathrm{E}'}^{\mathrm{N}-1} \, \hat{\mathrm{d}}_j \, \hat{\mathcal{P}}_{\mathrm{NE}} \, T_{ij}^{\eta}(\mathrm{E} - \mathrm{E}') \, f_{\eta}^{+}\left(\mathrm{E} - \mathrm{E}'\right) \Big\}.
\end{aligned} \tag{3.52}$$

We can also write Eq. (3.52) as a linear differential equation in matrix form:

$$\dot{\rho}_{red} = \mathcal{L}\rho_{red}, \tag{3.53}$$

where $\mathcal{L}$ is called the Liouvillian of the system. To obtain the stationary solution ρ_{red}^{stat}, we evaluate Eq. (3.52) under the condition that the time derivative of the RDM is equal to zero for $t \to \infty$:

$$\lim_{t\to\infty} \dot{\rho}_{red} = 0. \tag{3.54}$$

Considering Eq. (3.53), this implies:

$$0 = \mathcal{L}\rho_{red}^{stat}, \tag{3.55}$$

$$\Rightarrow \rho_{red}^{stat} = \ker(\mathcal{L}), \tag{3.56}$$

where $\ker(\mathcal{L})$ denotes the kernel of the Liouvillian $\mathcal{L}$.

3.2. Calculating the current

We will now calculate an expression for the current operator $\hat{I}$. Its expectation value is given by:

$$\langle \hat{I} \rangle = e \, \mathrm{tr}_{mol} \left\{ \hat{N} \dot{\hat{\rho}}^S_{red} \right\}. \tag{3.57}$$

After projecting the right hand side of Eq. (3.57) onto the subspace with particle number N and energy E using Eq. (A.19), we get for the current:

$$\langle \hat{I} \rangle = e \sum_{\mathrm{N,\,E}} \mathrm{tr}_{mol} \left\{ \mathrm{N} \dot{\rho}^{\mathrm{N}}_{\mathrm{E}} \right\}. \tag{3.58}$$

If we insert Eq. (3.52), the expression for the current reads:

$$\begin{aligned} \langle \hat{I} \rangle = -e \sum_{\eta} \sum_{i,j} \sum_{\mathrm{N}} \sum_{\mathrm{E,\,E'}} \mathrm{N} \, \mathrm{tr}_{mol} \Big\{ & \hat{\mathcal{P}}_{\mathrm{NE}} \, \hat{\mathrm{d}}_i \, \hat{\mathcal{P}}_{(\mathrm{N}+1)\mathrm{E'}} \, \hat{\mathrm{d}}^\dagger_j \, \rho^{\mathrm{N}}_{\mathrm{E}} \, T^\eta_{ij}(\mathrm{E'} - \mathrm{E}) \, f^+_\eta \left(\mathrm{E'} - \mathrm{E} \right) \\ & + \hat{\mathcal{P}}_{\mathrm{NE}} \, \hat{\mathrm{d}}^\dagger_i \, \hat{\mathcal{P}}_{(\mathrm{N}-1)\mathrm{E'}} \, \hat{\mathrm{d}}_j \, \rho^{\mathrm{N}}_{\mathrm{E}} \, T^\eta_{ij}(\mathrm{E} - \mathrm{E'}) \, f^-_\eta \left(\mathrm{E} - \mathrm{E'} \right) \\ & - \hat{\mathcal{P}}_{\mathrm{NE}} \, \hat{\mathrm{d}}_i \, \rho^{\mathrm{N}+1}_{\mathrm{E'}} \, \hat{\mathrm{d}}^\dagger_j \, \hat{\mathcal{P}}_{\mathrm{NE}} \, T^\eta_{ij}(\mathrm{E'} - \mathrm{E}) \, f^-_\eta \left(\mathrm{E'} - \mathrm{E} \right) \\ & - \hat{\mathcal{P}}_{\mathrm{NE}} \, \hat{\mathrm{d}}^\dagger_i \, \rho^{\mathrm{N}-1}_{\mathrm{E'}} \, \hat{\mathrm{d}}_j \, \hat{\mathcal{P}}_{\mathrm{NE}} \, T^\eta_{ij}(\mathrm{E} - \mathrm{E'}) \, f^+_\eta \left(\mathrm{E} - \mathrm{E'} \right) \Big\}. \end{aligned} \tag{3.59}$$

Now we use the fact that the tunneling matrix elements $T^\eta_{ij}(ij)$ are invariant under interchanging i and j. Then exchanging N by $\mathrm{N} \pm 1$ and E by E′ in the third and fourth line of Eq. 3.59 yields:

$$\begin{aligned} \langle \hat{I} \rangle = -e \sum_{\eta} \sum_{i,j} \sum_{\mathrm{N}} \sum_{\mathrm{E,\,E'}} \mathrm{tr}_{mol} \Big\{ & \mathrm{N} \hat{\mathcal{P}}_{\mathrm{NE}} \, \hat{\mathrm{d}}_i \, \hat{\mathcal{P}}_{(\mathrm{N}+1)\mathrm{E'}} \, \hat{\mathrm{d}}^\dagger_j \, \rho^{\mathrm{N}}_{\mathrm{E}} \, T^\eta_{ij}(\mathrm{E'} - \mathrm{E}) \, f^+_\eta \left(\mathrm{E'} - \mathrm{E} \right) \\ & + \mathrm{N} \hat{\mathcal{P}}_{\mathrm{NE}} \, \hat{\mathrm{d}}^\dagger_i \, \hat{\mathcal{P}}_{(\mathrm{N}-1)\mathrm{E'}} \, \hat{\mathrm{d}}_j \, \rho^{\mathrm{N}}_{\mathrm{E}} \, T^\eta_{ij}(\mathrm{E} - \mathrm{E'}) \, f^-_\eta \left(\mathrm{E} - \mathrm{E'} \right) \\ & - (\mathrm{N}-1) \hat{\mathcal{P}}_{(\mathrm{N}-1)\mathrm{E'}} \, \hat{\mathrm{d}}_j \, \rho^{\mathrm{N}}_{\mathrm{E}} \, \hat{\mathrm{d}}^\dagger_i \, \hat{\mathcal{P}}_{(\mathrm{N}-1)\mathrm{E'}} \, T^\eta_{ij}(\mathrm{E} - \mathrm{E'}) \, f^-_\eta \left(\mathrm{E} - \mathrm{E'} \right) \\ & - (\mathrm{N}+1) \hat{\mathcal{P}}_{(\mathrm{N}+1)\mathrm{E'}} \, \hat{\mathrm{d}}^\dagger_j \, \rho^{\mathrm{N}}_{\mathrm{E}} \, \hat{\mathrm{d}}_i \, \hat{\mathcal{P}}_{(\mathrm{N}+1)\mathrm{E'}} \, T^\eta_{ij}(\mathrm{E'} - \mathrm{E}) \, f^+_\eta \left(\mathrm{E'} - \mathrm{E} \right) \Big\}. \end{aligned} \tag{3.60}$$

Furthermore we can use the cyclic properties of the trace and the fact that the projection operators are idempotent to obtain:

$$\begin{aligned} \langle \hat{I} \rangle = e \sum_{\eta} \sum_{i,j} \sum_{\mathrm{N}} \sum_{\mathrm{E,\,E'}} \mathrm{tr}_{mol} \Big\{ & \hat{\mathcal{P}}_{\mathrm{NE}} \, \hat{\mathrm{d}}_i \, \hat{\mathcal{P}}_{(\mathrm{N}+1)\mathrm{E'}} \, \hat{\mathrm{d}}^\dagger_j \, \rho^{\mathrm{N}}_{\mathrm{E}} \, T^\eta_{ij}(\mathrm{E'} - \mathrm{E}) \, f^+_\eta \left(\mathrm{E'} - \mathrm{E} \right) \\ & - \hat{\mathcal{P}}_{\mathrm{NE}} \, \hat{\mathrm{d}}^\dagger_i \, \hat{\mathcal{P}}_{(\mathrm{N}-1)\mathrm{E'}} \, \hat{\mathrm{d}}_j \, \rho^{\mathrm{N}}_{\mathrm{E}} \, T^\eta_{ij}(\mathrm{E} - \mathrm{E'}) \, f^-_\eta \left(\mathrm{E} - \mathrm{E'} \right) \Big\}. \end{aligned} \tag{3.61}$$

In Eq. (3.61) we are able to identify the desired current operator $\hat{I}_\eta$ with $\eta = tip, sub$:

$$\hat{I}_\eta = e \sum_{i,j} \sum_{\mathrm{N}} \sum_{\mathrm{E},\mathrm{E}'} \hat{\mathcal{P}}_{\mathrm{NE}} \Big\{ \hat{\mathrm{d}}_i \, \hat{\mathcal{P}}_{(\mathrm{N}+1)\mathrm{E}'} \, \hat{\mathrm{d}}_j^\dagger \, T_{ij}^\eta(\mathrm{E}' - \mathrm{E}) \, f_\eta^+ \left(\mathrm{E}' - \mathrm{E}\right) \\ - \hat{\mathrm{d}}_i^\dagger \, \hat{\mathcal{P}}_{(\mathrm{N}-1)\mathrm{E}'} \, \hat{\mathrm{d}}_j \, T_{ij}^\eta(\mathrm{E} - \mathrm{E}') \, f_\eta^- \left(\mathrm{E} - \mathrm{E}'\right) \Big\} \hat{\mathcal{P}}_{\mathrm{NE}}. \tag{3.62}$$

Now that we have finally built up the formalism, enabling us to compute the tunneling onto and out of the molecule, we will turn our attention towards the latter to investigate its quantum mechanical properties.

4. Phthalocyanine

In this work we wish to study the properties of electronic transport through phthalocyanine molecules on a thin insulating layer. To this end, we first have to understand their geometrical and physical properties.

Phthalocyanines (Pc's) are organic macrocycles built of an inner ring of alternating carbon and nitrogen atoms to which four benzene rings are bonded, so that the whole molecule has a cross-shaped appearance. Two of the inner nitrogen atoms of the inner ring are each bonded to a hydrogen atom. Although this constellation is named phthalocyanine in most literature, for reasons of clearness we will refer to it from now on as hydrogen phthalocyanine (H_2Pc). The central hydrogen atoms can be substituted by a huge variety of metals, including Fe, Cu, Ni, Co, Zn and Mg.

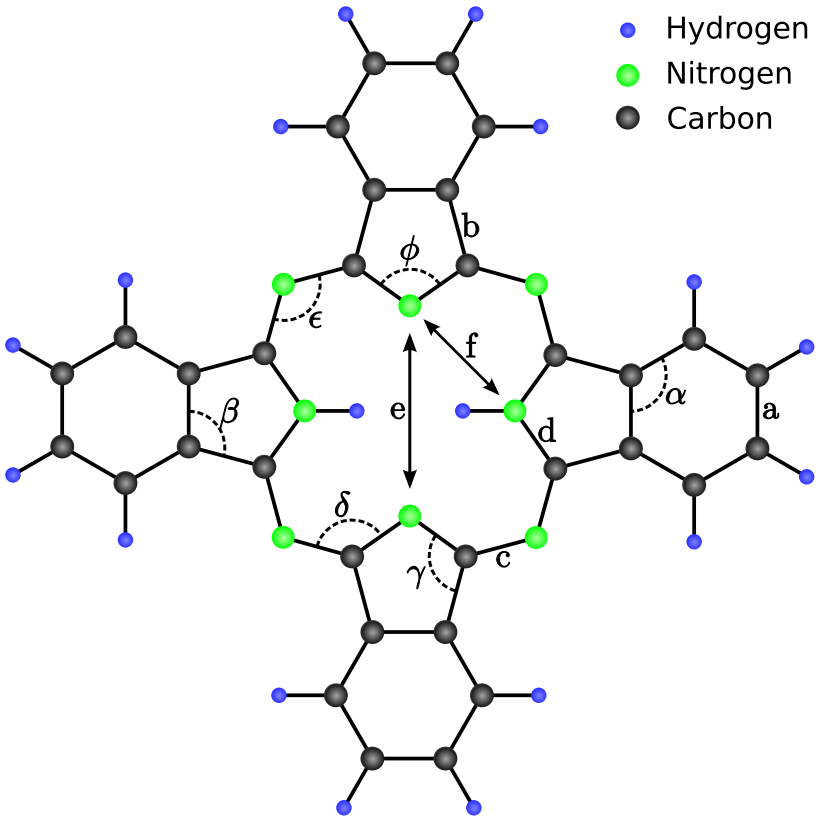

Figure 4.1.: *Hydrogen Phthalocyanine and its geometrical parameters.*

Parameter	Value	Taken from	Value used in thesis
d_{CH}	1.09 Å	[LS01]	1.09 Å
d_{NH}	1.00 Å	[DWP98]	1.00 Å
a	1.40 Å	[DH03]	1.40 Å
b	1.50 Å	[DH03]	1.50 Å
c	1.40 Å	[DH03]	1.40 Å
d	1.35 Å	[DH03]	1.35 Å
e	3.65 Å - 4.50 Å	[DH03]	4.03 Å
f	2.60 Å - 2.85 Å	[DH03]	2.85 Å
α	120°	[DH03]	120°
β	105°	[DH03]	105°
γ	110°	[DH03]	110°
δ	120° - 130°	[DH03]	130°
ϵ	115° - 125°	[DH03]	120°
ϕ	100° - 110°	[DH03]	110°

Table 4.1.: *Parameters for H_2Pc.*

In the unsubstituted (Pc) case, where the two central hydrogen atoms are not taken into account, the molecule can be split into four rotational unit cells, so that it can be described by only a small number of parameters. For some of them, definite values are given in the literature, whereas other parameters have to be matched to reproduce the geometry of the phthalocyanine ring. These parameters are listed in Tab. 4.1. In the case of naked Pc, each unit cell consists of two nitrogen, eight carbon and four hydrogen atoms. Like in benzene, the carbon and nitrogen atoms in Pc have a sp^2 hybridization built up by their 2s, $2p_x$ and $2p_y$ orbitals, so the structure of the molecule is planar. The remaining $2p_z$ orbitals are pointing out of that plane.

4.1. Hydrogen phthalocyanine

4.1.1. Extended Hückel Hamiltonian and Slater-Koster tight-binding method

In a first step we set up the single particle Hamiltonian for the H_2Pc molecule. The approximation used in this thesis is based on an extended Hückel [Hof63] approach on the one hand and an approach proposed by Slater and Koster [SK54] on the other hand. The goal of our approach is to set up molecular orbitals (MOs) from the localized atomic orbitals. Unlike e.g. for benzene, where the molecule consists of the same type of atoms with identical angles and distances between each other, for H_2Pc we have to take into account the contribution of the σ-system. The σ-system consists of MOs that are built of atomic orbitals lying in the molecular plane. At the end of the day, the σ-system

in hydrogen phthalocyanine contributes in a shifting of the onsite energies in the H_2Pc molecule. However, in benzene this contribution can be neglected. The π-system is made up of p_z orbitals pointing out of the molecular plane. Note that these definitions are a bit misleading and have not to be confused with the definition of π- and σ-bonds, since a bond between two atoms that is lying in plane can also be of π-type actually.
The extended Hückel Hamiltonian we have to set up for H_2Pc has the form:

$$\mathcal{H} = \sum_{\nu} \epsilon_\nu \hat{\mathrm{d}}_\nu^\dagger \hat{\mathrm{d}}_\nu + \sum_{\langle \nu, \nu' \rangle} b_{\nu\nu'} \hat{\mathrm{d}}_\nu^\dagger \hat{\mathrm{d}}_{\nu'}, \tag{4.1}$$

where $\nu = (\alpha, l_m, \tau)$ and $\nu' = (\alpha', l'_{m'}, \tau')$ are multi-indices consisting of the site number, e.g. in the case of H_2Pc $\alpha \in \{1, 2, \ldots 58\}$, the orbital quantum number l_m and a spin index τ, which again will be omitted in the following. To specify an atomic orbital it suffices to have only the indices l, denoting its angular momentum, and their magnetic quantum number m, as we only take into account the valence electrons of each atom. Hence the corresponding atomic orbitals are clearly defined $l \in \{0, 1, 2, \ldots\}$ and $m \in \{-l, \ldots, l\}$. For carbon and nitrogen it is clear that their valence electrons are in $2s$ and $2p$ orbitals, while for hydrogen the electron would be in a $1s$ orbital. However, we will use the common notation $l \in \{s, p, d, f, \ldots\}$ and, by using the real representation of the atomic orbitals as shown in Eq. (2.41), let $m \in \{x, y, z, z^2, \ldots\}$ depict their spatial orientation.

$\nu = (\alpha, l_m)$	(H, s)	(C, s)	(C, p)	(N, s)	(N, p)
ϵ_ν [eV]	-13.6	-19.38	-11.07	-26.22	-13.84

Table 4.2.: *Relevant orbital energies, taken from [Har99]. Here α depicts the type of atom at the corresponding site.*

The parameter $\epsilon_\nu = \langle \nu | \mathcal{H} | \nu \rangle$ is the onsite energy of an electron with a set of quantum numbers ν. The different ϵ_ν are listed in Tab. 4.2. The hopping parameter $b_{\nu\nu'} = \langle \nu | \mathcal{H} | \nu' \rangle$ describes the interaction between atomic orbitals of neighbouring atoms and is calculated by using the approach proposed by Slater and Koster. Here the overlap integrals $\langle \nu | \mathcal{H} | \nu' \rangle$ are expressed in terms of two-center integrals $V_{ll'\varsigma}$ and several geometrical factors, which depend on the direction cosines of the bond vector towards the coordinate axes and the spatial orientation of the contributing orbitals. The type of the overlapping orbitals is denoted by l and l'. The index ς labels the type of bonding (π, σ or δ).
Hence, a general expression for the matrix element $\langle \nu | \mathcal{H} | \nu' \rangle$ between two states with quantum numbers ν and ν' is given by:

$$\langle \nu | \mathcal{H} | \nu' \rangle = b_{\nu\nu'} = \sum_{\varsigma} V_{\nu\nu'\varsigma} f_\varsigma(\alpha, \beta, \gamma), \tag{4.2}$$

where $f_\varsigma(\alpha, \beta, \gamma)$ is a function of the direction cosines α, β and γ calculated between the x-, y- and z-axis and the bond vector of two neighbouring atoms. The function $f_\varsigma(\alpha, \beta, \gamma)$ cannot be given universally but has to be worked out for different orientations of the participating orbitals; either by following the rules given by Harrison [Har99] and decomposing

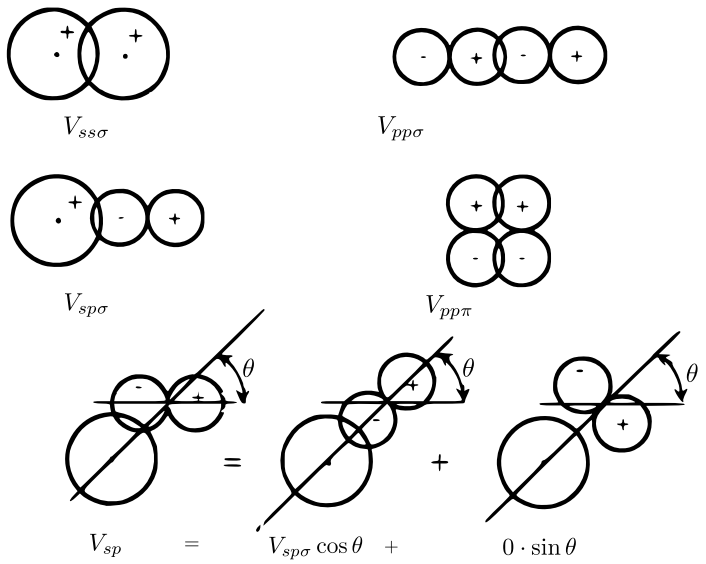

Figure 4.2.: *Several interatomic matrix elements for s- and p-orbitals. By decomposing p-orbitals in components parallel and perpendicular to the bond, one can set up the matrix elements for orbitals which are orientated in a different way. If the configuration is different from the above ones respective to the ± orientation of the involved p orbitals, the sign of the overlap integral changes. Picture taken from [Har99].*

the orbitals into components parallel and perpendicular to their bond as seen in Fig. 4.2 or by using the relations derived by Slater and Koster (see Tab. 4.4). The overlap integrals $V_{\nu\nu'\varsigma}$ are given by [Har99]:

$$V_{\nu\nu'\varsigma} = \eta_{ll'\varsigma} \frac{\hbar^2}{m_e d_{\alpha\alpha'}^2}, \tag{4.3}$$

where m_e is the mass of the electron and $d_{\alpha\alpha'}$ is the distance between the corresponding atomic sites α and α'. The $\eta_{ll'\varsigma}$ have been calculated by W. A. Harrison and are considered to be universal parameters [Har81]. In App. A.3 we show how the matrix elements are computed considering the orbitals of the nitrogen atom at site 1 and the carbon atom at site 2 (see Fig. 4.3).

$\eta_{ss\sigma}$	$\eta_{sp\sigma}$	$\eta_{pp\sigma}$	$\eta_{pp\pi}$
-1.32	1.42	2.22	-0.63

Table 4.3.: *Overlap integral coefficients, taken from [Har99].*

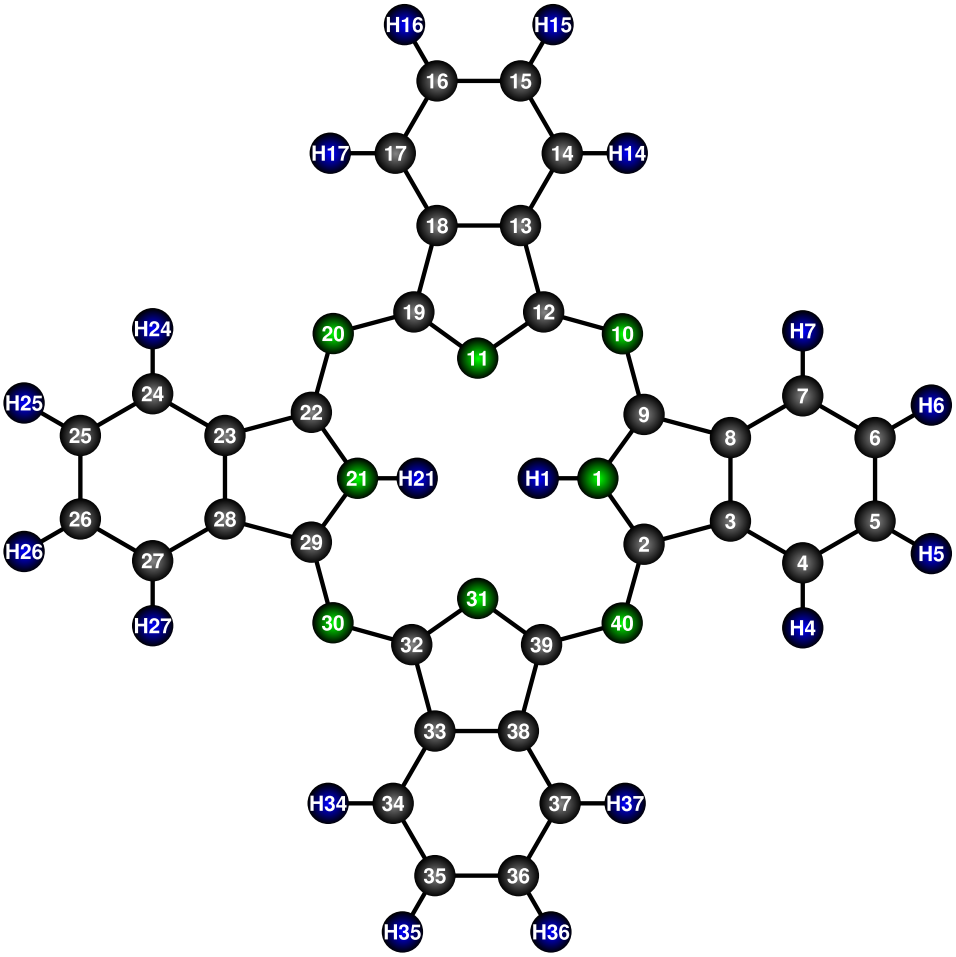

Figure 4.3.: *Numbering scheme for* H_2Pc.

Orientations $l_m, l'_{m'}$	$b_{\nu\nu'}$
s, s	$V_{ss\sigma}$
s, p_x	$\alpha\, V_{sp\sigma}$
p_x, p_x	$\alpha^2\, V_{pp\sigma} + (1-\alpha^2)\, V_{pp\pi}$
p_x, p_y	$\alpha\beta\, V_{pp\sigma} - \alpha\beta\, V_{pp\pi}$
p_x, p_z	$\alpha\gamma\, V_{pp\sigma} - \alpha\gamma\, V_{pp\pi}$
s, d_{xy}	$\sqrt{3}\,\alpha\beta\, V_{sd\sigma}$
$s, d_{x^2-y^2}$	$\frac{1}{2}\sqrt{3}\,(\alpha^2-\beta^2)\, V_{sd\sigma}$
s, d_{z^2}	$(\gamma^2 - \frac{1}{2}(\alpha^2+\beta^2))\, V_{sd\sigma}$
p_x, d_{xy}	$\sqrt{3}\,\alpha^2\beta\, V_{pd\sigma} + \beta(1-2\alpha^2)\, V_{pd\pi}$
p_x, d_{yz}	$\sqrt{3}\,\alpha\beta\gamma\, V_{pd\sigma} - 2\alpha\beta\gamma\, V_{pd\pi}$
p_x, d_{zx}	$\sqrt{3}\,\alpha^2\gamma\, V_{pd\sigma} + \gamma(1-2\alpha^2)\, V_{pd\pi}$
$p_x, d_{x^2-y^2}$	$\frac{1}{2}\sqrt{3}\,\alpha(\alpha^2-\beta^2)\, V_{pd\sigma} + \alpha(1-\alpha^2+\beta^2)\, V_{pd\pi}$
$p_y, d_{x^2-y^2}$	$\frac{1}{2}\sqrt{3}\,\beta(\alpha^2-\beta^2)\, V_{pd\sigma} - \beta(1+\alpha^2-\beta^2)\, V_{pd\pi}$
$p_z, d_{x^2-y^2}$	$\frac{1}{2}\sqrt{3}\,\gamma(\alpha^2-\beta^2)\, V_{pd\sigma} - \gamma(\alpha^2-\beta^2)\, V_{pd\pi}$
p_x, d_{z^2}	$\alpha(\gamma^2 - \frac{1}{2}(\alpha^2+\beta^2))\, V_{pd\sigma} - \sqrt{3}\,\alpha\gamma^2\, V_{pd\pi}$
p_y, d_{z^2}	$\beta(\gamma^2 - \frac{1}{2}(\alpha^2+\beta^2))\, V_{pd\sigma} - \sqrt{3}\,\beta\gamma^2\, V_{pd\pi}$
p_z, d_{z^2}	$\gamma(\gamma^2 - \frac{1}{2}(\alpha^2+\beta^2))\, V_{pd\sigma} - \sqrt{3}\,\gamma(\alpha^2+\beta^2)\, V_{pd\pi}$

Table 4.4.: *Some overlap integrals in terms of two-center integrals as derived by Slater and Koster [SK54]. Here symbols α, β, and γ are the direction cosines of the bond vector respective to the x-, the y- and the z-axis. Other matrix elements can be obtained by cyclically permuting the indices and cosines.*

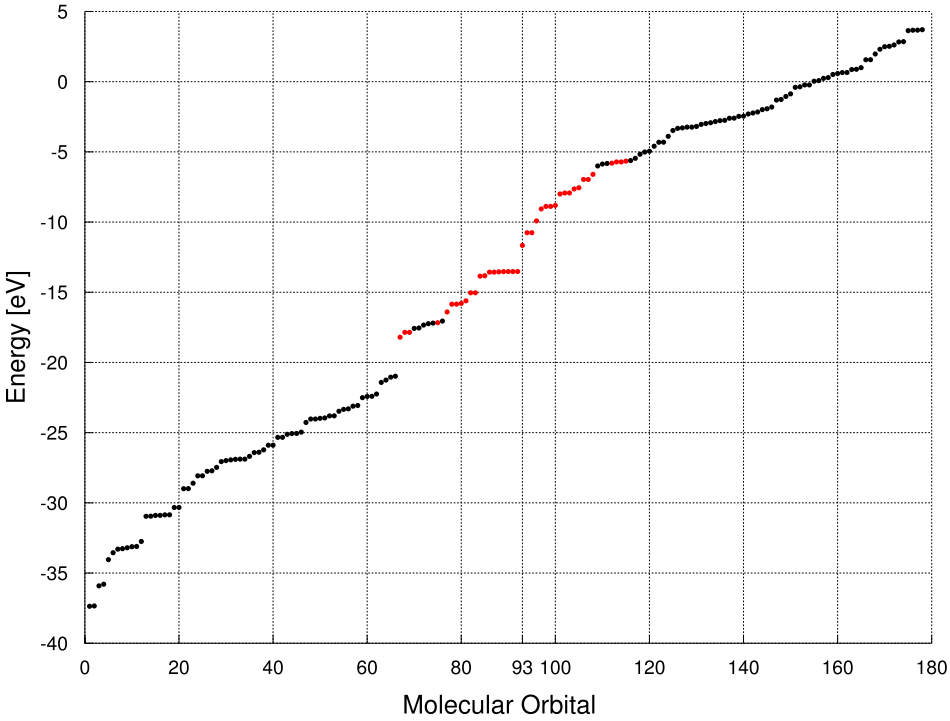

Figure 4.4.: *Calculated single particle spectrum of* H_2Pc *before Mulliken correction of the energies. Red and black dots depict energies corresponding to* π *or* σ *molecular orbitals respectively.*

4.1.2. Effective Hamiltonian for hydrogen phthalocyanine

Considering five valence electrons for nitrogen, four for carbon and one valence electron for hydrogen, the total number of valence electrons in H_2Pc sums up to 186. If we are assuming that the MOs, each containing two electrons (one with spin up and one with spin down), are filled ascending with their energies, a total number of 93 molecular orbitals will be occupied. By construction, the numerical diagonalization of the Hamiltonians associated with the π and the σ system can be performed separately. From this we get the eigenstates $|i\rangle$ which are the molecular orbitals, together with the corresponding eigenenergies:

$$|i\rangle = \sum_{\nu} c_{\nu i} |\nu\rangle , \tag{4.4}$$

$$\mathcal{H} |i\rangle = \epsilon_i |i\rangle . \tag{4.5}$$

The lowest 93 eigenenergies are those from occupied MOs. In our numerical calculations, we can sort the calculated eigenvalues from the π- together with those of the σ-system energetically. If we keep track of which eigenvalue comes from either system, we see that, on the one hand, 72 σ-type MOs are occupied. On the other hand, in a wide range around the Fermi level the only occupied molecular orbitals are π-type MOs.

As for transport the states in this range are the most relevant ones, we want to focus only on the π-system in our further calculations. Because the effects of the two hydrogen atoms can only come into our model through the σ-system, we somehow have to transfer these effects onto the π-system. This can be done by calculating the Mulliken charge for each atomic site α [Rei06]:

$$Q_\alpha^M = 2e \sum_{i,\, l_m} |c_{(\alpha,l_m)i}|^2. \tag{4.6}$$

The index i runs through all occupied σ molecular orbitals. The Mulliken charge reflects the delocalization of each atomic valence electron in the σ-system due to the forming of molecular orbitals. Carbon for example has four valence electrons. Three of them occupy orbitals in the σ-system, so one would expect that the remaining electron in the p_z orbital experiences a charge of $3e$. For nitrogen, lending five valence electrons from which four belong to the σ system, one consequently would expect a charge of $4e$. However, due to delocalization the Mulliken charge has a different value which can be calculated using Eq. (4.6). This difference then can be connected with an altering of the onsite energies of the p_z orbitals at the respective atomic sites. The energy difference is given by:

$$\Delta\epsilon_{(\alpha,p_z)} = \frac{Q_\alpha^0 - Q_\alpha^M}{Q_\alpha^0}\, \epsilon_{(\alpha,p_z)}. \tag{4.7}$$

At a nitrogen atom, where a hydrogen is bonded to (e.g. site 1), the calculated Mulliken charge is $3.4e$, which is lower than the expected charge of $4e$. In a simple electrostatic picture this means an electron will experience less repulsion than expected. Therefore the onsite energy of its p_z orbital is effectively lowered. As the Mulliken charge represents the average number of σ electrons localized at a specific atom, we can conclude, that at this nitrogen atom approximately two electrons from the π system are occupying the p_z orbital. On the other hand, the effective charge of a nitrogen atom which is not coupled to a hydrogen atom (e.g. site 11) is $4.13e$, which results in a higher repulsion of an electron populating its p_z orbital. Because of this, the effective onsite energy of the p_z orbital at this atomic site is scaled up. With this in hand, we are able to set up an effective Hamiltonian for the π-system which reflects the contribution of the σ-system:

$$\mathcal{H} = \sum_\alpha (\epsilon_{(\alpha,p_z)} + \Delta\epsilon_{(\alpha,p_z)})\, \hat{\mathrm{d}}_\alpha^\dagger \hat{\mathrm{d}}_\alpha + \sum_{\langle \alpha,\, \alpha' \rangle} b_{(\alpha,p_z)(\alpha',p_z)\pi}\, \hat{\mathrm{d}}_\alpha^\dagger \hat{\mathrm{d}}_{\alpha'}. \tag{4.8}$$

Diagonalizing this Hamiltonian gives us new molecular orbitals which are respecting the geometrical and symmetrical properties of the molecule. From the eigenvalues of the molecular orbitals we also see that the highest occupied molecular orbital (HOMO) in H_2Pc is the 21^{st} orbital from the π-system. The lowest unoccupied molecular orbital (LUMO) and the MO below the HOMO (HOMO-1), which are very important for transport calculations, also stem from the π-system. So we can safely restrict our further calculations to the π-system and thus to the 40 p_z orbitals pointing out of the molecular plane.
In order to do transport calculations, we need a suitable many-body representation of our system, that is, we have to introduce some sort of electron-electron interaction. However,

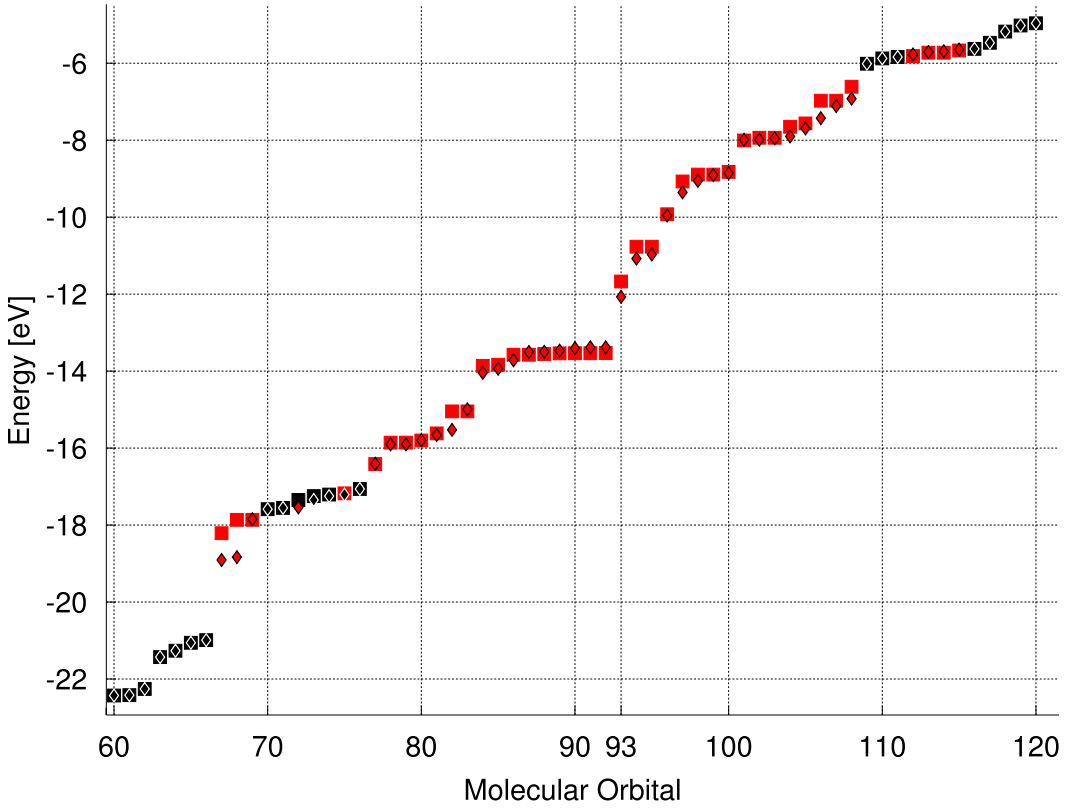

Figure 4.5.: *Comparison of calculated molecular orbital energies of* H_2Pc *around the fermi level before (squares) and after (diamonds) Mulliken correction. Again, red and black markers depict energies corresponding to* π *and* σ *orbitals respectively. Orbital 93 is the highest occupied molecular orbital.*

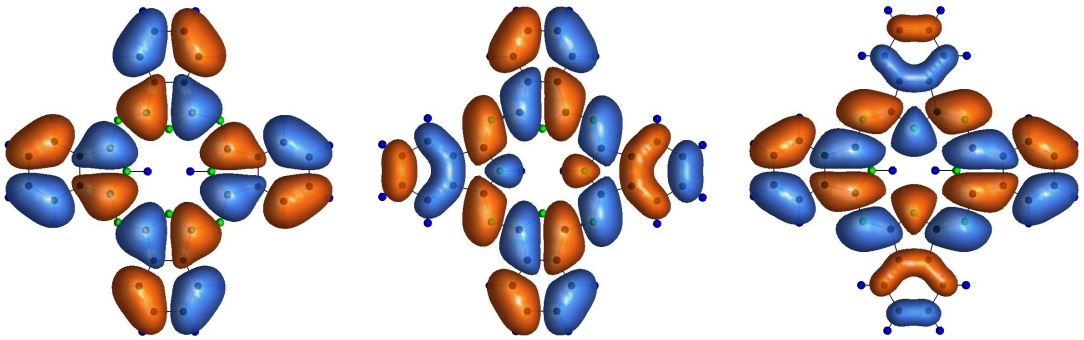

(a) HOMO (b) LUMO (c) LUMO+1

Figure 4.6.: *Depiction of the HOMO, LUMO and LUMO+1 molecular orbitals of* H_2Pc.

including full Coulomb interaction between all electrons occupying the different molecular orbitals of hydrogen phthalocyanine turns out to be a bad strategy: with 40 molecular orbitals being available for occupation, the resulting Fock space would have dimension 4^{40}. We therefore restrict to a much simpler constant-interaction model [KAT01].

4.1.3. Constant-interaction model

The constant-interaction model [KAT01] approximates the total energy E_N of an N-particle ground state of the molecule by the following equation:

$$E_N = \sum_{\substack{i,\sigma \\ \sum n_{i\sigma}=N}} \epsilon_i n_{i\sigma} + \frac{U}{2}\left(N - N_0\right)^2, \tag{4.9}$$

where ϵ_i is the energy of the single particle molecular orbital i that is occupied by $n_{i\sigma}$ electrons with spin σ. N_0 is the total number of π orbitals and U accounts for the Coulomb interaction. The parameter U is related to a constant charging energy for an electron on a capacitor with capacitance C:

$$U = \frac{e^2}{C}. \tag{4.10}$$

Thus, the corresponding Hamilton operator for the molecule including the constant interaction is given by:

$$\hat{\mathcal{H}} = \sum_{i,\sigma} \epsilon_i \hat{\mathrm{d}}^\dagger_{i\sigma}\hat{\mathrm{d}}_{i\sigma} + \frac{U}{2}\left(\hat{N} - N_0\right)^2, \tag{4.11}$$

with

$$\hat{N} = \sum_{i,\sigma} \hat{\mathrm{d}}^\dagger_{i\sigma}\hat{\mathrm{d}}_{i\sigma}. \tag{4.12}$$

The two main assumptions of the constant-interaction model are that all electronic interactions can be put into a constant capacitance C and that the single particle molecular orbitals and eigenenergies are unsensible against changes arising due to the presence of metallic contacts. Hence, we have to find a reasonable value for the parameter U, such that the molecule is in its neutral state when there is no bias voltage applied.

Determining the parameter for the Coulomb interaction

We are considering a system with variable particle number which is capacitively coupled to two reservoirs. At zero bias voltage, their chemical potentials are equal to $-\phi_0^{sub}$ or $-\phi_0^{tip}$, respectively, since we put the zero of the energy to the "vacuum" (see Fig. 2.2). As an approximation we choose both workfunctions to be equal $\phi_0^{sub} = \phi_0^{tip} \equiv \phi_0$, meaning that for the chemical potential at zero bias we have $\mu_G = -\phi_0$. Thus we have to ensure that the expectation value of the Hamilton operator $\hat{\mathcal{H}}_G$, which corresponds to a grand

canonical ensemble, is minimal at the particle number N that refers to the neutral state of the molecule [LP80, BF04]. Hence in the case of H_2Pc this minimum must lie at $N = 42$. The Hamiltonian $\hat{\mathcal{H}}_G$ is given by:

$$\hat{\mathcal{H}}_G = \hat{\mathcal{H}} - \mu_G \hat{N}. \tag{4.13}$$

The corresponding expectation value with an N-particle wavefunction is:

$$E'_N = \langle N|\hat{\mathcal{H}}_G|N\rangle = E_N - \mu_G N. \tag{4.14}$$

Work functions of common materials used in STM measurements are in the range of 4 to 5 eV. Thus, using $\mu_G = -4$ eV we obtain a range 2.82 eV $\leq U \leq$ 5.38 eV for which the expectation value $\langle N|\hat{\mathcal{H}}_G|N\rangle$ for the neutral state of H_2Pc is minimal.

Comparison with experimental results

Based on results in STS (scanning tunneling spectroscopy) and photoemission spectroscopy experiments on phthalocyanines (for example in [TT05] for CoPc, [ZGG06]), we expect that the HOMO-LUMO gap Δ_{HL} is about 1.5 eV to 2.5 eV. This is given by

$$\Delta_{\mathrm{HL}} = E_{43} - E_{42} - (E_{42} - E_{41}). \tag{4.15}$$

It is related to the distance of the resonant peaks corresponding to the frontier orbitals (HOMO and LUMO) in STS spectra . However, with the empirical value found for the Coulomb interaction U we obtain a rather big HOMO-LUMO gap. It ranges in the interval 2.82 eV $\leq \Delta_{\mathrm{HL}} \leq$ 5.38 eV. To figure out which factors contribute to this deviation, we will now decompose the occuring quantities. The electron affinity (or EA) is the change in energy when an electron is added to the neutral molecule. Thus, by exploiting the definition of the total energy E_N, we get:

$$\mathrm{EA} = E_{43} - E_{42} = \epsilon_{\mathrm{L}} + \frac{5}{2}U, \tag{4.16}$$

where ϵ_{L} is the single particle energy of the LUMO orbital. The ionization potential (IP) is the change in energy when removing an electron from the neutral molecule. Again,

$$\mathrm{IP} = E_{42} - E_{41} = \epsilon_{\mathrm{H}} + \frac{3}{2}U. \tag{4.17}$$

Consequently, ϵ_{H} denotes the single particle energy of the HOMO orbital. By writing $\delta_{\mathrm{HL}} = \epsilon_{\mathrm{L}} - \epsilon_{\mathrm{H}}$ for the difference between the single particle HOMO and LUMO energies, we get for the HOMO-LUMO gap:

$$\Delta_{\mathrm{HL}} = \mathrm{EA} - \mathrm{IP} = \delta_{\mathrm{HL}} + U. \tag{4.18}$$

The quantity δ_{HL} is determined by the single particle spectrum of phthalocyanine calculated in Sec. 4.1.2. Its value is $\delta_{\mathrm{HL}} = 1.0$ eV. So one contribution to the deviation is caused by our emprical choice of U. If we want to make it smaller we have to renormalize the single

particle energies as they appear in both EA and IP. To this end we compare EA, IP and Δ_{HL} with results from a combined VB-PES (valence band photoemission spectroscopy) and IPES (inverse PES) experiment done for organic semiconductors including various types of phthalocyanines [ZGG06]. They found a HOMO-LUMO gap $\tilde{\Delta}_{\mathrm{HL}} = 2.2$ eV, an electron affinity $\tilde{\mathrm{EA}} = -2.74$ eV and an ionization potential $\tilde{\mathrm{IP}} = -4.96$ eV. With these numbers we are now able to derive

$$\tilde{U} = \tilde{\Delta}_{\mathrm{HL}} - \delta_{\mathrm{HL}} = 1.2 \text{ eV}, \tag{4.19}$$

$$\tilde{\epsilon}_{\mathrm{L}} = \tilde{\mathrm{EA}} - \frac{5}{2}\tilde{U} = -5.74 \text{ eV}, \tag{4.20}$$

$$\tilde{\epsilon}_{\mathrm{H}} = \tilde{\mathrm{IP}} - \frac{3}{2}\tilde{U} = -6.76 \text{ eV}. \tag{4.21}$$

We notice that $\tilde{\epsilon}_{\mathrm{L}} - \epsilon_{\mathrm{L}} \approx \tilde{\epsilon}_{\mathrm{H}} - \epsilon_{\mathrm{H}} \approx 5.3$ eV. Thus, if we renormalize the single particle energies by this energy, we can render our many-body spectrum more comparable to the experimental situation. Also, if we check the expectation values $\langle N|\hat{\mathcal{H}}_G|N\rangle$ of our system using the new parameter $\tilde{U}$ for the Coulomb interaction and the renormalized energies we find its minimum still at the neutral state. We have for the differences in E':

$$\begin{aligned} E'_{41} - E'_{40} &= -2.18 \text{ eV}, \\ E'_{42} - E'_{41} &= -0.98 \text{ eV}, \\ E'_{43} - E'_{42} &= 1.22 \text{ eV}, \\ E'_{44} - E'_{43} &= 2.42 \text{ eV}. \end{aligned}$$

In a recent publication [KF11] it has been proposed, that image charge effects play a large role in single-molecule junctions. According to the authors, for benzene, they result in a large shifting of the onsite energies and the Coulomb interaction. Referring to this, we can justify the renormalization of our single-particle energies. However, an analytic proof would require solving Poisson's equation for our system, which is out of the scope of the present thesis.

4.2. Metal phthalocyanine

In metal phthalocyanine (MPc) one central metal atom instead of two hydrogen atoms is bonded to the organic macrocycle. A prominent member in the family of metal phthalocyanines is copper phthalocyanine (CuPc) which, as a dye, is very well known under the name phthalo blue. Copper has 11 valence electrons: the 3d shell is completely filled and one unpaired electron is populating the 4s shell.

4.2.1. Single particle Hamiltonian for copper phthalocyanine

Again we use the Slater-Koster tight binding method to set up the single particle Hamiltonian for metal phthalocyanine. Considering the type of metal we will focus on copper;

$\epsilon_{(Cu,s)}$	$\epsilon_{(Cu,d)}$	r_d	r_p	$\eta_{sd\sigma}$	$\eta_{pd\sigma}$	$\eta_{pd\pi}$
$-7.72\,\mathrm{eV}$	$-20.26\,\mathrm{eV}$	$0.688\,\text{Å}$	$5.29\,\text{Å}$	-3.16	$-\frac{3\sqrt{15}}{2\pi}$	$\frac{3\sqrt{5}}{2\pi}$

Table 4.5.: *Parameters needed to set up the Hamiltonian for* CuPc. *Taken from [Har99, Har89].*

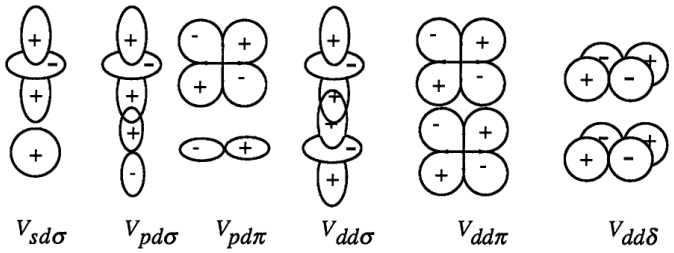

Figure 4.7.: *Interatomic matrix elements involving d orbitals. Taken from [Har99].*

other metals can be included in a similar way, provided the resulting compound also has a planar shape. This is the case for Be and Mg and metals in the periodic table between Cr and Zn [DH03]. Due to the central position of the metal atom, the in-plane direction cosines α and β needed for the matrix elements are either zero or one and the direction cosine γ respective to the z-axis actually is always zero. This significantly reduces the amount of different matrix elements. The general form of overlap integrals $V_{\nu\nu'\varsigma}$ involving d orbitals is given by [Har99]:

$$V_{(i,s)(i',d)\sigma} = \eta_{sd\sigma}\frac{\hbar^2 r_d^{3/2}}{m_e d_{ii'}^{7/2}}, \tag{4.22}$$

$$V_{(i,p)(i',d)\varsigma} = \eta_{pd\varsigma}\frac{\hbar^2\sqrt{r_p r_d^3}}{m_e d_{ii'}^4}, \tag{4.23}$$

where r_p and r_d are the element-specific p-state and d-state radii, here from nitrogen and copper respectively. These and the other parameters needed to calculate the matrix elements are given in Tab. 4.5.
Using Tab. 4.4 and Fig. 4.7 we now demonstrate the calculation of the matrix elements regarding the copper orbitals at site 57 with the orbitals of the nitrogen atom at site 1. As the bond vector of the two atoms lies on the x-axis, the first few matrix elements involving s and p orbitals are rather easy to evaluate. The only nonvanishing are:

$$b_{(57,s)(1,s)} = \eta_{ss\sigma}\frac{\hbar^2}{m_e d_{57,1}^2}, \tag{4.24}$$

$$b_{(57,s)(1,p_x)} = \eta_{sp\sigma}\frac{\hbar^2}{m_e d_{57,1}^2}. \tag{4.25}$$

Again, only two of the matrix elements between the d_{z^2} orbital and the orbitals of the nitrogen atom are different from zero:

$$b_{(57,d_{z^2})(1,s)} = -\frac{1}{2}\eta_{sd\sigma}\frac{\hbar^2 r_d^{3/2}}{m_e d_{57,1}^{7/2}}, \tag{4.26}$$

$$b_{(57,d_{z^2})(1,p_x)} = \frac{1}{2}\eta_{pd\sigma}\frac{\hbar^2\sqrt{r_p r_d^3}}{m_e d_{57,1}^4}. \tag{4.27}$$

The matrix elements involving the $d_{x^2-y^2}$ orbital are:

$$b_{(57,d_{x^2-y^2})(1,s)} = \frac{\sqrt{3}}{2}\eta_{sd\sigma}\frac{\hbar^2 r_d^{3/2}}{m_e d_{57,1}^{7/2}}, \tag{4.28}$$

$$b_{(57,d_{x^2-y^2})(1,p_x)} = -\frac{\sqrt{3}}{2}\eta_{pd\sigma}\frac{\hbar^2\sqrt{r_p r_d^3}}{m_e d_{57,1}^4}. \tag{4.29}$$

The last orbital that gives nonvanishing matrix elements with the in-plane orbitals is the d_{xy} orbital. Its contribution reads:

$$b_{(57,d_{xy})(1,p_y)} = -\eta_{pd\pi}\frac{\hbar^2\sqrt{r_p r_d^3}}{m_e d_{57,1}^4}. \tag{4.30}$$

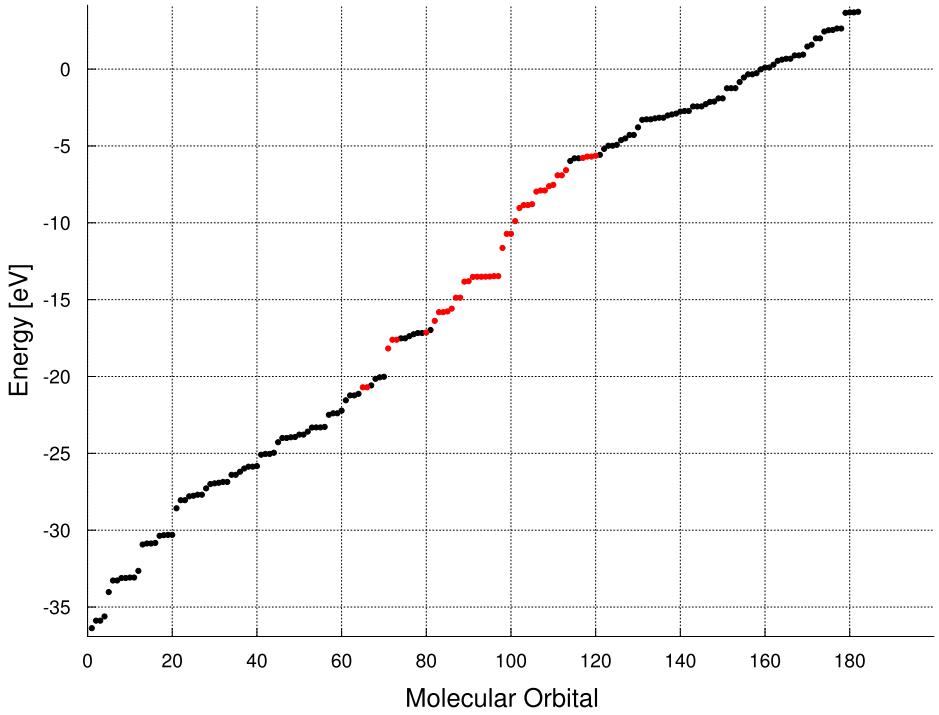

Figure 4.8.: *Calculated molecular orbital eigenenergies of the* CuPc *molecule. Black and red dots depict energies of orbitals from the σ and the π system, respectively.*

There is only one nonvanishing matrix element for the p_z orbital of the nitrogen atom at site 1 . It results from an overlap with the d_{xz} orbital of copper:

$$b_{(57,d_{xz})(1,p_z)} = -\eta_{pd\pi}\frac{\hbar^2\sqrt{r_p r_d^3}}{m_e d_{57,1}^4}. \tag{4.31}$$

After calculating all matrix elements, we are finally able to write down the single particle Hamiltonian for CuPc:

$$\mathcal{H} = \sum_{\nu} \epsilon_\nu \hat{\mathrm{d}}_\nu^\dagger \hat{\mathrm{d}}_\nu + \sum_{\langle \nu,\nu' \rangle} b_{\nu\nu'} \hat{\mathrm{d}}_\nu^\dagger \hat{\mathrm{d}}_{\nu'}. \tag{4.32}$$

Again, we use the multi-index notation $\nu = (i, l_m, \tau)$, where now the site index i can have values $i \in \{1, 2, \ldots 57\}$. For l and m we now have $l \in \{s, p, d\}$ and $m \in \{x, y, z, z^2, x^2 - y^2, xy, yz, xz\}$. After the numerical diagonalization of this Hamiltonian we obtain the molecular orbitals of CuPc; among those we have to distribute the 195 valence electrons, meaning that the expected HOMO will be the 98st molecular orbital. Around this orbital all other molecular orbitals stem from the π system. The lowest 75 molecular orbitals of the σ system are occupied.

4.2.2. Many-body representation for copper phthalocyanine

Also for copper phthalocyanine we have to set up a many-body representation. However, if we proceed like in the case of H_2Pc and consecutively fill each molecular orbital with two electrons, we end up with a HOMO orbital that is half filled, due to the odd number of total valence electrons in the molecule. With this situation, being greatly counterintuitive, the question arises where to put this single electron, or, in other words, which molecular orbital lying energetically below the HOMO should lend an electron to it to fill the vacancy. There are several papers [ECS+07, dOea10, CFN07] that predict the existence of a SOMO (singly occupied molecular orbital) lying in the gap between HOMO and LUMO and revealing $d_{x^2-y^2}$ character, thus stemming from the σ-system. But if we look at our single particle spectrum of CuPc (Fig. 4.8), we find no such orbital that could play the role of a SOMO. By shifting the onsite energies of the central copper atom we can achieve that an orbital from the σ-system rises energetically between HOMO and LUMO and we see that it has the desired $d_{x^2-y^2}$ character, too. How to justify this shifting and how to deal with the degenerate HOMO-1 and LUMO orbitals needs further examination and is still work in progress.

5. Transport spectroscopy and imaging of hydrogen phthalocyanine

Now we are finally able to study the transport properties of single phthalocyanine molecules underlying an STM setup. Different from the typical setup of a lateral quantum dot, the STM setup implicates an asymmetrical tunneling junction [vdML10]. This means that the chemical potentials of the substrate μ_S and the tip μ_T, appearing in the Fermi functions, do not change symmetrically with the applied bias voltage $eV_b = \mu_T - \mu_S$. This asymmetry is realized by defining the chemical potentials of the contacts as

$$\mu_T = \mu_G + c \cdot eV_b, \tag{5.1}$$
$$\mu_S = \mu_G - (1-c) \cdot eV_b, \tag{5.2}$$

where the factor c accounts for the drop of the electrostatic potential between the electrodes. In a symmetrical junction c would be 0.5, in our case it can be estimated by $c = \frac{\epsilon_r}{1+\epsilon_r}$, with ϵ_r being the relative permittivity of the insulating layer lying atop of the substrate. For NaCl we have $\epsilon_r = 5.9$, thus yielding a factor $c = 0.86$.
In order to do transport calculations, we have to evaluate the GME to obtain the stationary solution of the reduced density matrix. Thereby we restrict our calculations to molecular orbitals around the HOMO orbital and, as pointed out in Sec. 4.1.3, neglect excited states of our system. This means that we allow only transitions that result in a ground state for the corresponding particle number. This approximation can be justified by the fact that we are doing the calculations in the low-bias regime, meaning that excited states are energetically out of reach.
Finally, we get a set of coupled differential equations for the diagonal entries of the reduced density matrix, called populations. As an example we give the differential equations for the 42- and 43-particle populations. In the 42-particle configuration all molecular orbitals up to the HOMO are doubly filled, consequently in the 43-particle configuration one additional electron is occupying the LUMO orbital. The corresponding differential equations read:

$$\dot{\rho}_{42} = \sum_{\sigma} \left(\Gamma^{+}_{21}(\mu_{42})\rho_{41\sigma} - \left(\Gamma^{+}_{22}(\mu_{43}) + \Gamma^{-}_{21}(\mu_{42}) \right) \rho_{42} + \Gamma^{-}_{22}(\mu_{43})\rho_{43\sigma} \right), \tag{5.3}$$
$$\dot{\rho}_{43\sigma} = \Gamma^{+}_{22}(\mu_{43})\rho_{42} - \left(\Gamma^{+}_{22}(\mu_{44}) + \Gamma^{-}_{22}(\mu_{43}) \right) \rho_{43\sigma} + \Gamma^{-}_{22}(\mu_{44})\rho_{44}, \tag{5.4}$$

where we defined $\mu_N = E_N - E_{N-1}$ as the chemical potential of the N-particle ground state. Due to the fact that we focus only on the ground states of the system, energies are

uniquely identified by the corresponding particle numbers. Thus we omit the index for the energy in $\rho_{\mathrm{E}}^{\mathrm{N}}$. The factors $\Gamma_i^{\pm}(\mu_N)$ are containing tunneling matrix elements and Fermi functions. They are given by:

$$\Gamma_i^{\pm}(\mu_N) = \sum_{\eta} T_{i,i}^{\eta}(\mu_N) f_{\eta}^{\pm}(\mu_N). \tag{5.5}$$

With the set of differential equations at hand we are able to set up a Liouvillian matrix and finally calculate the stationary current through the molecule as already discussed in Sec. 3.2.

5.1. Theoretical considerations

First of all we discuss when we expect transitions that enable transport. At zero bias, no current is flowing and the molecule is in its neutral state (Fig. 5.1(a)). When increasing the bias we do not see a current as long as the chemical potential of the tip reaches the chemical potential of the 43-particle state (see Fig. 5.1(b)). The condition for the transition then is:

$$\mu_T = \mu_G + c \cdot eV_b \geq \mu_{43}. \tag{5.6}$$

During this transition, often referred to as the LUMO transition, an electron from the tip tunnels onto the molecule by occupying the LUMO orbital and then tunnels out into the substrate. Given the many-body energies of H_2Pc, we expect this transition to occur at bias voltages of about 1.4 V and 3.7 V for the renormalized and the unrenormalized spectrum, respectively. Consequently, for negative bias voltages the current is blocked until the chemical potential of the tip hits the chemical potential of the 42-particle state (see Fig. 5.1(c)):

$$\mu_T = \mu_G + c \cdot eV_b \leq \mu_{42}. \tag{5.7}$$

In this configuration an electron from the HOMO orbital tunnels into the tip while the substrate delivers an electron that reoccupies the half-filled orbital. Due to the involvement of the HOMO orbital, this transition is named HOMO transition. The expected bias voltages for this transition are about -1.1 V for the renormalized and -2.2 V for the unrenormalized spectrum.

One may ask why only the chemical potential of the tip and not the chemical potential of the substrate is determining when tunneling of an electron is allowed. A reason for this is the asymmetric adjustment of μ_T and μ_S with the applied bias due to the parameter c. Consider a transition $N \to N+1$. Using Eq. (5.6) we get a condition for the bias voltage:

$$eV_{b,1} \geq \frac{\mu_{N+1} - \mu_G}{c}, \tag{5.8}$$

with the tip playing the role of the source. Analogously,

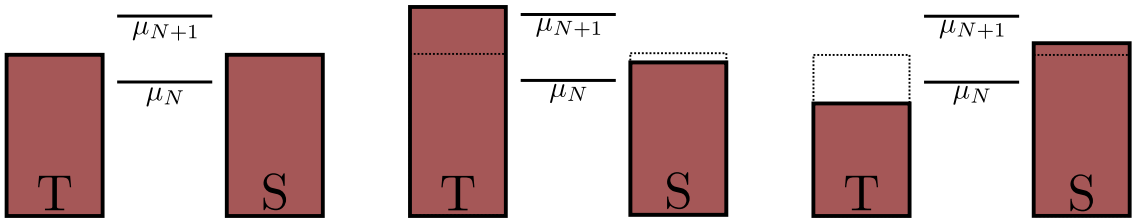

(a) $V_b = 0$ (b) $V_b > 0$ (c) $V_b < 0$

Figure 5.1.: *Arrangement of the chemical potentials depending on the applied bias voltage.*

$$\mu_S = \mu_G - (1-c) \cdot eV_b \geq \mu_{N+1}, \tag{5.9}$$

$$\Rightarrow |eV_{b,2}| \geq \frac{\mu_{N+1} - \mu_G}{(1-c)}, \tag{5.10}$$

if the event would be mediated by the substrate. Since tunneling from N to $N+1$ with the substrate acting as a source would generally require negative bias voltage (Fig. 5.1(c)), we put the absolute value of $eV_{b,2}$ in Eq. (5.10). Using the definition of c, the ratio of these two quantities is given by:

$$\frac{|eV_{b,2}|}{eV_{b,1}} = \frac{c}{1-c} = \epsilon_r. \tag{5.11}$$

This means that we do expect transitions that are determined by the relative alignment of the substrate's chemical potential. These will occur at much higher absolute values of the bias voltage. There is also another point of view regarding the relative alignment of the different chemical potentials. In the configuration depicted in Fig. (5.1), the chemical potentials of the tip and the substrate are changing with the bias, while the chemical potential of the molecule remains fixed. However, if we take a look at the Fermi functions appearing in our formulas,

$$f_T^+(\mu_N) = f(\mu_N - [\mu_G + c \cdot eV_b]), \tag{5.12}$$

$$f_S^+(\mu_N) = f(\mu_N - [\mu_G - (1-c) \cdot eV_b]), \tag{5.13}$$

we can shift the order of terms of their arguments like:

$$f_T^+(\mu_N) = f([\mu_N - c \cdot eV_b] - \mu_G), \tag{5.14}$$

$$f_S^+(\mu_N) = f([\mu_N - c \cdot eV_b] - [\mu_G - eV_b]). \tag{5.15}$$

We notice that from this point of view that the chemical potential of the tip remains fixed at μ_G, while the potential of the molecule moves with $-c \cdot eV_b$. Due to the negative sign of

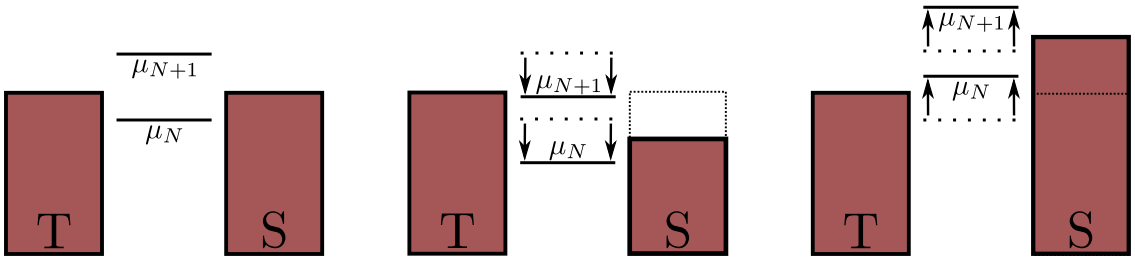

(a) $V_b = 0$ (b) $V_b > 0$ (c) $V_b < 0$

Figure 5.2.: *From the tip's point of view the chemical potentials of the molecule and the substrate move contrary to the applied bias voltage.*

$-eV_b$, the chemical potential of the substrate moves in the same direction as the chemical potential of the molecule, yet with the full bias voltage. Again, the chemical potential of the tip determines when the first transition in either direction is occuring, altough it is not moving with the bias. As we see in Fig. 5.2, the current is blocked as long as either μ_N or μ_{N+1} are passing the chemical potential of the tip, while again μ_S plays a subordinate role as it moves faster than the chemical potential of the molecule.

Our model formally allows us to access configurations with even higher or lower particle numbers, respectively, by increasing the range of the bias voltage (this applies only to the case of the renormalized spectrum, as we will see later). Though, we have to be careful, as for higher bias voltages we are not allowed anymore to neglect excited states. However, we can make at least qualitative predictions about the transport properties of hydrogen phthalocyanine, as long as we restrict to low bias voltages and keep these limitations in mind. In the following sections we discuss the results of our numerical calculations.

5.2. I-V characteristics and differential conductance for hydrogen phthalocyanine

The recording of the current-voltage characteristics and the differential conductance in dependence of the applied bias voltage are two main applications of scanning tunneling microscopy. They are generated by sweeping the bias voltage at a fixed position of the tip. Current-voltage curves allow the inspection of the general behaviour of the molecule when applying a bias voltage. Often, the differential conductance, which is a measure of how the current changes with the bias is more interesting. As we will see, the plots of the differential conductance give hints about the spectral properties of the examined molecule. First, we show current-voltage curves for both renormalized (Fig. 5.3) and nonrenormalized (Fig. 5.4) many-body energies. We see that until the bias voltage reaches a certain value, the current is blocked, as no tunneling is allowed.
The current in Fig. (5.3) shows a staircase-like behaviour. Reminding the theoretical considerations in the section before we can explain this easily: At positive bias the first

step occurs when the LUMO-transition is allowed; one electron tunnels from the tip into the system and out into the substrate again. Then, as long as the chemical potential of the 44-particle state lies above the chemical potential of the tip, the current stays constant. If we further raise the bias voltage the 44-particle ground state becomes accessible, so that the current increases, as another channel which allows tunneling into the system becomes available.
At negative bias the current is negative since electrons tunnel out of the system. In analogy to the case of positive bias voltage, the current is blocked until the applied bias voltage surpasses a certain value which corresponds to the HOMO transition. At even lower bias voltages there is another step of the current due to the possibility to access the 40-particle ground state. Note that physical interpretations of these transitions have to be taken with care, since for higher bias voltages excited states can not be excluded anymore.

In the case of the unrenormalized many-body spectrum in Fig. 5.4 we only see the HOMO and LUMO transitions, because the next transitions lie outside of a range of reasonable bias voltages: Considering Eq. (5.8), we see that the bias voltage needed for a transition is proportional to a difference $\mu_{N+1} - \mu_G$. However, in the unrenormalized case these energy differences for states with higher particle number simply become too large. For example regarding the 44- and the 43-particle states we already have $\mu_{44} - \mu_G = 7.3$ eV, implying a bias voltage of $V_b = 8.5$ V. As we derived the tunneling matrix elements under the condition that the energy of an electron which tunnels into the system is limited by the energy window that is determined by the Fermi levels and workfunctions of the contacts (see Fig. 2.2), such high energies are not consistent with the model. Thus, the bias voltage can be varied only in a very limited range for the unrenormalized spectrum. Altough this spectrum is obviously not physical, we still give it as an example, also to substantiate the necessity for the renormalization of the single particle energies.

In Figs. 5.5 and 5.6 we show plots of the differential conductance for the renormalized or the unrenormalized case, respectively. The peaks that appear in these curves correspond to the bias voltages which are needed to enable transitions into the different many-body states. Again, there are less transitions visible in the unrenormalized case.
Hence, we will focus on the renormalized case in our further considerations. The two peaks at positive bias voltage correspond to transitions between 42 and 43 particles at $V_b \approx 1.4$ V and to transitions between states with 43 and 44 particles at $V_b = 2.8$ V. At negative bias voltages we have the transition between 41 and 42 particles at $V_b = -1.1$ V and the transition between 40 and 41 electrons at $V_b \approx -2.6$ V.
With Eq. (5.8) we are directly able to relate the positions of the peaks to the chemical potentials of the corresponding ground states and find that they coincide. The voltage difference between the peaks for the HOMO and the LUMO transition is related to the HOMO-LUMO gap by:

$$eV_{b,LUMO} - eV_{b,HOMO} = \frac{\Delta_{HL}}{c} = 2.55 \text{ eV}. \tag{5.16}$$

Thus we have a HOMO-LUMO gap of $\Delta_{HL} = 2.2$ eV. Another quantity we can read out

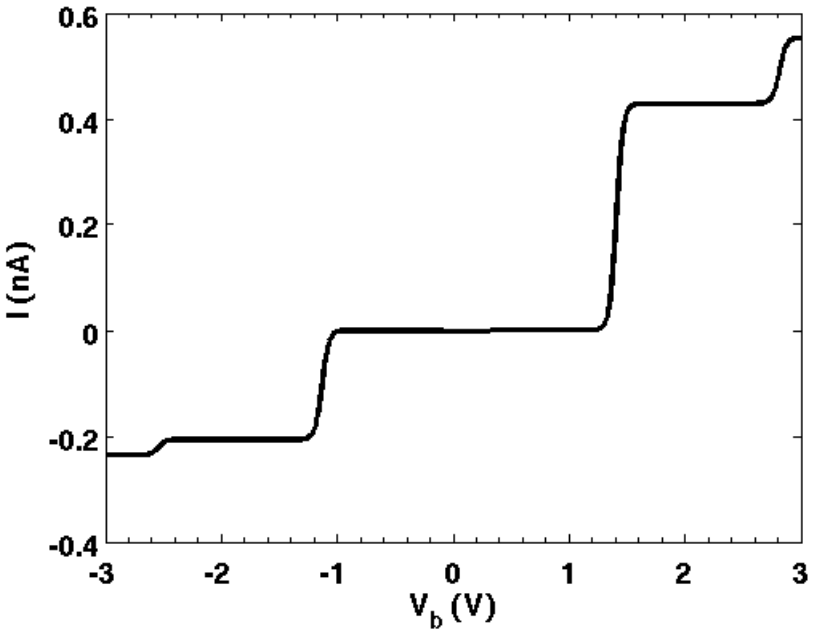

Figure 5.3.: *Current-voltage curve for renormalized spectrum.*

from the distance of the peaks is the charging energy we used to describe the Coulomb interaction in the constant-interaction model. Given

$$E_{44} - E_{43} = \epsilon_L + \frac{7}{2}U, \tag{5.17}$$

$$E_{43} - E_{42} = \epsilon_L + \frac{5}{2}U, \tag{5.18}$$

$$E_{42} - E_{41} = \epsilon_H + \frac{3}{2}U, \tag{5.19}$$

$$E_{41} - E_{41} = \epsilon_H + \frac{1}{2}U, \tag{5.20}$$

the voltage difference ΔV between two peaks in positive or negative direction of the bias is:

$$\Delta V = \frac{U}{c \cdot e}. \tag{5.21}$$

Amongst other things these results allowed us to check whether our numerical results are reflecting the expected behaviour. Hence we can now proceed to spatially resolve the properties of the current through the molecule.

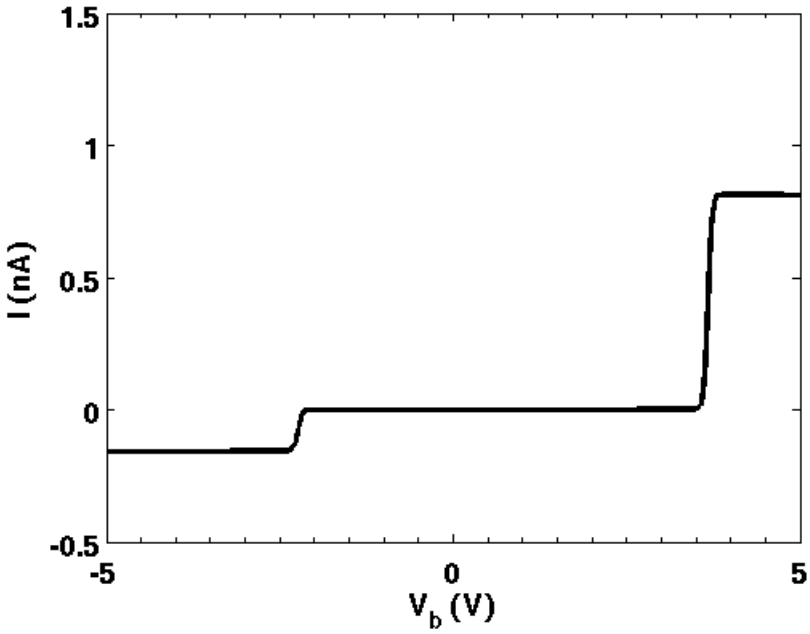

Figure 5.4.: *Current-voltage curve for unrenormalized spectrum.*

5.3. STM imaging

The main application of scanning tunneling microscopy is, as its name implies, the scanning of samples and surfaces to investigate their structural properties. Most STM pictures are in the constant-current mode. Here the microscope is adjusted to a certain value of the tunneling current. Then, when scanning a surface or a sample, this current is held constant by variing the relative distance of the tip towards the sample or surface. The outcome of these measurements then reveals the topography of the surface.

However, our numerical calculations are done in constant-height mode, where the distance between the tip and the sample is fixed. Thus, our plots reflect the spatial change of the tunneling current through the sample. They are recorded at a tip-sample distance of 4 Å. If not stated otherwise, we use a d_{z^2}-oriented tip state, because for tungsten tips mainly this state is contributing to tunneling [Che90]. For reasons of visibility all current plots are showing the absolute value of the current measured at the tip. However, we keep in mind that for negative bias voltages the measured current is negative (see Fig. 5.3).

The first image we present in Fig. 5.7 is recorded at the peak in the differential conductance curve for $V_b = -1.12$ V (Fig. 5.5). At this bias voltage transport is happening via the HOMO molecular orbital, whereby an electron from this orbital is tunneling into the tip. Thus we expect that the shape of this orbital is reflected in the current map. By checking Fig. 5.7 we see that this is the case (for comparison, see Fig. 4.6(a) in section 4.1.2).

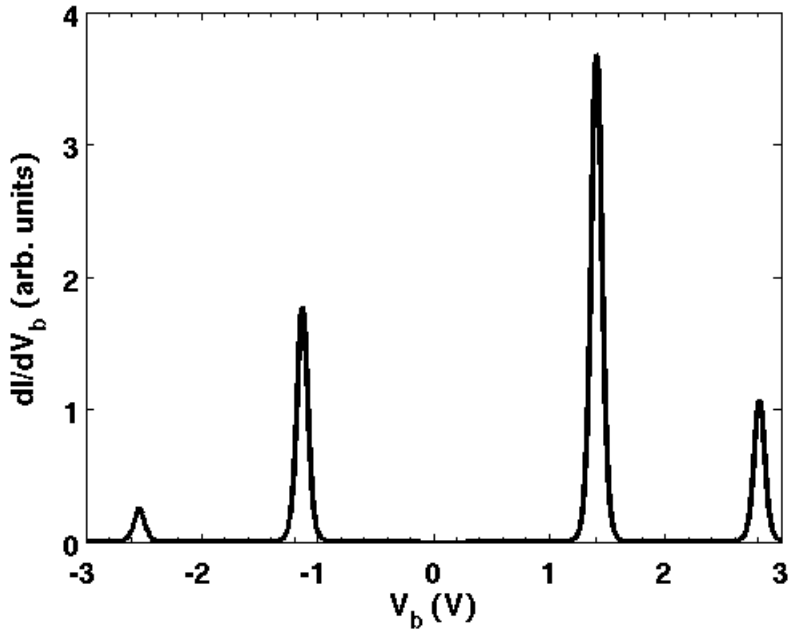

Figure 5.5.: *Differential conductance for renormalized spectrum.*

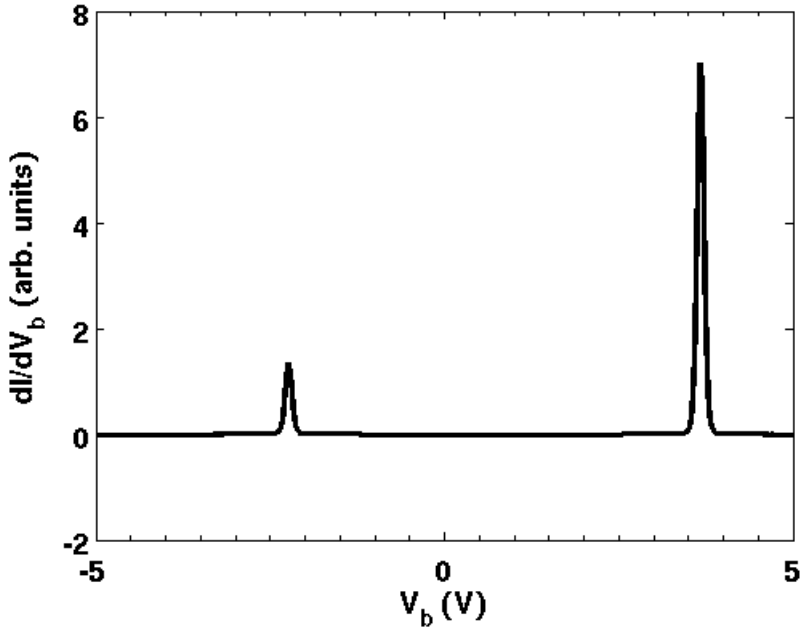

Figure 5.6.: *Differential conductance for unrenormalized spectrum*

In Fig. 5.8 we show the recorded current at $V_b = 1.4$ V, which is the first peak for positive bias voltage in the conductance plot in Fig. 5.5. As already discussed in Sec. 5.1, we expect that the image reflects the shape of the LUMO orbital, since now this orbital receives an electron which is tunneling out of the tip onto the molecule. Again, the image is in good agreement with the calculated shape of the LUMO orbital shown in Fig. 4.6(b).

Up to now, we only considered pure tip states; more precisely, we used tunneling matrix elements for a d_{z^2} oriented tip state. However, since we put such effort in deriving the tunneling matrix elements for the tip, we will now examine the effects resulting from a change of the spatial orientation of the tip state. We try to reproduce the results of a recently published work by L. Gross and his group [GMM+11], where a CO-functionalized tip was used to image the molecular orbitals of pentacene and naphthalocyanine molecules. Naphthalocyanine is closely related to phthalocyanine. The only difference is an additional benzene ring attached to each "arm" of naphthalocyanine compared to H_2Pc. Since also their HOMO and LUMO orbitals have a similar shape (see Fig. 1(b) in [GMM+11]), we can compare our results to those presented in [GMM+11].
The key result of [GMM+11] is, that one can enhance the lateral resolution of STM images by using a CO tip. This enhancement is caused by the parallel alignment of the p_x and p_y orbitals of CO with the sample and the different phases of their lobes (see App. A.4). Fig. 5.11 contains an excerpt of their paper, showing the main results. In [GMM+11] the measurements were rechecked with numerical, in their case DFT, calculations. These calculations showed excellent agreement with the experimental data when using a mixed state (s, p_x and p_y contributions) for the tip and scanning in constant-height mode.
Implementing a mixed tip state in our model is not difficult. It can be achieved by simply using the relations given in Sec. 2.2.2.

The result of our calculations for the HOMO transition is given in Fig. 5.9. We see a good agreement with both the experimental and numerical results presented in 5.11, where also eight maxima can be seen in the middle of the molecule. These are lying at the positions of the nodes of the HOMO orbital. Also in the outer part of the molecule our image resembles both calculated and experimental images in Fig. 5.11 very well. The only difference is that in Fig. 5.11 there are two additional bulbs at each arm of the molecule. However, this is due to the fact that H_2Pc is missing the extra benzene rings of naphthalocyanine. The bulbs in Fig. 5.9 lie at the same positions as the lobes of the HOMO orbital, indicating that here the s-wave character of the tip is dominating the tunneling transport. Also at the crossing of two nodal planes of the HOMO orbital we see pronounced minima in Fig. 5.9.
In the case of the image of the LUMO orbital in Fig. 5.10, there are good agreements with the images presented in [GMM+11]. In the upper and lower part of Fig. 5.10 we see two prominent bulbs, lying at the positions of the lobes of the LUMO orbital and hence revealing the s-wave contribution to the tip state. Comparing with Fig. 5.11 testifies the coincidences. Considering the inner part of the molecule, we see five tubular lobes connecting the bulbs in the left and right arms of H_2Pc in Fig. 5.10. These tube-shaped maxima

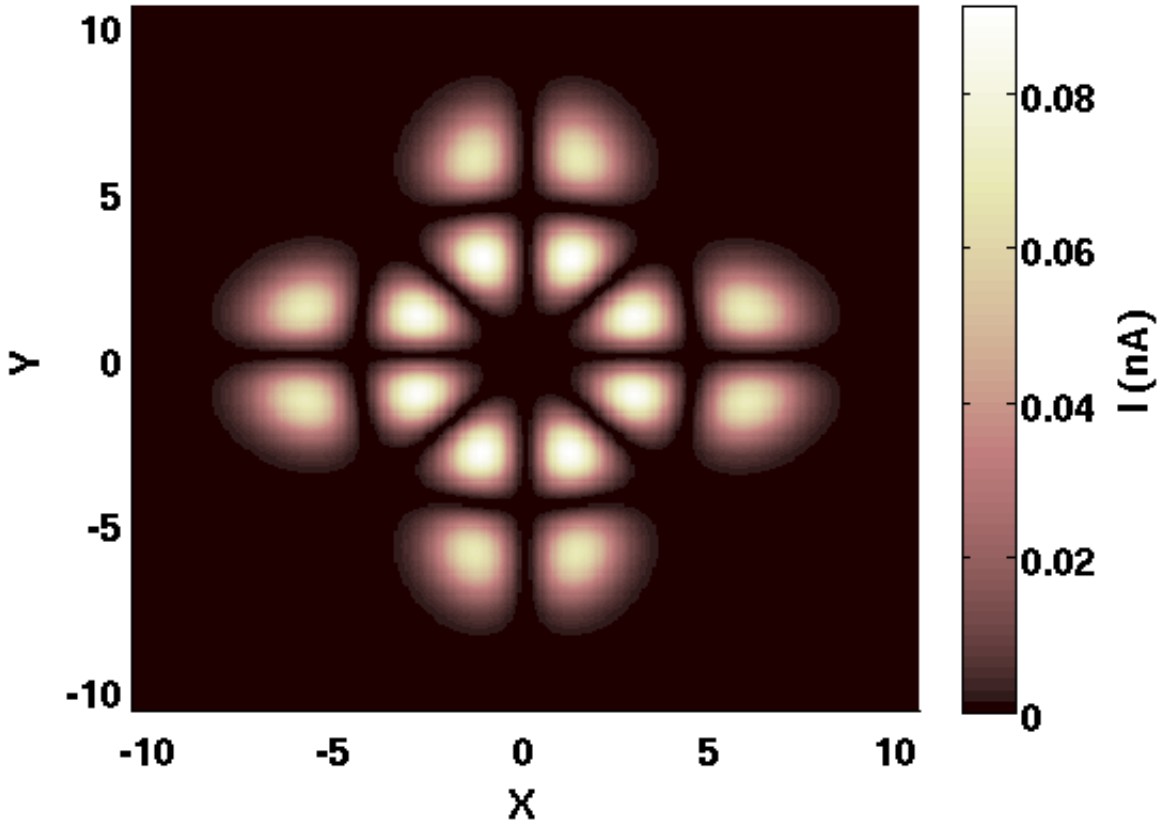

Figure 5.7.: *STM image of* H_2Pc*, recorded at* $V_b = -1.12$ *V with a* d_{z^2} *oriented tip. At this transition, the HOMO orbital is involved. Spatial units in Å.*

coincide with the nodal planes of the LUMO orbital. The two outer bulbs again correspond to a predominant s-wave contribution at this position of the tip. The comparison with Fig. 5.11 shows good agreement, where additional bulbs can be seen in the upper and lower part of the molecule, again atrributable to the given of a different type of investigated molecule. This reason also applies to the appearance of seven tube-shaped lobes in Fig. 5.11, which however, in analogy to our result for H_2Pc in Fig. 5.10, lie at the same positions where the LUMO orbital of naphthalocyanine has nodal planes.

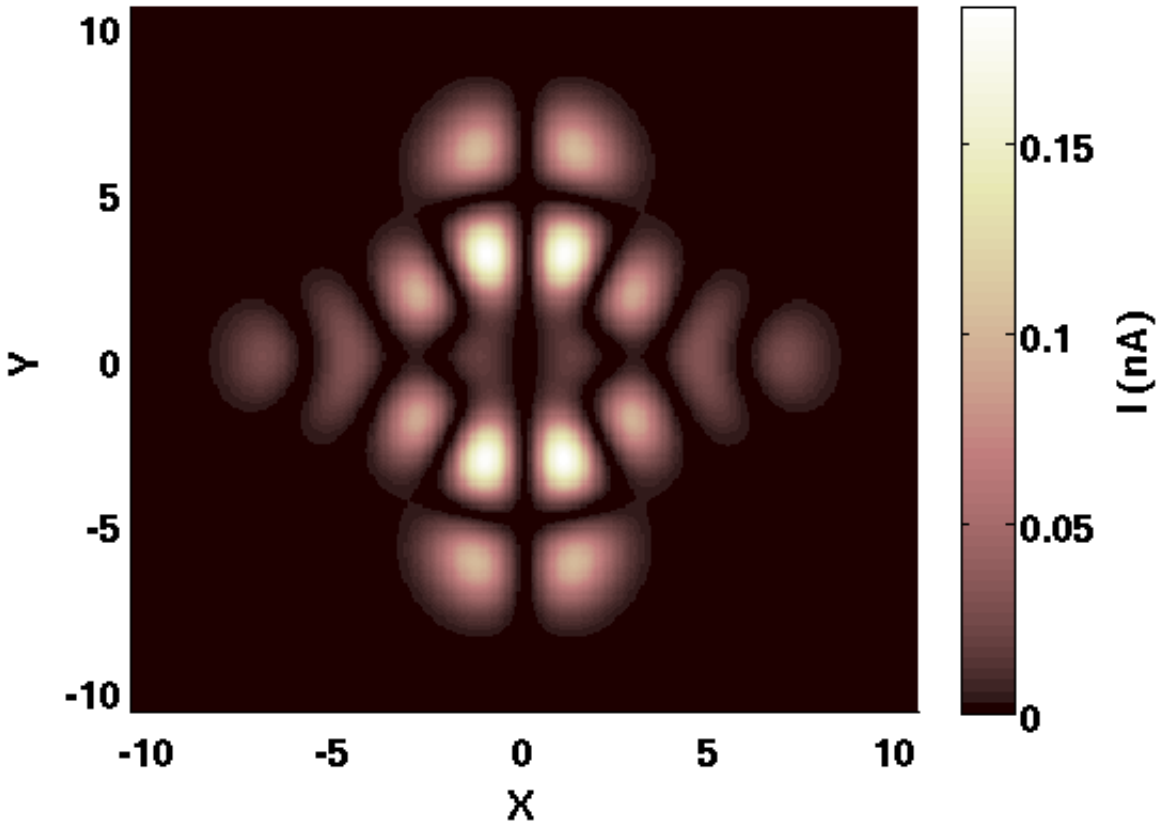

Figure 5.8.: *STM image of* H_2Pc*, recorded at* $V_b = 1.4$ *V with a* d_{z^2} *oriented tip. At this transition, the LUMO orbital is involved. Spatial units in Å.*

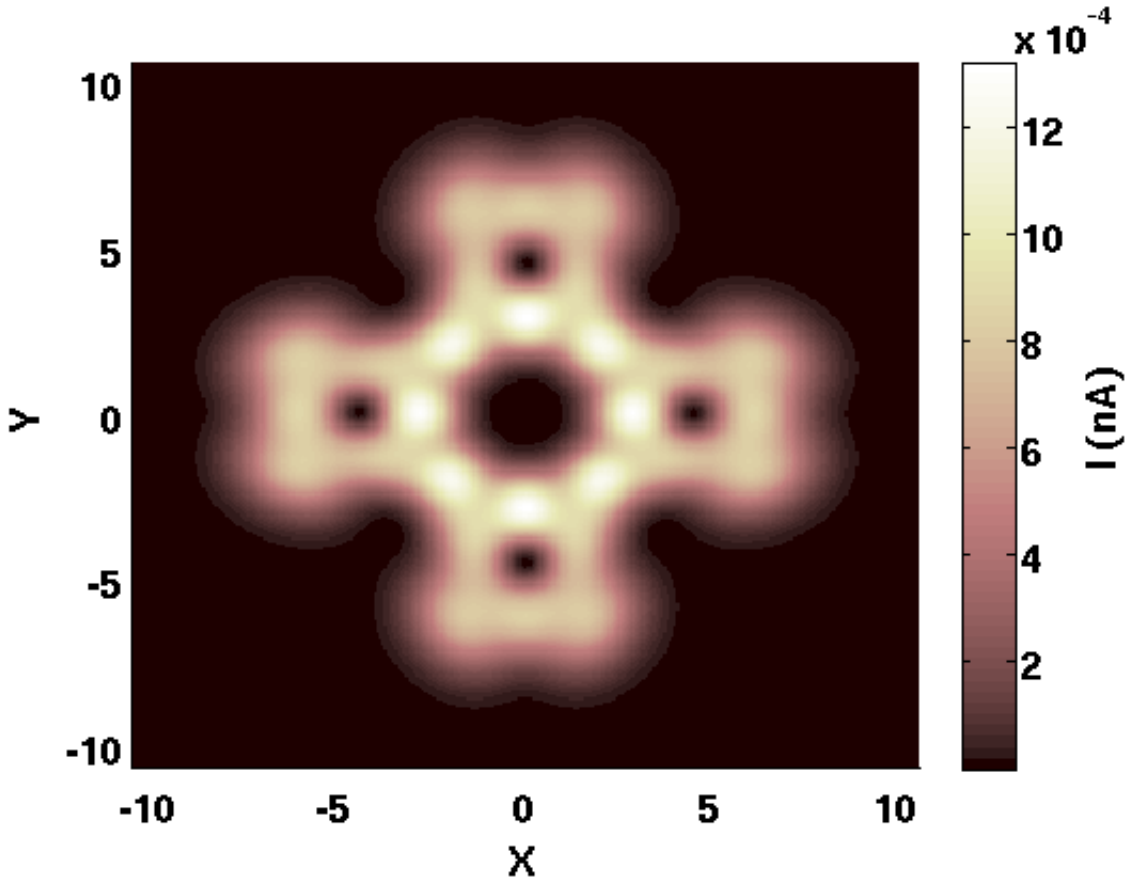

Figure 5.9.: *STM image of the HOMO orbital of* H_2Pc *with a mixed s-p-wave tip. Spatial units in Å.*

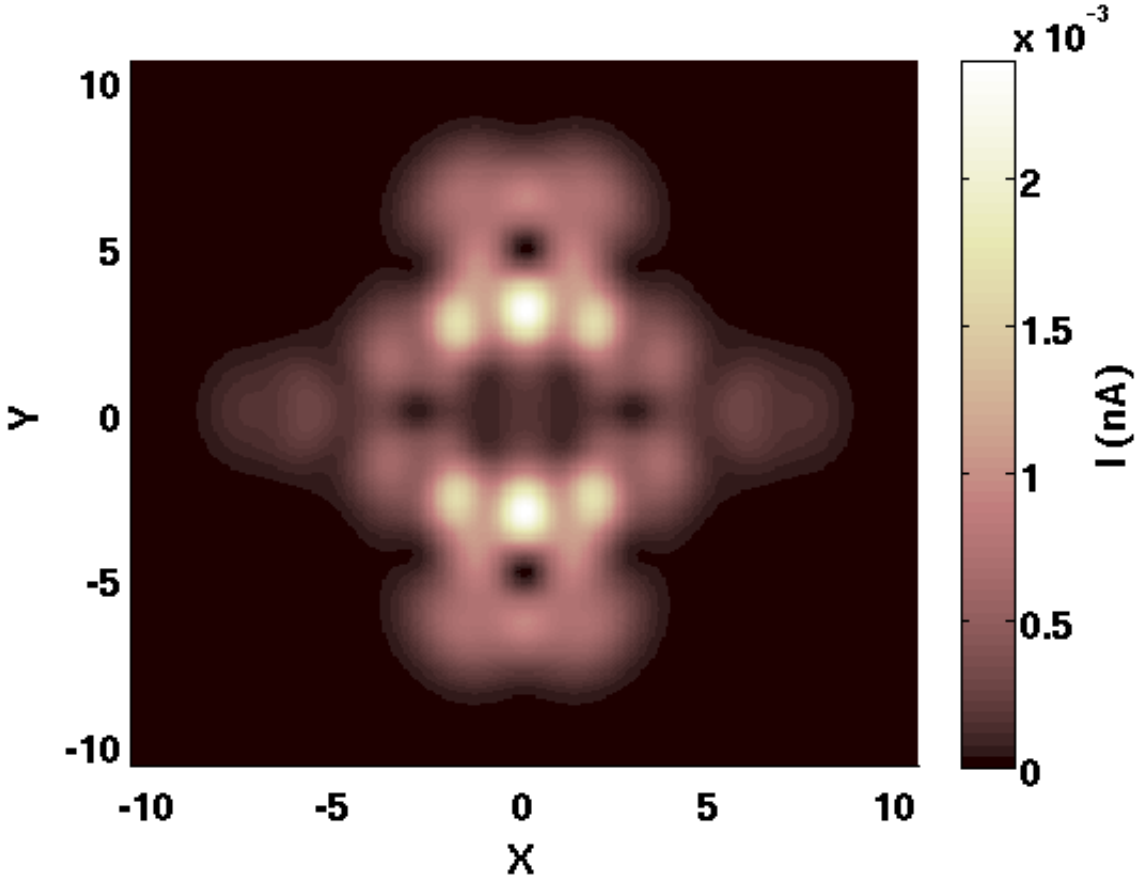

Figure 5.10.: *STM image of the LUMO orbital of* H_2Pc *with a mixed s-p-wave tip. Spatial units in Å.*

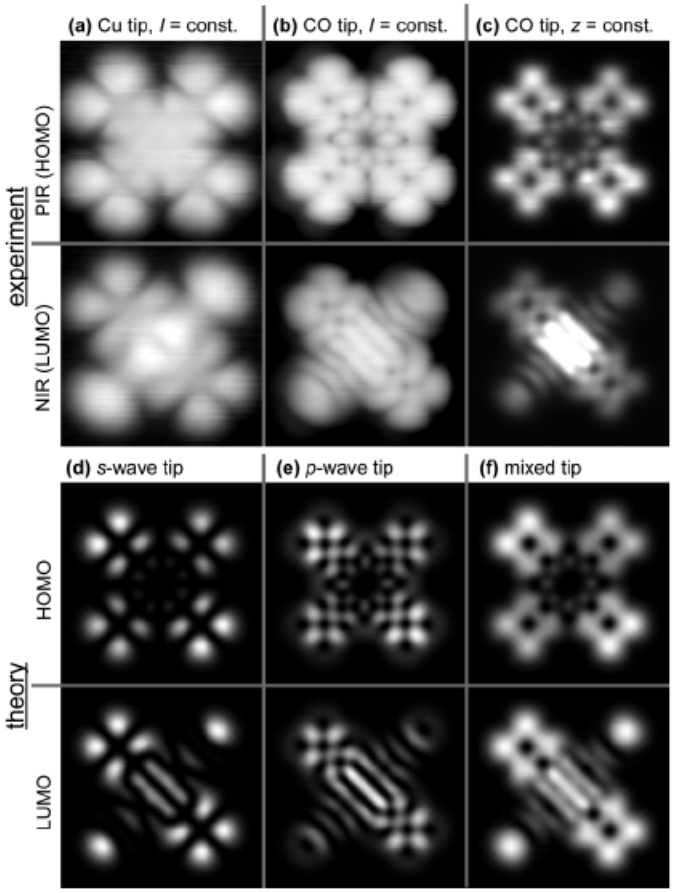

FIG. 4. Naphthalocyanine on NaCl(2 ML) on Cu(111) measured using a Cu tip (a) and a CO tip (b) in constant-current mode, and with a CO tip in constant-height mode (c). The PIR (1st row) is measured at $V = -1.65$ V and the NIR (2nd row) at $V = 0.60$ V. Calculated images at $z_0 = 5.0$ Å of the HOMO (3rd row) and LUMO (4th row) with an s-wave tip (d), a p-wave tip (e), and with a mixed tip (f). The molecule is oriented as depicted in Fig. 1(b). All images: 27 Å × 27 Å.

Figure 5.11.: *Excerpt from [GMM+11].*

6. Conclusion

We systematically developed a formalism to describe transport through organic moleculs underlying an STM setup. For this purpose we derived tunneling matrix elements that distinguish under which conditions tunneling between the molecule and the contacts takes place. They depend on various quantities, such as energy and the quantum number denoting the different molecular orbitals. For the substrate, we started from a microscopic point of view, using the solutions of a Schrödinger equation for a potential well in z-direction. Plane waves are describing the behavior of the wavefunction of the substrate perpendicular to the z-direction. For the tunneling matrix elements that describe the tunneling between the molecule and the tip, however, we used a different approach proposed by Julian Chen [Che90]. This approach considers the shape of the tip wavefunction in the vacuum between tip and sample. This did not only enable us to derive the tunneling matrix elements for the tip with much less effort in comparison to the case of the substrate, but also enriched our formalism with the possibility to include the effects of different spatially orientated tip states.
Finally, we derived the General Master Equation for the reduced density matrix in secular approximation with the tunneling Hamiltonian treated in second order. A Markov approximation was applied to render the resulting differential equation local in time. The current through the system was calculated using the stationary solution of the reduced density matrix
In order to model the investigated molecule we used the Slater-Koster LCAO approach [SK54]. Based on this we set up a single particle Hamiltonian for both H_2Pc and CuPc. However, due to the decoupling of the π and the σ system induced by this approach, The π orbitals of H_2Pc did not show the symmetry properties of the molecule. To counteract we performed a Mulliken population analysis for the σ orbitals of H_2Pc and projected its outcome onto the onsite energies of the p_z orbitals. For the many-body representation of H_2Pc we used the constant-interaction model to calculate the energies of the many-particle ground states of the molecule. Nevertheless, to reflect experimental facts, we had to renormalize the energies of the single particle molecular orbitals using experimental data from photoemission spectroscopy. In the case of copper phthalocyanine the problem arose that there is an odd number of total valence electrons, which led to the non-intuitive situation of the HOMO orbital being singly filled. At the time being, this problem is not solved completely. In addition to that, also the implementation of the degenerate LUMO and HOMO-1 orbitals could not be fully understood yet.
Finally, we presented our numerical calculations for the case of hydrogen phthalocyanine and compared them to our theoretical expectations as well as to experimental results. In both cases we achieved good agreement. Also the effect of a non-standard tip state was examined. By comparison with a recent paper [GMM+11], which adressed the same

question we found that different tip states play a prominent role considering the lateral resolution of STM images. All in all we showed, that our formalism is able to mirror experimental findings quite well, keeping always in mind the limitations induced by our applied approximations.

With regard to the general formalism, we expect that implementing excited electronic states in our model could lead to many interesting features, as e.g interference effects and negative differential conductance. Especially screening and image charge effects, induced by the contacts, have recently been proven to be responsible for negative differential conductance and the breaking of molecular symmetries [KF11]. Also the role of vibronic excitations would be an interesting topic to adress. For the case of H_2Pc a striking feature considering its use in molecular electronics would be a current-induced switching of the positions of the central hydrogen atoms, which already has been adressed for naphthalocyanine [LRM07]. Regarding copper phthalocyanine, the implementation of Coulomb and spin interactions together with image charge effects could be a promising task for further investigations.

A. Appendix

A.1. Derivation of the Generalized Master Equation for the reduced density matrix

A.1.1. Time dependence of the tunneling Hamiltonian

We start with Eq. (3.23). Expanding the double commutators in Eq. (3.23) yields:

$$\begin{aligned}\dot{\hat{\rho}}^I_{red}(t) = -\frac{1}{\hbar^2}\int_0^\infty \mathrm{d}t_2 \Big[& \operatorname{tr}_{sub,\,tip}\left\{\hat{\mathcal{H}}^I_T(t)\,\hat{\mathcal{H}}^I_T(t-t_2)\,\hat{\rho}^I_{red}(t)\hat{\rho}_{tip}\hat{\rho}_{sub}\right\} \\ & + \operatorname{tr}_{sub,\,tip}\left\{\hat{\rho}^I_{red}(t)\hat{\rho}_{tip}\hat{\rho}_{sub}\,\hat{\mathcal{H}}^I_T(t-t_2)\,\hat{\mathcal{H}}^I_T(t)\right\} \\ & - \operatorname{tr}_{sub,\,tip}\left\{\hat{\mathcal{H}}^I_T(t)\,\hat{\rho}^I_{red}(t)\hat{\rho}_{tip}\hat{\rho}_{sub}\,\hat{\mathcal{H}}^I_T(t-t_2)\right\} \\ & - \operatorname{tr}_{sub,\,tip}\left\{\hat{\mathcal{H}}^I_T(t-t_2)\,\hat{\rho}^I_{red}(t)\hat{\rho}_{tip}\hat{\rho}_{sub}\,\hat{\mathcal{H}}^I_T(t)\right\} \Big]. \end{aligned} \tag{A.1}$$

Now we first have to consider the time dependence of the various parts of Eq. (A.1). Remember that $\hat{\mathcal{H}}^I_T(t)$ is given by

$$\begin{aligned}\hat{\mathcal{H}}^I_T(t) = \sum_{\mathbf{k},\,i}\Big(& t^T_{\mathbf{k}i}\,\hat{\mathrm{a}}^\dagger_{\mathbf{k}}(t)\hat{\mathrm{d}}_i(t) + \left(t^T_{\mathbf{k}i}\right)^*\,\hat{\mathrm{d}}^\dagger_i(t)\hat{\mathrm{a}}_{\mathbf{k}}(t) \\ & + t^S_{\mathbf{k}i}\,\hat{\mathrm{c}}^\dagger_{\mathbf{k}}(t)\hat{\mathrm{d}}_i(t) + \left(t^S_{\mathbf{k}i}\right)^*\,\hat{\mathrm{d}}^\dagger_i(t)\hat{\mathrm{c}}_{\mathbf{k}}(t)\Big). \end{aligned} \tag{A.2}$$

As an example, for the annihilation operator of the tip we have:

$$\hat{\mathrm{a}}_{\mathbf{k}}(t) = e^{\frac{i}{\hbar}\hat{\mathcal{H}}_0 t}\,\hat{\mathrm{a}}_{\mathbf{k}}\,e^{-\frac{i}{\hbar}\hat{\mathcal{H}}_0 t}. \tag{A.3}$$

We now derive its explicit time dependence. The easiest way to do this is to first differentiate the above equation,

$$\begin{aligned}\dot{\hat{a}}_{\mathbf{k}}(t) &= \frac{i}{\hbar}\left[\hat{\mathcal{H}}_0,\,\hat{\mathrm{a}}_{\mathbf{k}}(t)\right] \\ &= \frac{i}{\hbar}\,e^{\frac{i}{\hbar}\hat{\mathcal{H}}_0 t}\left[\hat{\mathcal{H}}_0,\,\hat{\mathrm{a}}_{\mathbf{k}}\right]e^{-\frac{i}{\hbar}\hat{\mathcal{H}}_0 t}, \end{aligned} \tag{A.4}$$

and then to compute the emerging commutator. As $\hat{\mathcal{H}}_0$ consists of pairs of one creation and one annihilation operator, the relation $[ab,\,c] = a\{b,\,c\} - \{a,\,c\}b$ is very useful to calculate commutators like:

$$
\begin{aligned}
[\hat{a}^\dagger_{\mathbf{k}'}\hat{a}_{\mathbf{k}'},\, \hat{a}_{\mathbf{k}}] &= \hat{a}^\dagger_{\mathbf{k}'}\,\{\hat{a}_{\mathbf{k}'},\, \hat{a}_{\mathbf{k}}\} - \{\hat{a}^\dagger_{\mathbf{k}'},\, \hat{a}_{\mathbf{k}}\}\,\hat{a}_{\mathbf{k}'} \\
&= 0 - \delta_{\mathbf{k}'\mathbf{k}}\hat{a}_{\mathbf{k}'}.
\end{aligned} \tag{A.5}
$$

With this we arrive at a differential equation for $\hat{a}_{\mathbf{k}}(t)$:

$$
\dot{\hat{a}}_{\mathbf{k}}(t) = -\frac{i}{\hbar}\epsilon_{\mathbf{k}}\,\hat{a}_{\mathbf{k}}(t), \tag{A.6}
$$

which is easily solved by:

$$
\hat{a}_{\mathbf{k}}(t) = \hat{a}_{\mathbf{k}}\, e^{-\frac{i}{\hbar}\epsilon_{\mathbf{k}}t}. \tag{A.7}
$$

For its hermitian conjugate and the electron operators of the substrate it follows analogously:

$$
\begin{aligned}
\hat{a}^\dagger_{\mathbf{k}}(t) &= \hat{a}_{\mathbf{k}}\, e^{+\frac{i}{\hbar}\epsilon_{\mathbf{k}}t}, \\
\hat{c}_{\mathbf{k}}(t) &= \hat{c}_{\mathbf{k}}\, e^{-\frac{i}{\hbar}\epsilon_{\mathbf{k}}t}, \\
\hat{c}^\dagger_{\mathbf{k}}(t) &= \hat{c}^\dagger_{\mathbf{k}}\, e^{+\frac{i}{\hbar}\epsilon_{\mathbf{k}}t}.
\end{aligned} \tag{A.8}
$$

A.1.2. Applying the partial trace

Each term in Eq. (3.23) contains a product of two fermionic operators. For any operator $\hat{O}$ it holds:

$$
\mathrm{tr}\left\{\hat{\rho}\hat{O}\right\} = \langle\hat{O}\rangle\,. \tag{A.9}
$$

Thus we can give the following relations for a product of two fermionic operators:

$$
\mathrm{tr}_{sub}\left\{\hat{\rho}_{sub}\hat{c}_{\mathbf{k}}\hat{c}_{\mathbf{k}'}\right\} = \mathrm{tr}_{sub}\left\{\hat{\rho}_{sub}\hat{c}^\dagger_{\mathbf{k}}\hat{c}^\dagger_{\mathbf{k}'}\right\} = 0 \tag{A.10}
$$

$$
\mathrm{tr}_{tip}\left\{\hat{\rho}_{tip}\hat{a}_{\mathbf{k}}\hat{a}_{\mathbf{k}'}\right\} = \mathrm{tr}_{tip}\left\{\hat{\rho}_{tip}\hat{a}^\dagger_{\mathbf{k}}\hat{a}^\dagger_{\mathbf{k}'}\right\} = 0 \tag{A.11}
$$

$$
\mathrm{tr}_{sub}\left\{\hat{\rho}_{sub}\hat{c}^\dagger_{\mathbf{k}}\hat{c}_{\mathbf{k}'}\right\} = \delta_{\mathbf{k}\mathbf{k}'}f^+_{sub}(\epsilon_{\mathbf{k}}) \tag{A.12}
$$

$$
\mathrm{tr}_{sub}\left\{\hat{\rho}_{sub}\hat{c}_{\mathbf{k}}\hat{c}^\dagger_{\mathbf{k}'}\right\} = \delta_{\mathbf{k}\mathbf{k}'}f^-_{sub}(\epsilon_{\mathbf{k}}) \tag{A.13}
$$

$$
\mathrm{tr}_{tip}\left\{\hat{\rho}_{tip}\hat{a}^\dagger_{\mathbf{k}}\hat{a}_{\mathbf{k}'}\right\} = \delta_{\mathbf{k}\mathbf{k}'}f^+_{tip}(\epsilon_{\mathbf{k}}) \tag{A.14}
$$

$$
\mathrm{tr}_{tip}\left\{\hat{\rho}_{tip}\hat{a}_{\mathbf{k}}\hat{a}^\dagger_{\mathbf{k}'}\right\} = \delta_{\mathbf{k}\mathbf{k}'}f^-_{tip}(\epsilon_{\mathbf{k}}). \tag{A.15}
$$

For a detailed calculation of the expectation value of two fermionic operators the reader may be referred to [BF04]. Using the cyclic properties of the partial trace and the above relations enables us to derive Eq. (3.24).

A.1.3. Transformation of the GME into the Schrödinger picture

We can go back to the Schrödinger picture by performing the transformation

$$\hat{\rho}^S_{red}(t) = \hat{U}_0(t)\hat{\rho}^I_{red}(t)\hat{U}_0^\dagger(t). \tag{A.16}$$

This yields for the time derivative of the RDM:

$$\begin{aligned}\dot{\hat{\rho}}^S_{red}(t) &= -\frac{i}{\hbar}\hat{U}_0(t)[\hat{\mathcal{H}}_0,\, \hat{\rho}^I_{red}(t)]\hat{U}_0^\dagger(t) + \hat{U}_0(t)\dot{\hat{\rho}}^I_{red}(t)\hat{U}_0^\dagger(t) \\ &= -\frac{i}{\hbar}[\hat{\mathcal{H}}_0,\, \hat{\rho}^S_{red}(t)] + \hat{U}_0(t)\dot{\hat{\rho}}^I_{red}(t)\hat{U}_0^\dagger(t).\end{aligned} \tag{A.17}$$

Inserting into Eq. (3.24) gives:

$$\begin{aligned}\dot{\hat{\rho}}^S_{red}(t) = -\frac{i}{\hbar}[\hat{\mathcal{H}}_{mol},\, \hat{\rho}^S_{red}(t)] - \frac{1}{\hbar^2}\int_0^\infty \mathrm{d}t_2 \sum_{\mathbf{k}}\sum_{i,\,j}\sum_{\eta}\Big[\\ + t^\eta_{\mathbf{k}i}(t^\eta_{\mathbf{k}j})^*\, f^+_\eta\,(\epsilon_{\mathbf{k}})\; \hat{\mathrm{d}}_i\hat{\mathrm{d}}_j^\dagger(-t_2)\,\hat{\rho}^S_{red}(t)\, e^{\frac{i}{\hbar}\epsilon_{\mathbf{k}}t_2} \\ + (t^\eta_{\mathbf{k}i})^* t^\eta_{\mathbf{k}j}\, f^-_\eta\,(\epsilon_{\mathbf{k}})\; \hat{\mathrm{d}}_i^\dagger\hat{\mathrm{d}}_j(-t_2)\,\hat{\rho}^S_{red}(t)\, e^{-\frac{i}{\hbar}\epsilon_{\mathbf{k}}t_2} \\ + t^\eta_{\mathbf{k}i}(t^\eta_{\mathbf{k}j})^*\, f^+_\eta\,(\epsilon_{\mathbf{k}})\; \hat{\rho}^S_{red}(t)\,\hat{\mathrm{d}}_i(-t_2)\hat{\mathrm{d}}_j^\dagger\, e^{-\frac{i}{\hbar}\epsilon_{\mathbf{k}}t_2} \\ + (t^\eta_{\mathbf{k}i})^* t^\eta_{\mathbf{k}j}\, f^-_\eta\,(\epsilon_{\mathbf{k}})\; \hat{\rho}^S_{red}(t)\,\hat{\mathrm{d}}_i^\dagger(-t_2)\hat{\mathrm{d}}_j\, e^{\frac{i}{\hbar}\epsilon_{\mathbf{k}}t_2} \\ - t^\eta_{\mathbf{k}i}(t^\eta_{\mathbf{k}j})^*\, f^-_\eta\,(\epsilon_{\mathbf{k}})\; \hat{\mathrm{d}}_i\hat{\rho}^S_{red}(t)\hat{\mathrm{d}}_j^\dagger(-t_2)\, e^{\frac{i}{\hbar}\epsilon_{\mathbf{k}}t_2} \\ - (t^\eta_{\mathbf{k}i})^* t^\eta_{\mathbf{k}j}\, f^+_\eta\,(\epsilon_{\mathbf{k}})\; \hat{\mathrm{d}}_i^\dagger\hat{\rho}^S_{red}(t)\hat{\mathrm{d}}_j(-t_2)\, e^{-\frac{i}{\hbar}\epsilon_{\mathbf{k}}t_2} \\ - t^\eta_{\mathbf{k}i}(t^\eta_{\mathbf{k}j})^*\, f^-_\eta\,(\epsilon_{\mathbf{k}})\; \hat{\mathrm{d}}_i(-t_2)\hat{\rho}^S_{red}(t)\hat{\mathrm{d}}_j^\dagger\, e^{-\frac{i}{\hbar}\epsilon_{\mathbf{k}}t_2} \\ - (t^\eta_{\mathbf{k}i})^* t^\eta_{\mathbf{k}j}\, f^+_\eta\,(\epsilon_{\mathbf{k}})\; \hat{\mathrm{d}}_i^\dagger(-t_2)\hat{\rho}^S_{red}(t)\hat{\mathrm{d}}_j\, e^{\frac{i}{\hbar}\epsilon_{\mathbf{k}}t_2}\Big].\end{aligned} \tag{A.18}$$

A.1.4. Application of the projection operators

The projection operators $\hat{\mathcal{P}}_{\mathrm{NE}}$ have the following properties:

$$\hat{\mathcal{P}}_{\mathrm{NE}} = \sum_l |\mathrm{N\,E}\,l\rangle\langle \mathrm{N\,E}\,l| \tag{A.19}$$

$$\mathbb{1} = \sum_{\mathrm{N,\,E}} \hat{\mathcal{P}}_{\mathrm{NE}} \tag{A.20}$$

$$\rho^{\mathrm{N}}_{\mathrm{EE'}} = \hat{\mathcal{P}}_{\mathrm{NE}}\,\hat{\rho}^S_{red}(t)\,\hat{\mathcal{P}}_{\mathrm{NE'}} \tag{A.21}$$

$$\dot{\rho}^{\mathrm{N}}_{\mathrm{EE'}} = \hat{\mathcal{P}}_{\mathrm{NE}}\,\dot{\hat{\rho}}^S_{red}(t)\,\hat{\mathcal{P}}_{\mathrm{NE'}}. \tag{A.22}$$

In the following we give two examples how the projection operators $\hat{\mathcal{P}}_{\mathrm{NE}}$ have to be applied. In the first example the RDM is e.g. to the right of a creation and annihilation operator pair of the molecule. So we have to insert a unity between the pair of electron operators and the RDM:

$$\hat{\mathcal{P}}_{\mathrm{NE}}\,\hat{\mathrm{d}}_i\,\hat{\mathrm{d}}_j^\dagger(-t_2)\,\hat{\rho}_{red}^S(t)\,\hat{\mathcal{P}}_{\mathrm{NE}'} = \sum_{\mathrm{M,\,F}} \hat{\mathcal{P}}_{\mathrm{NE}}\,\hat{\mathrm{d}}_i\,\hat{\mathrm{d}}_j^\dagger(-t_2)\hat{\mathcal{P}}_{\mathrm{MF}}\,\hat{\rho}_{red}^S(t)\,\hat{\mathcal{P}}_{\mathrm{NE}'}. \tag{A.23}$$

The pair $\hat{\mathrm{d}}_i\,\hat{\mathrm{d}}_j^\dagger$ effectively conserves the number of particles and, as $\hat{\rho}_{red}^S$ is considered to be diagonal in particle number, the indices M and N have to be equal. In addition, we can resolve the time dependence of the molecule electron operators $\hat{\mathrm{d}}_i^\dagger(t) = \hat{U}_0^\dagger(t)\hat{\mathrm{d}}_i^\dagger\hat{U}_0(t)$ and get:

$$\hat{\mathcal{P}}_{\mathrm{NE}}\,\hat{\mathrm{d}}_i\,\hat{\mathrm{d}}_j^\dagger(-t_2)\,\hat{\rho}_{red}^S(t)\,\hat{\mathcal{P}}_{\mathrm{NE}'} = \sum_{\mathrm{F}} \hat{\mathcal{P}}_{\mathrm{NE}}\,\hat{\mathrm{d}}_i\,e^{-\frac{i}{\hbar}\hat{\mathcal{H}}_0 t_2}\,\hat{\mathrm{d}}_j^\dagger\,e^{\frac{i}{\hbar}\mathrm{F}t_2}\rho_{\mathrm{FE}'}^{\mathrm{N}}. \tag{A.24}$$

In the second example, the position of the RDM is between two electron operators. Thus we have to insert an additional unity in comparison to the previous example:

$$\hat{\mathcal{P}}_{\mathrm{NE}}\,\hat{\mathrm{d}}_i\,\hat{\rho}_{red}^S(t)\,\hat{\mathrm{d}}_j^\dagger(-t_2)\,\hat{\mathcal{P}}_{\mathrm{NE}'} = \sum_{\mathrm{M,\,F}}\sum_{\mathrm{M}',\,\mathrm{F}'} \hat{\mathcal{P}}_{\mathrm{NE}}\,\hat{\mathrm{d}}_i\,\hat{\mathcal{P}}_{\mathrm{MF}}\hat{\rho}_{red}^S(t)\,\hat{\mathcal{P}}_{\mathrm{M}'\mathrm{F}'}\,\hat{\mathrm{d}}_j^\dagger(-t_2)\,\hat{\mathcal{P}}_{\mathrm{NE}'}. \tag{A.25}$$

We see from that M and M′ have to be equal to $\mathrm{N}+1$. According to this, the term takes the following form:

$$\hat{\mathcal{P}}_{\mathrm{NE}}\,\hat{\mathrm{d}}_i\,\hat{\rho}_{red}^S(t)\,\hat{\mathrm{d}}_j^\dagger(-t_2)\,\hat{\mathcal{P}}_{\mathrm{NE}'} = \sum_{\mathrm{F,\,F}'} \hat{\mathcal{P}}_{\mathrm{NE}}\,\hat{\mathrm{d}}_i\rho_{\mathrm{FF}'}^{\mathrm{N}+1}\,e^{-\frac{i}{\hbar}\mathrm{F}'t_2}\,\hat{\mathrm{d}}_j^\dagger\,e^{\frac{i}{\hbar}\mathrm{E}'t_2}\hat{\mathcal{P}}_{\mathrm{NE}'}. \tag{A.26}$$

Applying these relations to Eq. (A.18) yields

$$
\begin{aligned}
\dot{\rho}^{\mathrm{N}}_{\mathrm{EE}'} = -\frac{i}{\hbar}(\mathrm{E}-\mathrm{E}')\rho^{\mathrm{N}}_{\mathrm{EE}'} - \frac{1}{\hbar^2}\int_0^\infty \mathrm{d}t_2 \sum_{\mathbf{k}}\sum_{i,\,j}\sum_{\mathrm{F}}\sum_{\eta}\Big\{ & \\
\hat{\mathcal{P}}_{\mathrm{NE}}\,\hat{\mathrm{d}}_i\Big[t^{\eta}_{\mathbf{k}i}(t^{\eta}_{\mathbf{k}j})^*\,f^+_\eta\,(\epsilon_{\mathbf{k}})\;e^{\frac{i}{\hbar}(\mathrm{F}-\hat{\mathcal{H}}_{mol})t_2+\frac{i}{\hbar}\epsilon_{\mathbf{k}}t_2}\Big]\hat{\mathrm{d}}^\dagger_j\,\rho^{\mathrm{N}}_{\mathrm{FE}'} & \\
+\hat{\mathcal{P}}_{\mathrm{NE}}\,\hat{\mathrm{d}}^\dagger_i\Big[(t^{\eta}_{\mathbf{k}i})^*t^{\eta}_{\mathbf{k}j}\,f^-_\eta\,(\epsilon_{\mathbf{k}})\;e^{\frac{i}{\hbar}(\mathrm{F}-\hat{\mathcal{H}}_{mol})t_2-\frac{i}{\hbar}\epsilon_{\mathbf{k}}t_2}\Big]\hat{\mathrm{d}}_j\,\rho^{\mathrm{N}}_{\mathrm{FE}'} & \\
+\rho^{\mathrm{N}}_{\mathrm{EF}}\,\hat{\mathrm{d}}_i\Big[t^{\eta}_{\mathbf{k}i}(t^{\eta}_{\mathbf{k}j})^*\,f^+_\eta\,(\epsilon_{\mathbf{k}})\;e^{\frac{i}{\hbar}(\hat{\mathcal{H}}_{mol}-\mathrm{F})t_2-\frac{i}{\hbar}\epsilon_{\mathbf{k}}t_2}\Big]\hat{\mathrm{d}}^\dagger_j\,\hat{\mathcal{P}}_{\mathrm{NE}'} & \\
+\rho^{\mathrm{N}}_{\mathrm{EF}}\,\hat{\mathrm{d}}^\dagger_i\Big[(t^{\eta}_{\mathbf{k}i})^*t^{\eta}_{\mathbf{k}j}\,f^-_\eta\,(\epsilon_{\mathbf{k}})\;e^{\frac{i}{\hbar}(\hat{\mathcal{H}}_{mol}-\mathrm{F})t_2+\frac{i}{\hbar}\epsilon_{\mathbf{k}}t_2}\Big]\hat{\mathrm{d}}_j\,\hat{\mathcal{P}}_{\mathrm{NE}'} & \\
-\hat{\mathcal{P}}_{\mathrm{NE}}\,\hat{\mathrm{d}}_i\sum_{\mathrm{F}'}\rho^{\mathrm{N}+1}_{\mathrm{FF}'}\Big[t^{\eta}_{\mathbf{k}i}(t^{\eta}_{\mathbf{k}j})^*\,f^-_\eta\,(\epsilon_{\mathbf{k}})\;e^{\frac{i}{\hbar}(\mathrm{E}'-\mathrm{F}')t_2+\frac{i}{\hbar}\epsilon_{\mathbf{k}}t_2}\Big]\hat{\mathrm{d}}^\dagger_j\,\hat{\mathcal{P}}_{\mathrm{NE}'} & \\
-\hat{\mathcal{P}}_{\mathrm{NE}}\,\hat{\mathrm{d}}^\dagger_i\sum_{\mathrm{F}'}\rho^{\mathrm{N}-1}_{\mathrm{FF}'}\Big[(t^{\eta}_{\mathbf{k}i})^*t^{\eta}_{\mathbf{k}j}\,f^+_\eta\,(\epsilon_{\mathbf{k}})\;e^{\frac{i}{\hbar}(\mathrm{E}'-\mathrm{F}')t_2-\frac{i}{\hbar}\epsilon_{\mathbf{k}}t_2}\Big]\hat{\mathrm{d}}_j\,\hat{\mathcal{P}}_{\mathrm{NE}'} & \\
-\hat{\mathcal{P}}_{\mathrm{NE}}\,\hat{\mathrm{d}}_i\sum_{\mathrm{F}'}\rho^{\mathrm{N}+1}_{\mathrm{FF}'}\Big[t^{\eta}_{\mathbf{k}i}(t^{\eta}_{\mathbf{k}j})^*\,f^-_\eta\,(\epsilon_{\mathbf{k}})\;e^{\frac{i}{\hbar}(\mathrm{F}-\mathrm{E})t_2-\frac{i}{\hbar}\epsilon_{\mathbf{k}}t_2}\Big]\hat{\mathrm{d}}^\dagger_j\,\hat{\mathcal{P}}_{\mathrm{NE}'} & \\
-\hat{\mathcal{P}}_{\mathrm{NE}}\,\hat{\mathrm{d}}^\dagger_i\sum_{\mathrm{F}'}\rho^{\mathrm{N}-1}_{\mathrm{FF}'}\Big[(t^{\eta}_{\mathbf{k}i})^*t^{\eta}_{\mathbf{k}j}\,f^+_\eta\,(\epsilon_{\mathbf{k}})\;e^{\frac{i}{\hbar}(\mathrm{F}-\mathrm{E})t_2+\frac{i}{\hbar}\epsilon_{\mathbf{k}}t_2}\Big]\hat{\mathrm{d}}_j\,\hat{\mathcal{P}}_{\mathrm{NE}'}\Big\}, &
\end{aligned}
\tag{A.27}
$$

for the non-secular part of the GME, and

$$
\begin{aligned}
\dot{\rho}^{\mathrm{N}}_{\mathrm{E}} = -\frac{1}{\hbar^2}\int_0^\infty \mathrm{d}t_2 \sum_{\mathbf{k}}\sum_{i,\,j}\sum_{\eta}\Big\{ & \\
\hat{\mathcal{P}}_{\mathrm{NE}}\,\hat{\mathrm{d}}_i\Big[t^{\eta}_{\mathbf{k}i}(t^{\eta}_{\mathbf{k}j})^*\,f^+_\eta\,(\epsilon_{\mathbf{k}})\;e^{\frac{i}{\hbar}(\mathrm{E}-\hat{\mathcal{H}}_{mol})t_2+\frac{i}{\hbar}\epsilon_{\mathbf{k}}t_2}\Big]\hat{\mathrm{d}}^\dagger_j\,\rho^{\mathrm{N}}_{\mathrm{E}} + \mathrm{h.c.} & \\
+\hat{\mathcal{P}}_{\mathrm{NE}}\,\hat{\mathrm{d}}^\dagger_i\Big[(t^{\eta}_{\mathbf{k}i})^*t^{\eta}_{\mathbf{k}j}\,f^-_\eta\,(\epsilon_{\mathbf{k}})\;e^{\frac{i}{\hbar}(\mathrm{E}-\hat{\mathcal{H}}_{mol})t_2-\frac{i}{\hbar}\epsilon_{\mathbf{k}}t_2}\Big]\hat{\mathrm{d}}_j\,\rho^{\mathrm{N}}_{\mathrm{E}} + \mathrm{h.c.} & \\
-\hat{\mathcal{P}}_{\mathrm{NE}}\,\hat{\mathrm{d}}_i\sum_{\mathrm{E}'}\rho^{\mathrm{N}+1}_{\mathrm{E}'}\Big[t^{\eta}_{\mathbf{k}i}(t^{\eta}_{\mathbf{k}j})^*\,f^-_\eta\,(\epsilon_{\mathbf{k}})\;e^{\frac{i}{\hbar}(\mathrm{E}-\mathrm{E}')t_2+\frac{i}{\hbar}\epsilon_{\mathbf{k}}t_2}\Big]\hat{\mathrm{d}}^\dagger_j\,\hat{\mathcal{P}}_{\mathrm{NE}} & \\
-\hat{\mathcal{P}}_{\mathrm{NE}}\,\hat{\mathrm{d}}^\dagger_i\sum_{\mathrm{E}'}\rho^{\mathrm{N}-1}_{\mathrm{E}'}\Big[(t^{\eta}_{\mathbf{k}i})^*t^{\eta}_{\mathbf{k}j}\,f^+_\eta\,(\epsilon_{\mathbf{k}})\;e^{\frac{i}{\hbar}(\mathrm{E}-\mathrm{E}')t_2-\frac{i}{\hbar}\epsilon_{\mathbf{k}}t_2}\Big]\hat{\mathrm{d}}_j\,\hat{\mathcal{P}}_{\mathrm{NE}} & \\
-\hat{\mathcal{P}}_{\mathrm{NE}}\,\hat{\mathrm{d}}_i\sum_{\mathrm{E}'}\rho^{\mathrm{N}+1}_{\mathrm{E}'}\Big[t^{\eta}_{\mathbf{k}i}(t^{\eta}_{\mathbf{k}j})^*\,f^-_\eta\,(\epsilon_{\mathbf{k}})\;e^{\frac{i}{\hbar}(\mathrm{E}'-\mathrm{E})t_2-\frac{i}{\hbar}\epsilon_{\mathbf{k}}t_2}\Big]\hat{\mathrm{d}}^\dagger_j\,\hat{\mathcal{P}}_{\mathrm{NE}} & \\
-\hat{\mathcal{P}}_{\mathrm{NE}}\,\hat{\mathrm{d}}^\dagger_i\sum_{\mathrm{E}'}\rho^{\mathrm{N}-1}_{\mathrm{E}'}\Big[(t^{\eta}_{\mathbf{k}i})^*t^{\eta}_{\mathbf{k}j}\,f^+_\eta\,(\epsilon_{\mathbf{k}})\;e^{\frac{i}{\hbar}(\mathrm{E}'-\mathrm{E})t_2+\frac{i}{\hbar}\epsilon_{\mathbf{k}}t_2}\Big]\hat{\mathrm{d}}_j\,\hat{\mathcal{P}}_{\mathrm{NE}}\Big\}, &
\end{aligned}
\tag{A.28}
$$

for the secular part.

A.2. The overlap between the substrate wavefunction and an atomic p orbital

Here we show the evaluation of Eq. (2.22). The integral we have to solve is:

$$\langle \mathbf{k}|\alpha\rangle = S^{-1/2} \int \mathrm{d}^3 r \, e^{-ik_x x} e^{-ik_y y} \, \Psi(z) p_z(\mathbf{r} - \mathbf{r}_\alpha). \tag{A.29}$$

As a first step, we use the identity

$$\Psi(z) = \int \mathrm{d}z' \Psi(z') \delta(z' - z). \tag{A.30}$$

Inserting Eq. (A.30) in Eq. (A.29) yields:

$$\langle \mathbf{k}|\alpha\rangle = S^{-1/2} \int \mathrm{d}z' \, \Psi(z') \int \mathrm{d}^3 r \, \delta(z' - z) \, e^{-ik_x x} e^{-ik_y y} \, p_z(\mathbf{r} - \mathbf{r}_\alpha). \tag{A.31}$$

After replacing the delta function by its Fourier transform,

$$\delta(z' - z) = \frac{1}{2\pi} \int_{-\infty}^{\infty} \mathrm{d}\ell_z \, e^{i\ell_z (z' - z)}, \tag{A.32}$$

a variable transformation $\mathbf{r} \longrightarrow \mathbf{r} + \mathbf{r}_\alpha$ and choosing $\boldsymbol{\ell} := (k_x, k_y, \ell_z)$, we arrive at the following equation for the overlap integral:

$$\langle \mathbf{k}|\alpha\rangle = \frac{S^{-1/2}}{8\sqrt{2\pi^3}} \left(\frac{Q_\alpha}{a_0}\right)^{\frac{5}{2}} \int \mathrm{d}z' \int \mathrm{d}\ell_z \, \Psi(z') \, e^{i\ell_z z'} e^{-i\boldsymbol{\ell}\cdot\mathbf{r}_\alpha} \int \mathrm{d}^3 r \, e^{-i\boldsymbol{\ell}\cdot\mathbf{r}} \, r \cos(\vartheta) \, e^{-\frac{Q_\alpha}{2a_0} r}. \tag{A.33}$$

To solve the last part of the integral we first have to expand the exponential $e^{-i\vec{\ell}\cdot\vec{r}}$ into spherical harmonics:

$$e^{i\boldsymbol{\ell}\cdot\mathbf{r}} = 4\pi \sum_{l=0}^{\infty} \sum_{m=-l}^{l} i^l j_l(\ell r) Y_{lm}(\vartheta_r, \varphi_r) Y_{lm}^*(\vartheta_\ell, \varphi_\ell). \tag{A.34}$$

Here j_l are the spherical Bessel function and $(\vartheta_\ell, \phi_\ell)$ denote the angles in the space of the wavevector $\boldsymbol{\ell}$. Note that for our problem we have to use the complex conjugate of Eq. (A.34). After applying the relation

$$\cos(\vartheta_r) = 2\sqrt{\frac{\pi}{3}} Y_{10}(\vartheta_r, \varphi_r) \tag{A.35}$$

and the orthonormality of the spherical harmonics, we can bring the last integral of Eq. (A.33) into the form:

$$\int \mathrm{d}^3r\, e^{-i\boldsymbol{\ell}\cdot\mathbf{r}}\, r\cos(\vartheta)\, e^{-\frac{Q_\alpha}{2a_0}r} = -4\pi i\, 2\sqrt{\frac{\pi}{3}}Y_{10}(\vartheta_\ell,\varphi_\ell)\int_0^\infty \mathrm{d}r\, r^3\, e^{-\frac{Q_\alpha}{2a_0}r}\, j_1(\ell r) \tag{A.36}$$

$$= -4\pi i\,\frac{\ell_z}{\ell}\int_0^\infty \mathrm{d}r\, r^3\, e^{-\frac{Q_\alpha}{2a_0}r}\, j_1(\ell r) \tag{A.37}$$

$$= -32\pi i\,\frac{\ell_z}{\ell}\,\frac{Q_\alpha}{2a_0}\,\ell\left[\left(\tfrac{Q_\alpha}{2a_0}\right)^2+\ell^2\right]^{-3}. \tag{A.38}$$

Here we again used Eq. (A.35), but this time with argument ϑ_ℓ obeying $\cos(\vartheta_\ell)=\frac{\ell_z}{\ell}$. After inserting the above solution into Eq. (A.33) and renaming z' to z again, we obtain the following equation:

$$\langle\mathbf{k}|\alpha\rangle = \frac{-2\pi i S^{-1/2}}{\sqrt{2\pi^3}}\left(\tfrac{Q_\alpha}{a_0}\right)^{\frac{7}{2}}\int \mathrm{d}z\,\mathrm{d}\ell_z\,\Psi(z)\,e^{i\ell_z z}e^{-i\boldsymbol{\ell}\cdot\mathbf{r}_\alpha}\,\ell_z\left[\left(\tfrac{Q_\alpha}{2a_0}\right)^2+\ell^2\right]^{-3}. \tag{A.39}$$

The next integration we have to solve is the integral over ℓ_z which can be done by following the standard procedure of applying the residue theorem. After splitting $\mathbf{r}_\alpha$ and $\boldsymbol{\ell}$ into components parallel to the x-y plane, $\mathbf{r}_{\alpha\parallel}=(x_\alpha,\,y_\alpha,\,0)$ and $\boldsymbol{\ell}_\parallel=(k_x,\,k_y,\,0)\equiv\mathbf{k}_\parallel$, and components in z-direction, d and ℓ_z, the matrix element $\langle\mathbf{k}|\alpha\rangle$ is given by:

$$\langle\mathbf{k}|\alpha\rangle = \frac{-2\pi i S^{-1/2}}{\sqrt{2\pi^3}}\left(\tfrac{Q_\alpha}{a_0}\right)^{\frac{7}{2}}\,e^{-i\mathbf{k}_\parallel\cdot\mathbf{r}_{\alpha\parallel}}\int_{z_0}^{0}\mathrm{d}z\,\Psi(z)J(z), \tag{A.40}$$

with

$$J(z)=\int_{-\infty}^{\infty}\mathrm{d}\ell_z\,e^{i\ell_z(z-d)}\,\frac{\ell_z}{\left[(\ell_z+i\ell_\alpha)(\ell_z-i\ell_\alpha)\right]^3}. \tag{A.41}$$

The integrand has two third order poles at $\ell_z=\pm i\ell_\alpha$, with

$$\ell_\alpha=\frac{Q_\alpha}{2a_0}\sqrt{1+\frac{4a_0^2k_\parallel^2}{Q_\alpha^2}}. \tag{A.42}$$

Using the abbreviation ℓ_α greatly simplifies the results. The sign of the difference $(z-d)$ in the exponential determines in which half-plane we have to close our contour to get the correct results. Consequently, the integral splits into two parts: The first one, $J^-(z)$, corresponds to $z_0<z<d$. Hence $(z-d)<0$. meaning that we have to close the contour in the lower half plane to hinder the integrand from diverging. The enclosed pole is $-i\ell_\alpha$ and we get the winding number $\nu=-1$. The second part, $J^+(z)$, is associated with values $z>d$, meaning that we have to close the contour in the upper half plane. Therefore the enclosed pole is $+i\ell_\alpha$ and the winding number ν is $+1$. Using

$$\operatorname{Res} f(z)\Big|_{z=z_0}=\frac{1}{(n-1)!}\lim_{z\to z_0}\frac{\partial^{n-1}}{\partial z^{n-1}}\left[(z-z_0)^n f(z)\right]. \tag{A.43}$$

we get:

$$J^{\pm}(z) = \frac{\pm\ell_\alpha (z-d)^2 + (z-d)}{32\pi i \ell_\alpha^3}\, e^{\mp\ell_\alpha (z-d)}. \tag{A.44}$$

Now we are able to take the final integral. As we are not concerned with the behaviour of the piecewise-defined $\Psi(z)$ for $z < z_0$, only two of its three regions of definition are of interest. $\Psi(z)$ then reads:

$$\Psi(z) = \begin{cases} \Psi_a(z) = \frac{\Omega}{2}\left(\xi e^{ik_z z} + \xi^* e^{-ik_z z}\right), & z_0 < z < 0 \\ \Psi_b(z) = \Omega\, e^{-\kappa z}, & z > 0 \end{cases}. \tag{A.45}$$

Nevertheless, the integration consists of three parts, as in one region the difference $(z-d)$ changes sign. Therefore, we have to split up $\langle \mathbf{k}|\alpha\rangle$ as follows:

$$\begin{aligned} z_0 < z < 0: \quad & \langle \mathbf{k}|\alpha\rangle_1 = \mathcal{N}\, e^{-i\mathbf{k}_\parallel \cdot \mathbf{r}_{\alpha\parallel}} \int_{z_0}^{0} \mathrm{d}z\, \Psi_a(z) J^-(z) \\ 0 < z < d: \quad & \langle \mathbf{k}|\alpha\rangle_2 = \mathcal{N}\, e^{-i\mathbf{k}_\parallel \cdot \mathbf{r}_{\alpha\parallel}} \int_{0}^{d} \mathrm{d}z\, \Psi_b(z) J^-(z) \\ z > d: \quad & \langle \mathbf{k}|\alpha\rangle_3 = \mathcal{N}\, e^{-i\mathbf{k}_\parallel \cdot \mathbf{r}_{\alpha\parallel}} \int_{d}^{\infty} \mathrm{d}z\, \Psi_b(z) J^+(z). \end{aligned}$$

For brevity, here we introduced a temporary prefactor $\mathcal{N}$. After introducing the abbreviations

$$\mathcal{A}_1 = \frac{1}{(\ell_\alpha + ik_z)^2}\left\{1 - (\ell_\alpha + ik_z)d - \left[1 - (\ell_\alpha + ik_z)(d - z_0)\right] e^{(\ell_\alpha + ik_z)z_0}\right\}, \tag{A.46}$$

$$\mathcal{A}_2 = \frac{1}{\ell_\alpha + ik_z}\left\{d^2 - (d - z_0)^2\, e^{(\ell_\alpha + ik_z)z_0} - 2\mathcal{A}_1\right\}, \tag{A.47}$$

the first part of the overlap integral is given by:

$$\langle \mathbf{k}|\alpha\rangle_1 = \tilde{\Omega}_\alpha\, e^{-i\mathbf{k}_\parallel \cdot \mathbf{r}_{\alpha\parallel}}\, \Re\left\{\xi\left(\ell_\alpha \mathcal{A}_2 - \mathcal{A}_1\right)\right\} e^{-\ell_\alpha d}. \tag{A.48}$$

The prefactor $\tilde{\Omega}_\alpha$ (which also depends on k_z, $k_\parallel$ and κ) reads:

$$\tilde{\Omega}_\alpha = \frac{\Omega}{16\sqrt{2\pi^3 S}\ell_\alpha^3}\left(\frac{Q_\alpha}{a_0}\right)^{\frac{7}{2}} = \tilde{\Omega}_\alpha(k_z, k_\parallel, \kappa). \tag{A.49}$$

For convenience, we rewrite $\langle \mathbf{k}|\alpha\rangle_1$ as:

$$\langle \mathbf{k}|\alpha\rangle_1 = \tilde{\Omega}_\alpha\, V_\alpha^{(1)}(k_z, k_\parallel, \kappa)\, e^{-i\mathbf{k}_\parallel \cdot \mathbf{r}_{\alpha\parallel}}. \tag{A.50}$$

The second part of the overlap integral, defined in the region $0 < z < d$, is given by:

$$\langle \mathbf{k}|\alpha\rangle_2 = \tilde{\Omega}_\alpha\, e^{-i\mathbf{k}_\parallel\cdot\mathbf{r}_{\alpha\parallel}} \left\{ \frac{2\ell_\alpha}{(\ell_\alpha-\kappa)^3}\left[1-\left(1+(\ell_\alpha-\kappa)d+(\ell_\alpha-\kappa)^2\frac{d^2}{2}\right)\, e^{-(\ell_\alpha-\kappa)d}\right] + \frac{1}{(\ell_\alpha-\kappa)^2}\left[1-\left(1+(\ell_\alpha-\kappa)d\right)e^{-(\ell_\alpha-\kappa)d}\right]\right\} e^{-\kappa d}. \tag{A.51}$$

Again in a shortened form:

$$\langle \mathbf{k}|\alpha\rangle_2 = \tilde{\Omega}_\alpha\, V_\alpha^{(2)}(k_z,k_\parallel,\kappa)\, e^{-i\mathbf{k}_\parallel\cdot\mathbf{r}_{\alpha\parallel}}. \tag{A.52}$$

Finally, the third part reads:

$$\langle \mathbf{k}|\alpha\rangle_3 = \tilde{\Omega}_\alpha\, e^{-i\mathbf{k}_\parallel\cdot\mathbf{r}_{\alpha\parallel}}\left[-\frac{2\ell_\alpha}{(\ell_\alpha+\kappa)^3}-\frac{1}{(\ell_\alpha+\kappa)^2}\right] e^{-\kappa d} \tag{A.53}$$

$$= \tilde{\Omega}_\alpha\, V_\alpha^{(3)}(k_z,k_\parallel,\kappa)\, e^{-i\vec{k}_\parallel\cdot\vec{r}_{\alpha\parallel}}. \tag{A.54}$$

Collecting the results and defining $V_\alpha(k_z,k_\parallel,\kappa)=\tilde{\Omega}_\alpha(V_\alpha^{(1)}+V_\alpha^{(2)}+V_\alpha^{(3)})$, we arrive at the following expression for the tunneling matrix elements in the substrate region:

$$t_{\mathbf{k}i}^S = \epsilon_i \sum_\alpha c_{\alpha i} V_\alpha(k_z,k_\parallel,\kappa)\, e^{-i\mathbf{k}_\parallel\cdot\mathbf{r}_{\alpha\parallel}}. \tag{A.55}$$

A.3. Calculation of the overlap integrals for the Slater-Koster LCAO method

First, we will show the computation of matrix elements involving the orbitals of the nitrogen atom at site 1 and the carbon atom at site 2 for the σ-system (see Fig. 4.3). The bond vector between site 1 and site 2 forms angles of 55° and 35° to the x- and y-axis, respectively. In a first step we calculate the overlap between the 2s orbitals located at each of the two sites. This is rather simple and after looking at Tab. 4.4 we obtain:

$$b_{(1,s)(2,s)} = \eta_{ss\sigma}\,\frac{\hbar^2}{m_e d_{12}^2}. \tag{A.56}$$

Now we evaluate the matrix element between the s orbital at site 1 and the p_x orbital at site 2. Again, after consulting Tab. 4.4, we get:

$$b_{(1,s)(2,p_x)} = \eta_{sp\sigma}\,\frac{\hbar^2}{m_e d_{12}^2}\cos(55°). \tag{A.57}$$

A small difference occurs when we want to calculate the overlap between an s orbital at site 1 and a p_y orbital at site 2. If we look at Fig. 4.2, we see that, because of the respective

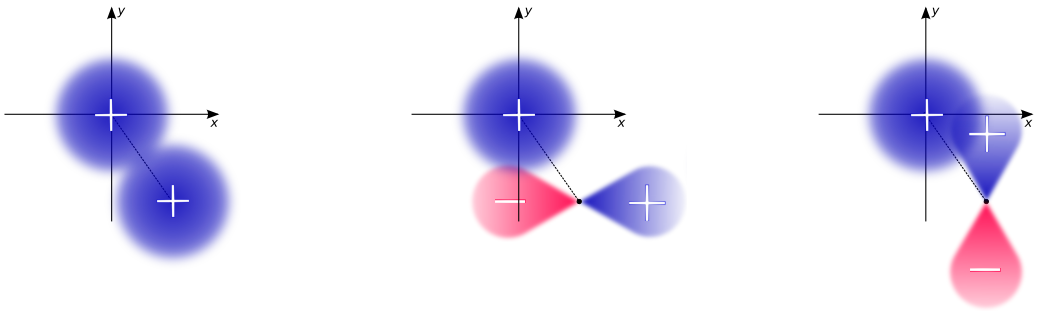

(a) $b_{(1,s)(2,s)}$ (b) $b_{(1,s)(2,p_x)}$ (c) $b_{(1,s)(2,p_y)}$

Figure A.1.: *Sketch of overlaps between an s orbital at site 1 and the different orbitals at site 2.*

orientation of the two orbitals, we have a minus sign in front. In addition we now have to use the direction cosine towards the y-axis:

$$b_{(1,s)(2,p_y)} = -\eta_{sp\sigma} \frac{\hbar^2}{m_e d_{12}^2} \cos(35°). \tag{A.58}$$

Now we calculate the matrix elements between the p_x orbital at site 1 and the different orbitals at site 2. By looking at the picture and checking Fig. 4.2, we see that the overlap with the s orbital is equivalent to $b_{(1,s)(2,p_x)}$ except for the sign:

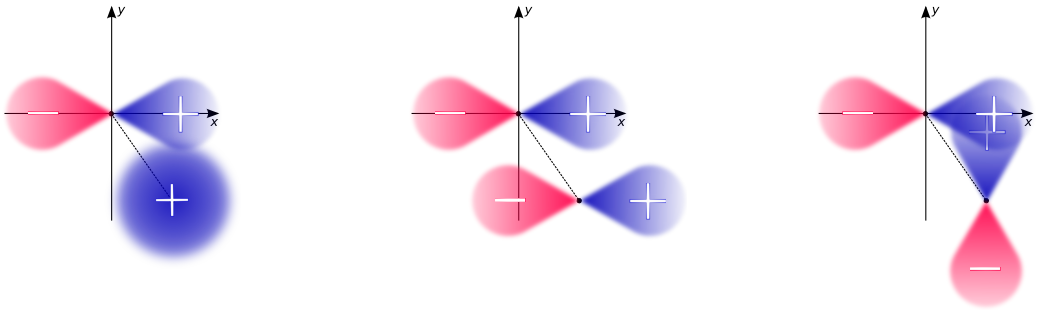

(a) $b_{(1,p_x)(2,s)}$ (b) $b_{(1,p_x)(2,p_x)}$ (c) $b_{(1,p_x)(2,p_y)}$

Figure A.2.: *Sketch of overlaps between a p_x orbital at site 1 and the different orbitals at site 2.*

$$b_{(1,p_x)(2,s)} = -b_{(1,s)(2,p_x)} = -\eta_{sp\sigma} \frac{\hbar^2}{m_e d_{12}^2} \cos(55°). \tag{A.59}$$

The next matrix element $b_{(1,p_x)(2,p_x)}$ can be evaluated easily just by looking at Tab. 4.4:

$$b_{(1,p_x)(2,p_x)} = \left(\eta_{pp\sigma} \cos^2(55°) + \eta_{pp\pi} \sin^2(55°)\right) \frac{\hbar^2}{m_e d_{12}^2}. \tag{A.60}$$

To calculate the overlap between the p_x orbital at site 1 and the p_y orbital at site 2, we first have to decompose the p_y orbital in components parallel and perpendicular to the bond. After consulting Fig. 4.2, we see that both overlap integrals $V_{(1,p_x)(2,p_y)\sigma}$ and $V_{(1,p_x)(2,p_y)\pi}$ have a minus sign in front of them due to the respective orientations of the orbitals. Checking Tab. 4.4 then finally gives us the functions $f_\varsigma(\alpha,\beta,\gamma)$:

$$b_{(1,p_x)(2,p_y)} = -\left(\eta_{pp\sigma} - \eta_{pp\pi}\right)\frac{\hbar^2}{m_e d_{12}^2}\cos(55°)\cos(35°). \tag{A.61}$$

The next matrix element follows analogously:

$$b_{(1,p_y)(2,s)} = \eta_{sp\sigma}\frac{\hbar^2}{m_e d_{12}^2}\cos(35°). \tag{A.62}$$

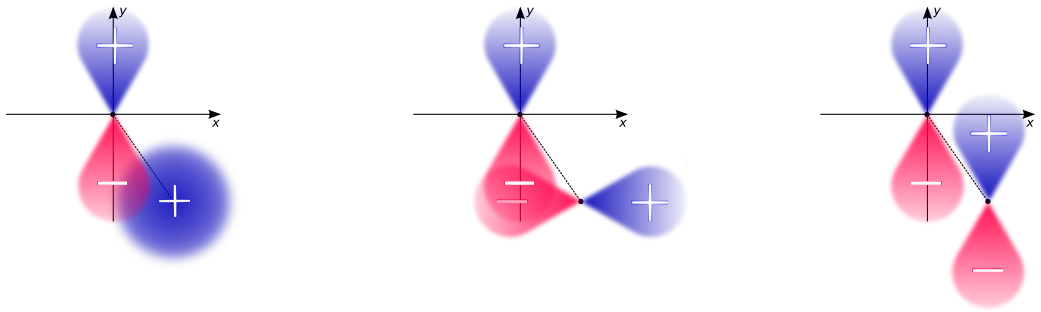

(a) $b_{(1,p_y)(2,s)}$ (b) $b_{(1,p_y)(2,p_x)}$ (c) $b_{(1,p_y)(2,p_y)}$

Figure A.3.: *Sketch of overlaps between a p_y orbital at site 1 and the different orbitals at site 2.*

For the matrix element $b_{(1,p_y)(2,p_x)}$ we again get a minus sign in front due to the orientations of the participating orbitals:

$$b_{(1,p_y)(2,p_x)} = -\left(\eta_{pp\sigma} - \eta_{pp\pi}\right)\frac{\hbar^2}{m_e d_{12}^2}\cos(55°)\cos(35°). \tag{A.63}$$

For the last matrix element $b_{(1,p_y)(2,p_y)}$ we get basically the same result as for $b_{(1,p_x)(2,p_x)}$, but now we have to use the direction cosine respective to the y-axis. Thus the argument of the cosine now is 35°:

$$b_{(1,p_y)(2,p_y)} = \left(\eta_{pp\sigma}\cos^2(35°) + \eta_{pp\pi}\sin^2(35°)\right)\frac{\hbar^2}{m_e d_{12}^2}. \tag{A.64}$$

After calculating all matrix elements corresponding to the σ-orbitals of the first atom, we only have to apply this recipe to the other 57 atoms to obtain the single particle Hamiltonian for the σ-system. For the π-system it does not take as much effort as in the σ case, since all p_z orbitals are alligned parallel. Hence, we get

$$b_{(i,p_z)(i',p_z)} = \eta_{pp\pi}\frac{\hbar^2}{m_e d^2_{\alpha\alpha'}} \tag{A.65}$$

for each matrix element of two p_z orbitals located at atom α and α', respectively.

A.4. Basic explanation of the functionality of a p-wave tip

When the tip is placed directly above the center of a p_z orbital (Fig. A.4(a)), we see that the corresponding tunneling matrix element has contributions from both the positive and the negative lobe of the p-wave orbital in the tip. If we would calculate the overlap between these two orbitals using the Slater-Koster LCAO method (App. A.3) we would find the result to vanish. Consequently, also the tunneling matrix element for this constellation and thus the current evaluated at this position is zero, as the contributions from the positive and the negative lobe of the tip orbital cancel out each other .

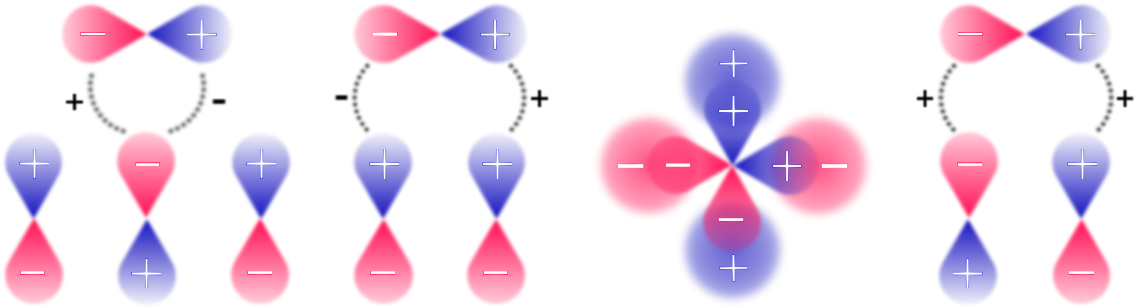

(a) $I = 0$ (b) $I = 0$ (c) Top view of (b) (d) $I \neq 0$

Figure A.4.: *Sketch of the three most important configurations in the case of a p-wave tip.*

Figs. A.4(b) and A.4(c) represent the placing of the tip above the crossing of two nodal planes, e.g. in the center of the arms of the HOMO orbital of H_2Pc. Again, the different phases of the lobes of the tip orbital cause a vanishing tunneling matrix element and zero current. When the tip is placed above one single node of the molecular orbital (Fig. A.4(d)) we have a situation similar to Fig. A.2(b), allowing for a non-vanishing current at this position of the tip.

Bibliography

[AR74] A. Aviram and M. A. Ratner. Molecular rectifiers. *Chem. Phys. Lett.*, 29:277–283, 1974.

[Arf85] G. Arfken. *Mathematical Methods for Physicists*, chapter 11, page 633ff. Academic Press, 1985.

[AS72] M. Abramovitz and I. A. Stegun. *Handbook of Mathematical Functions*, page 443ff. Dover Publications, 1972.

[Bar61] J. Bardeen. Tunneling from a many-particle point of view. *Phys. Rev. Lett.*, 6(2):57–59, 1961.

[BF04] H. Bruus and K. Flensbert. *Many-Body Quantum Theory in Condensed Matter Physics*. Oxford University Press, 2004.

[Blu96] K. Blum. *Density Matrix Theory and Applications*. Plenum Press, 1996.

[BR82] G. Binning and H. Rohrer. Surface Studies by Scanning Tunneling Microscopy. *Phys. Rev. Lett.*, 49(1):57–61, 1982.

[CFN07] A. Calzolari, A. Ferretti, and M. B. Nardelli. Ab initio correlation effects on the electronic and transport properties of metal(ii)-phthalocyanine-based devices. *Nanotechnology*, 18:42013, 2007.

[Che90] C. J. Chen. Tunneling matrix elements in three-dimensional space: The derivative rule and the sum rule. *Phys. Rev. B*, 42(14):8841–8857, 1990.

[DBDG09] D. Darau, G. Begemann, A. Donarini, and M. Grifoni. Interference effects on the transport characteristics of a benzene single-electron transistor. *Phys. Rev. B*, 79(23):235404, 2009.

[DH03] D. Dini and M. Hanack. Physical Properties of Phthalocyanine-based Materials. *The Porphyrin Handbook*, 17, 2003.

[dOea10] D. G. de Oteyza et al. Copper-phthalocyanine based metal–organic interfaces: The effect of fluorination, the substrate, and its symmetry. *J. Chem. Phys.*, 133:214703, 2010.

[DWP98] P. N. Day, Z. Wang, and R. Pachter. Calculation of the structure and absorption spectra of phthalocyanines in the gas-phase and solution. *Journal of Molecular Structure (Theochem)*, 455:33–50, 1998.

[ECS+07] F. Evangelista, V. Carravetta, G. Stefani, B. Jansik, M. Alagia, S. Stranges, and A. Ruocco. Electronic structure of copper phthalocyanine: An experimental and theoretical study of occupied and unoccupied levels. *J. Chem. Phys.*, 126(12), 2007.

[ES90] D.M. Eigler and E.K. Schweizer. Positioning single atoms with a scanning tunneling microscope. *Science*, 344:524–526, 1990.

[Fey60] R. P. Feynman. There's Plenty of Room at the Bottom. *Engineering & Science. Transcript of talk given on December 29th 1959 at annual meeting of American Physical Society at the California Institute of Technology*, 1960.

[GD92] H. Grabert and M. H. Devoret. *Single Charge Tunneling*. Plenum Press, 1992.

[GMM+11] L. Gross, N. Moll, F. Mohn, A. Curioni, G. Meyer, F. Hanke, and M. Petson. High-Resolution Orbital Imaging Using a p-Wave STM Tip. *Phys. Rev. Lett.*, 107(8):086101, 2011.

[GRM+05] L. Gross, K. H. Rieder, F. Moresco, S. M. Stojkovic, A. Gourdon, and C. Joachim. Trapping and moving metal atoms with a six-leg molecule. *Nature Materials*, pages 892–895, 2005.

[Har81] W. A. Harrison. New tight-binding parameters for covalent solids obtained using Louie peripheral states. *Phys. Rev. B*, 24(10):5835–5843, 1981.

[Har89] W. A. Harrison. *Electronic Structure and the Properties of Solids*. Dover Publications, 1989.

[Har99] W. A. Harrison. *Elementary Electronic Structure*. World Scientific, 1999.

[Hof63] R. Hoffmann. An Extended Hückel Theory. I. Hydrocarbons. *J. Chem. Phys.*, 39(6):1397–1412, 1963.

[KAT01] L. P. Kouwenhoven, D. G. Austing, and S. Tarucha. Few-electron quantum dots. *Rep. Prog. Phys.*, 64:701–736, 2001.

[KDH+03] S. Kubatkin, A. Danilov, M. Hjort, J. Cornil, J.-L. Brédas, N. Stuhr-Hansen, P. Hedegård, and T. Bjørnholm. Single-electron transistor of a single organic molecule with access to several redox states. *Nature*, 425:698–701, 2003.

[KF11] K. Kaasbjerg and K. Flensberg. Image charge effects in single-molecule junctions: Breaking of symmetries and negative-differential resistance in a benzene single-electron transistor. *Phys. Rev. B*, 84(11):115457, 2011.

[LP80] E. M. Lifschitz and L. P. Pitajewski. *Lehrbuch der theoretischen Physik*, volume 9, page 30. Akademie-Verlag, Berlin, 1980.

[LRM07] P. Liljeroth, J. Repp, and G. Meyer. Current-Induced Hydrogen Tautomerization and Conductance Switching of Naphthalocyanine Molecules. *Science*, 317:1203–1206, 2007.

[LS01] M.-S. Liao and S. Scheiner. Electronic structure and bonding in metal phthalocyanines, Metal=Fe,Co,Ni,Cu,Zn,Mg. *J. Chem. Phys.*, 114(22):9780–9791, 2001.

[PGAW11] J. Prasongkit, A. Grigoriev, R. Ahuja, and G. Wendin. Interference effects in phthalocyanine controlled by H-H tautomerization: a potential two-terminal unimolecular electronic switch. *Phys. Rev. B*, 84(16), 2011.

[PPL+00] H. Park, J. Park, A. K. L. Lim, E. H. Anderson, A. P. Alivisatos, and P. L. McEuen. Nanomechanical oscillations in a single-C_{60} transistor. *Nature*, 407:57–60, 2000.

[Rei95] H. J. Reittu. Fermi's golden rule and Bardeen's tunneling theory. 63(10):940–944, 1995.

[Rei06] J. Reinhold. *Quantentheorie der Moleküle. Eine Einführung.* Teubner, 2006.

[RM05] J. Repp and G. Meyer. Molecules on Isulating Films: Scanning-Tunneling Microscopy Imaging of Individual Molecular Orbitals. *Phys. Rev. Lett.*, 94:026803, 2005.

[SK54] J. C. Slater and G. F. Koster. Simplified LCAO Method for the Periodic Potential Problem. *Phys. Rev.*, 94(6):1498–1524, 1954.

[Tou00] J. M. Tour. Molecular Electronics. Synthesis and Testing of Components. *Acc. Chem. Res.*, 33(11):791–804, 2000.

[TT05] M. Takada and H. Tada. Scanning Tunneling Microscopy and Spectroscopy of Phthalocyanine Molecules on Metal Surfaces. *Jpn. J. Appl. Phys.*, 44(7B):5332–5335, 2005.

[vdML10] S. J. van der Molen and P. Liljeroth. Charge transport through molecular switches. *J. Phys.: Condens. Matter*, 22, 2010.

[ZGG06] D. R. T. Zahn, G. N. Gavrila, and M. Gorgoi. The transport gap of organic semiconductors studied using the combination of direct and inverse photoemission. *Chem. Phys.*, 325:99–112, 2006.

Danksagung

Zum Schluss möchte ich mich bei allen herzlich bedanken, die mich bei der Anfertigung dieser Arbeit unterstützt haben. Besonderer Dank gilt meiner Betreuerin Milena Grifoni. Danke dafür, dass sie immer ein offenes Ohr für meine Fragen und Probleme gehabt hat, für ihre Geduld besonders in den letzten Wochen meiner Arbeit und nicht zuletzt dafür, dass sie mich so herzlich in diese wundervolle Arbeitsgruppe integriert hat. Ich hätte sonst wahrscheinlich nicht so viele neue nette Menschen kennenlernen dürfen. An dieser Stille möchte ich der gesamten Arbeitsgruppe für meine herzliche Aufnahme danken.
Ein großes Dankeschön an Dana Darau und Sandra Kolmeder für die Vorarbeiten zum Thema meiner Diplomarbeit und für die vielen hilfreichen Gespräche. Vielen Dank auch an Andrea Donarini, der mir in wichtigen Fragen eine große Hilfe war. An meinen langjährigen guten Freund und Bürokollegen Sebastian Pfaller möchte ich ein herzliches Dankeschön richten: für das Korrekturlesen, für die vielen Unterhaltungen, Diskussionen und Anregungen und die viele Unterstützung bei allen möglichen Problemen. Ein großes Dankeschön geht an Björn Erbe, der meine Arbeit mit unheimlicher Präzision Korrektur gelesen hat und mir überhaupt in zahlreichen Ratschlägen und Diskussionen ein wertvoller Ansprechpartner war. Bei Lizy Lazar möchte ich mich für ihre herzliche und offene Art und ihre Unterstützung bei vielen organisatorischen Dingen bedanken.
Ein ganz großes Dankeschön gilt meiner Familie, ganz besonders meinen Eltern, für ihre selbstlose Unterstützung nicht nur während meines Studiums. Ohne sie wäre diese Arbeit sicher nicht möglich gewesen.
An letzter Stelle möchte ich meiner Freundin Christine danken, dafür, dass sie mir immer zur Seite gestanden und immer für mich da war.

Erklärung

Hiermit erkläre ich, dass ich die Diplomarbeit selbständig angefertigt und keine Hilfsmittel ausser den in der Arbeit angegebenen benutzt habe.

Regensburg, den 15.11.2010